Atomic Photoelectric Effect Above 10 keV*

R. H. PRATT, AKIVA RON,† H. K. TSENG

Department of Physics, University of Pittsburgh, Pittsburgh, Pennsylvania 15213

The current understanding of the theory of the atomic photoelectric effect is reviewed for incident photon energies above 10 keV, complementing the earlier review of Fano and Cooper (1968) at lower energies. The theoretical developments of the last two decades are of two types: (1) analytic results giving insight into many aspects of the photoelectric process and (2) exact numerical cross sections calculated with high speed electronic computers. The basic assumptions underlying the photoeffect calculations are described, and pertinent atomic models are discussed. In the energy range considered, satisfactory results are obtained with the process described as the ejection of an electron moving in a relativistic Hartree–Fock–Slater potential. Exchange, correlation, and other effects are discussed. Many features of the process can be understood with the realization that the important regions in configuration space in the photoeffect matrix element are of the order of an electron Compton wave length. This leads to the predictions that the photoeffect cross section in a screened potential can be obtained from a point-Coulomb result by a simple normalization, that angular distribution shapes and polarization correlations are the same in the two cases, and that results for photoeffect from different subshells of the same angular momentum are similarly related. The numerical methods, achieving total cross sections accurate to 1%, are described and compared with experiment. Different self-consistent atomic models yield cross sections which differ by 3%–8%; these agree with experiments of similar accuracy. New and more accurate cross section tabulations that have recently become available are discussed and recommendations are made concerning their use.

CONTENTS

1. INTRODUCTION AND NOTATION

1.1 Introduction

In the atomic photoeffect, an electron is ejected from an atom as a result of the absorption of a photon. The photoeffect, scattering, and pair production are the three processes primarily responsible for the attenuation of electromagnetic radiation in matter. Typically, for a given element the photoeffect dominates at low photon energies, scattering at intermediate energies, and pair production at high energies. This review paper is primarily concerned with the photoelectric effect for incident photon energies above 10 keV. At these energies

* Supported in part by the Lawrence Radiation Laboratory of the University of California through Subcontract No. 4738209 and in part by the National Science Foundation under Grant No. GP-32798.

† Permanent address: Racah Institute of Physics, Hebrew University of Jerusalem, Jerusalem, Israel.

the ejected electron usually comes from a tightly bound inner shell. Such electrons are well represented by central-field wave functions of Hartree–Fock–Slater type. At lower energies, and especially close to absorption edges, other effects, such as correlations among electrons, become prominent. With high-resolution experimental work, the structure resulting from such effects has been measured, and the low-energy region is now of considerable interest. However, it is beyond the scope of this review, though some comments and references are given in Secs. 2.1 and 3.2a; we refer the interested reader to the review of Fano and Cooper (1968). The data presented and discussed in this review concern total cross sections, though for the sake of completeness we give the general formulas for angular distributions and polarization correlations.

The photoelectric effect has been known for some time, although our present understanding is quite recent. Hertz in 1887 noted that ultraviolet light facilitated the passage of electric current across a spark gap. In 1905 Einstein explained the main features of the photoelectric effect with the hypothesis of quantized radiation. With the advent of modern quantum mechanics and radiation theory, a quantitative calculation of the photoionization of atoms became feasible. The main outline of the theory was established in 1936 when the review article of Hall (1936) appeared; little was added in the next two decades.

The books of Heitler (1954) and Bethe and Salpeter (1957) provide a good summary of the theory up to 1957. Theoretical knowledge of the process and resultant Tables of absorption cross sections were primarily based on four pieces of work: (1) exact nonrelativistic results in the point-Coulomb potential for ejection of K- and L-shell electrons (Stobbe, 1930) (see Sec. 6.1); (2) Sauter's relativistic Born result (Sauter, 1931a,b) for the K shell in the point-Coulomb potential; (3) Hall's high-energy limits (Hall and Rarita, 1934; Hall, 1936) for the K and L shells in the point-Coulomb potential; and (4) exact relativistic point-Coulomb K-shell total cross sections obtained numerically for six cases by Hulme, McDougall, Buckingham, and Fowler (1935). Atomic-electron screening was taken into account by considering cross sections as a function of atomic number Z, and replacing Z by a $Z_{\text{effective}}$ chosen to reproduce observed binding energies. Contributions of higher shells to the total cross section were accounted for by multiplying K-shell cross sections by 5/4. [Subsequent work has shown that the $Z_{\text{effective}}$ approximation is poor and that Hall's result is incorrect (Pratt, 1960a,b). The numerical work of Hulme, McDougall, Buckingham, and Fowler (1935) has been verified and the 5/4 rule has been found to be fair for high Z but not for low Z.]

Renewed interest in the photoelectric process began in the late 1950's. With the rapid development of nuclear physics, knowledge of photoelectric cross sections was needed in order to establish various nuclear properties (e.g., experimental internal conversion coefficients) and to perform calculations related to radiation shielding and astrophysical problems (e.g., opacity). On the other hand, some experimental improvements were introduced. Latyshev (1947) suggested the use of β spectrometers, and later improvements by Hultberg (1955, 1959) made possible measurements of separate shell contributions and angular distributions. Thus, more and better theoretical predictions were needed. Renewed analytical work corrected the high-energy limit results (Pratt, 1960a,b) and extended the relativistic Born approximation (Gavrila, 1959, 1961; Nagel, 1960). But only with the aid of modern electronic computers, beginning in the 1960's, has it become possible to obtain fairly precise (1%–5%) quantitative predictions of photoelectric cross sections, angular distributions, and polarization correlations, at least for $Z>13$, $k>10$ keV. Photoelectric cross sections are now available for all Z and for energies from 1 keV to 100 MeV, based on description of both the bound and ejected electrons with Dirac wave functions in a relativistic Hartree–Fock–Slater potential. The most complete theoretical Tables are due to Storm and Israel (1970) and Scofield (1972).

Simultaneous with the recent numerical work, it has become possible to understand in an analytical fashion the origins of many aspects of the photoelectric process. Thus, the normalization screening theory, introduced for the photoelectric process by Pratt (1960a), predicts the dependence of cross sections on electron screening, for energies away from threshold: (1) The main contribution to the photoeffect matrix element comes from regions in configuration space of the order of *one electron Compton wavelength*, and not where the bound wave function is largest. (2) At these distances, the bound wave function has a hydrogen-like shape and differs from a point-Coulomb wave function only by a normalization factor. (3) At these energies, the kinematic factor pE of the photoeffect cross section cancels the change in the normalization of the continuum wave function. Consequently, the effect of screening on the photoeffect cross section is simply to multiply it by the square of the change in normalization of the bound state wave function (Pratt and Tseng, 1972). Another consequence of the theory is that angular distributions and polarizations correlations are nearly independent of screening. For similar reasons, one may also predict that the ratios of the cross sections of certain subshells are independent of energy. Such subshells have the same angular distribution shapes and polarization correlations. Phenomena of this type are clearly not peculiar to photoeffect, but will occur in any process for which it can be argued that the small distance region dominates. An obvious example is orbital electron capture, discussed by Brysk and Rose (1958). Recently Band, Sliv, and Trzhaskovskaya (1970)

have shown that the arguments are valid in internal conversion. Tseng and Pratt (1971, 1972) have demonstrated these effects in pair production near threshold.

We have attempted to keep this review relatively self-contained. For this reason we discuss in some detail, in successive sections, the basic theoretical assumptions, atomic models, electron wave functions, and numerical methods. The reader who is interested only in a discussion of present results may proceed directly to Sec. 6. It should be noted that the list of references includes many items not explicitly mentioned in the text. This does not reflect on their quality, but on the desire to hold the text to manageable length. We wish to call attention to the comprehensive glossary which follows this subsection; symbols are also defined when first introduced.

1.2 Notation

Here we provide a brief summary of the notation used in this review. We generally follow the notation of *Relativistic Quantum Mechanics* by Bjorken and Drell (1964). Unrationalized units are used throughout, $\hbar=m_e=c=1$, unless otherwise specified. Here $\hbar=6.582183\times10^{-22}$ MeV sec is the (reduced) Planck's constant, $m_e=0.5110041$ MeV/c^2 is the electron rest mass, and $c=2.9979250\times10^{10}$ cm/sec is the speed of light (Taylor, Parker, and Langenberg, 1969). In this system, the unit of length is the electron Compton wavelength $\lambda\!\!\!^{-}_e=\hbar/m_ec=3.861592\times10^{-11}$ cm$=386.1592$ F, time is measured in multiples of the interval in which light travels one electron Compton wavelength, $\hbar/m_ec^2=1.288088\times10^{-21}$ sec, and the unit of energy is the electron rest energy $m_ec^2=0.5110041$ MeV.

α = Fine-structure constant$=e^2/\hbar c=1/137.03602$, where $e=-4.803250\times10^{-10}$ esu is the electron charge.

a_e = Bohr radius of the hydrogen atom, $\hbar^2/m_ee^2=0.52917715\times10^{-8}$ cm.

r_e = Classical electron radius$=e^2/m_ec^2=\alpha\lambda\!\!\!^{-}_e=\alpha^2a_e=2.817939\times10^{-13}$ cm.

Z = Atomic number of target elements.

a = $Z\alpha$.

k, $\mathbf{k}$ = Initial photon energy and momentum, respectively, in m_ec^2 and m_ec units in the laboratory system.

ϵ = Binding energy of the atomic electrons.

E, $\mathbf{p}$ = Total energy and momentum of the ejected electron in the laboratory system.

T = Kinetic energy of electrons.

$\mathbf{r}$ = Radius vector from the center of the atomic nucleus.

$\hat{r}$ = $\mathbf{r}/r$.

$\boldsymbol{\varepsilon}$ = Complex unit vector for photon polarization such that $\boldsymbol{\varepsilon}^*\cdot\boldsymbol{\varepsilon}=1$, $\boldsymbol{\varepsilon}\cdot\mathbf{k}=0$, i.e., the radiation gauge has been chosen.

$\boldsymbol{\xi}_i$ ζ_i $(i=1,2,3)$ = Polarization parameters for initial photons and ejected electron, respectively.

ψ_i, ψ_f = Wave functions for the initial bound-state electron and final continuum state electron

l, j, m = Quantum numbers for the orbital and total angular momentum of the ejected electron, and projection of j.

L, J, M = Quantum numbers of the orbital and total angular momentum of the initial bound electron, and projection of J.

κ = Quantum number which combines j and parity, $\kappa=\mp(j+1/2)$ as $j=l\pm1/2$ $(\equiv l'\mp1/2)$: In spectroscopic notation, l (not an eigenvalue) is used instead of parity. $\kappa=-1, +1, -2, +2, -3, \cdots$ correspond to $s_{1/2}$ (abbreviation s), $p_{1/2}(p)$, $p_{3/2}(\bar{p})$, $d_{3/2}(d)$, $d_{5/2}(\bar{d})$, $\cdots$ states, respectively.

K = Same as κ but for bound electrons

$\mathbf{S}$ = $\boldsymbol{\sigma}/2$= the spin of electrons

γ = $(\kappa^2-a^2)^{1/2}$

γ_B = $(\mathrm{K}^2-a^2)^{1/2}$

γ_β = $(1-\beta^2)^{-1/2}$, with $\beta=p/E$

$\gamma_\mu A^\mu$ = $\gamma^0A^0-\boldsymbol{\gamma}\cdot\mathbf{A}$, where γ_μ are γ matrices in Dirac equations and in spinor representation

$$\gamma^0=\begin{pmatrix}1 & 0\\ 0 & -1\end{pmatrix},\qquad \boldsymbol{\gamma}=\begin{pmatrix}0 & \boldsymbol{\sigma}\\ -\boldsymbol{\sigma} & 0\end{pmatrix},$$

with $\boldsymbol{\sigma}$ the familiar 2×2 Pauli matrices.

$\boldsymbol{\alpha}$ = $\begin{pmatrix}0 & \boldsymbol{\sigma}\\ \boldsymbol{\sigma} & 0\end{pmatrix}$ in spinor representation

$g_\kappa(r), f_\kappa(r)$ = Large and small components of Dirac radial wave function of continuum state electrons of κ-partial waves, satisfying the equations,

$$dg/dr=(E+1-V)f-\kappa g/r,$$

$$df/dr=-(E-1-V)g+\kappa f/r,$$

where $V(r)$ stands for the assumed atomic central potentials.

$G_\mathrm{K}(r), F_\mathrm{K}(r)$ = Same as g_κ and f_κ but for bound-state electrons.

δ_κ = Phase shift of κ partial waves.

n = The principal quantum number of bound electrons.

M_{fi} = Atomic photoeffect matrix elements between initial and final states i and f.

$d\Omega$ = $\sin\theta\, d\theta\, d\phi$= element of solid angle in the direction of $\mathbf{p}$ relative to $\mathbf{k}$, in steradian (abbreviation sr) units.

$d\sigma/d\Omega$ = Atomic photoeffect cross sections, differential with respect to the solid angle in the direction of $\mathbf{p}$ relative to $\mathbf{k}$, in b/sr-atom units (1 barn$=10^{-24}$ cm^2).

σ_{1s}, σ_{2s}, σ_{2p}, $\sigma_{2\tilde{p}}$, σ_K, σ_L, σ_M, σ_n, σ_a = Atomic photoeffect total cross sections of the K shell, the $L_{\rm I}$ subshell, the $L_{\rm II}$ subshell, the $L_{\rm III}$ subshell, the K shell, the L shell, the M shell, the shell with principal quantum number n, and the atom of target elements, respectively. Note that $\sigma_{1s}=\sigma_K=\sigma_1$, $\sigma_L=\sigma_2$, $\sigma_M=\sigma_3$, $\sigma_a=\sum_n \sigma_n$. See for example, Bethe and Salpeter (1957), p. 295.

$C(j_1 j_2 j; m_1 m_2)$ = The Clebsch–Gordan coefficient [we follow the Condon–Shortley (1935) phase convention].

$Y_{lm}(\hat{r})$ = Spherical harmonics

$\chi = \sum_s a_s \chi^s$ = The two-component spinors with

$$\chi^{\dagger}\chi=1, \qquad \chi^{1/2}=\begin{pmatrix}1\\0\end{pmatrix}$$

and

$$\chi^{-1/2}=\begin{pmatrix}0\\1\end{pmatrix}.$$

$\Omega_{\kappa m}(\hat{r}) = \sum_s C(l\tfrac{1}{2}j; m-s, s) Y_{l,m-s}(\hat{r})\chi^s$ is the spherical spinor.

$\nu = aE/p$.

$N_{\rm K}^2 = (G_{\rm K} r^{-\gamma_B})_{r=0}^2 + (F_{\rm K} r^{-\gamma_B})_{r=0}^2$ = Square of normalizations of bound electron wave functions with the quantum number K.

Ξ = The ratio of screened to point-Coulomb bound-state normalizations.

$j_l(x)$, $y_l(x)$ = Spherical Bessel functions of the first and second kind.

HFS = Hartree–Fock–Slater (relativistic unless otherwise specified).

HFS 2/3 = Hartree–Fock–Slater with two-thirds Slater's exchange (Kohn–Sham, relativistic unless otherwise specified).

TF = Thomas–Fermi.

TFC = Thomas–Fermi modified by Csavinsky (1968).

FAM = Fermi–Amaldi modified by Shalitin (1965).

${}_1F_1(a, c, z)$ = The confluent hypergeometric function, i.e., the Kummer function.

2. BASIC ASSUMPTIONS AND GENERAL FORMULATION

2.1 Basic Assumptions

The complete physical situation which we should describe is the absorption of a beam of photons by a material target, resulting in the ejection of electrons. This complex process includes numerous effects. Here we restrict our attention to the absorption of one photon by an isolated atom, resulting in the ejection of one electron. Once this basic cross section is known, additional effects can be included. We furthermore use a simplified model for the atom and for the absorption process which, we will argue, is adequate for a wide range of atoms and photon energies (particularly above the keV range). In certain experimental situations (e.g., with thin targets, see Sec. 6), the other physical effects are minor and we can make direct comparison with the predictions of this simplified theory. In summary, our simplifying assumptions are as follows:

(i) A single isolated atom is the target,
(ii) The target atom is neutral and in its ground state,
(iii) A central potential model describes the atom,
(iv) The process is treated as a one-photon, one-electron, and one-vertex one.

In the following paragraphs, we briefly discuss each of these assumptions:

(i) The first assumption concerns the neglect of extended structure in the target, responsible for primary molecular or solid-state effects in the photoelectric process (e.g., crystal structure, energy bands, etc.). Usually, these effects are most pronounced for the loosely bound electrons of the outer shells. The characteristic binding energies of such electrons are of the order of some tens of eV or less. We are considering the photoelectric effect for much higher energies, never less than 1 keV. The direct contribution of outer electrons to the total atomic cross section is then very small, as the photoeffect cross sections are largest for the most tightly bound electrons which can be ejected with the available energy. (Recall that energy-momentum conservation forbids transfer of energy to a free electron. We will show later that the important region contributing to the photoeffect matrix element is that for which $r\sim 1$. At these distances, contributions from inner shell electrons predominate; molecular and solid state effects are negligible.)

In the first few hundreds of electron volts on the high-energy side of the absorption edge in a solid, fine structure is observed in the cross section. Such structure is seen also for noncrystalline matter (usually only within tens of electron volts), and this phenomenon is attributed to purely "atomic" origins. These problems are beyond the scope of this review; we refer the reader to Fano and Cooper (1968) and Azaroff and Pease (1973). On the energy scale of concern in this review such fine structure can hardly be seen. Thus, we are justified in neglecting these effects.

Even though the primary process is influenced to a very small extent by molecular and solid-state effects, secondary effects exist, due to target thickness, which complicate measurements of photoelectric cross sections. However, in our present discussion the target is assumed to consist of a single, isolated atom.

(ii) The assumption of a neutral atom in its ground state clearly eliminates consideration of temperature and pressure effects, which may excite, ionize, or even completely strip the atom. Excitation can also arise from other causes. Such effects are important in stellar matter and plasmas. The standard methods used to

describe atomic models at zero temperature (see Sec. 3) can be extended to handle finite temperatures and pressures. At a finite temperature not all states are filled; the Fermi–Dirac distribution indicates the probability that a state of given energy is occupied. Results of this approach in the Thomas–Fermi model have been obtained by Feynman, Metropolis, and Teller (1949) (see also Gombás, 1949, 1956; and Latter, 1955). More recently, results for the Hartree–Fock–Slater model at finite temperatures have been reported by Rozsnyai (1972). Confining the atom to a specified volume by imposing suitable boundary conditions on the potential (e.g., for a neutral atom the force $-dV(r)/dr\,|_{r=R}=0$ at the preassigned radius R of the atom) is equivalent to making a statement about density. Through thermodynamic arguments, the pressure is then also determined. Rozsnyai's calculations, which were performed for Fe and Rb, show that for zero temperature the difference between binding energies calculated for normal density (D_0) and low density ($0.1D_0$) is small. His values of binding energies for low densities agree well with those of Herman and Skillman (1963). At a density of $20D_0$, binding energies change significantly even for the L shell ($\sim$30%) and one notices the disappearance of bound levels in the M shell. The occupation numbers for the inner (K, L) shells are not affected. The lowest finite temperature for which Rozsnyai presents results is $k_BT=100$ eV ($k_B=1.0/11604.85$ eV/°K, the Boltzmann constant; and T is the absolute temperature in °K unit), where the binding energies for the L shell increase by at most 20%, whereas the occupation numbers are practically unchanged. This is an extremely high temperature for our purposes (at room temperature $k_BT\approx0.03$ eV). Therefore, there is no need for us to consider effects of this nature, nor those arising from thermal agitation of the atoms. (We have assumed implicitly that small changes in binding energies reflect somewhat comparable changes in potentials and wave functions.)

(iii) For the purposes of this review we also assume that the whole atomic system can be treated as a central field in which a given electron (to be ejected) moves. The central-field assumption is very reasonable, as long experience with its use shows. Many atomic properties (e.g., binding energies) calculated on this assumption agree very well with experimental results. We discuss in Sec. 3 the circumstances in which the use of a central potential appears justified in photoeffect; if we are satisfied with cross sections accurate to within 1%–5% the assumption is satisfactory for incident photon energies above 10 keV on targets with atomic numbers $13<Z<100$. In Sec. 3 we also give the details regarding our description of the nucleus, the electronic interactions, etc., which underlie the central field assumption, and we discuss the resulting atomic models. It is shown that, within the subclass of atomic models of self-consistent type, there is at present no one choice that is clearly superior. For illustrative purpose, we have therefore used the relatively simple relativistic Hartree–Fock–Slater (HFS) potential, and assume that both bound and continuum states see the same potential.

(iv) We describe electrons with solutions of the Dirac equation; in Sec. 6 the rather limited situations are noted in which a Schrödinger description would suffice. We do not restrict ourselves to a perturbation expansion for the final continuum states (Born approximation) in the strength of the potential $a=Z\alpha$, because even at high energies such an approach is valid only for light elements. In the upper part of Fig. 1, we symbolically represent an electron by a double line, indicating that, whether bound or continuum, it is in the presence of the atomic field, considered as a central potential. We do not use the series decomposition for the continuum state into free-electron states and propagators (shown in the lower part of Fig. 1), which yield the usual Feynman diagrams. We apply perturbation theory only to the basic quantum-electrodynamic interaction of photons with electrons: We assume that the total Hamiltonian H consists of contributions from the electrons in the presence of the atomic field $H_{\rm el}$ ($H_{\rm el}$ includes the atomic field as well as the free electron Hamiltonian), from the radiation field of photons $H_{\rm rad}$, and from the interaction of electrons with the electromagnetic field, $H_{\rm int}$. Hence, we have $H=H_{\rm el}+H_{\rm rad}+H_{\rm int}$. In this review we consider only the first-order term in $H_{\rm int}$, i.e., we consider only the diagram corresponding to the absorption of one photon by one electron, as shown in the top of Fig. 1. This corresponds to neglecting radiative corrections and higher-order quantum-electrodynamic effects.

For processes involving only continuum-state electrons, such as bremsstrahlung and pair production, radiative corrections have been discussed by Guzenko and Fomin (1960), Fomin (1959), and recently Mork and Olsen (1965, 1968). These radiative corrections are important only in the high-energy region. However, as indicated later, errors in theoretical photoelectric cross sections in the high-energy region are already larger than the effect of such radiative corrections. Radiative corrections to processes involving bound electrons are still an open question. Lamb-shift results give no indication that such effects are unusually large. (See for example, Desiderio and Johnson, 1971.) Other higher-order quantum electrodynamic effects, such as diagrams corresponding to the atom being excited, also involve higher-order terms in $H_{\rm int}$. These are normally small corrections, since the electromagnetic interaction is comparatively weak.

2.2 General Formulation for the Absorption of a Photon by an Electron in a Central Potential

2.2a Formulation of Matrix Element and Cross Section

With the basic assumptions indicated in the preceding section, our formalism corresponds to Furry's extension

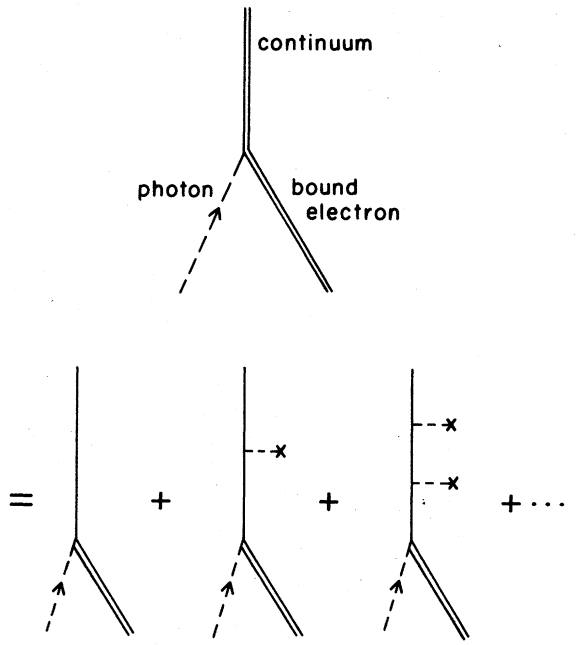

FIG. 1. Furry diagram (upper) and Feynman diagrams (lower) for atomic photoeffect.

(Furry, 1951) of the usual Feynman–Dyson formulation (Feynman, 1949; Dyson, 1949) of quantum electrodynamics, which includes the interaction of the electrons with the atomic field in the unperturbed Hamiltonian. The atomic field is considered as a central potential in this work. Symbolically, the photoeffect process is shown in Fig. 1.

The electrons in the atomic field and the photons are described by operators $\Psi(x)$ and $A^{\rm rad}(x)$, respectively, which satisfy the equations

$$[i(\gamma_\mu\nabla^\mu)-e(\gamma_\mu A^\mu)^{\rm Coul}-1]\Psi(x)=0 \quad (2.2.1)$$

and

$$\Box A^{\rm rad}(x)=0. \quad (2.2.2)$$

Here $A^{\rm Coul}$ is the vector potential describing the atomic field

$$\gamma_\mu\nabla^\mu=\gamma_0(\partial/\partial t)+\boldsymbol{\gamma}\cdot\boldsymbol{\nabla},$$
$$\gamma_\mu A^\mu=\gamma_0 A_0-\boldsymbol{\gamma}\cdot\mathbf{A},$$
$$\Box=(\partial/\partial x_\mu)(\partial/\partial x^\mu),$$

γ^μ are the Dirac matrices satisfying the anticommutation relations $\gamma_\mu\gamma_\nu+\gamma_\nu\gamma_\mu=2g_{\mu\nu}$; and the metric tensor $g_{\mu\nu}=0$ except $g_{00}=1$, $g_{11}=g_{22}=g_{33}=-1$. (The central-potential approximation plus the assumption that we are in the laboratory frame corresponding to an infinite-mass nucleus, implies that only $A_0^{\rm Coul}\neq 0$.) The solution of Eqs. (2.2.1) and (2.2.2) is written (see for example, Källen, 1958, 1962; Schweber, 1961; here we deal with particle densities normalized to one per unit volume)

$$\Psi(x)=\sum_E \psi_E(\mathbf{r})\exp(-iEt)b$$

for bound electrons, and

$$\Psi(x)=\sum_E[\psi_E^{(+)}(\mathbf{r})\exp(-iEt)b+\psi_E^{(-)}(\mathbf{r})\exp(iEt)\,d^\dagger] \quad (2.2.3)$$

for free electrons;

$$A_0^{\rm rad}=0,$$
$$\mathbf{A}^{\rm rad}(x)=(2\pi/k)^{1/2}\sum_{\mathbf{k},\boldsymbol{\varepsilon}}[\exp(-ikx)\boldsymbol{\varepsilon}a(\mathbf{k},\boldsymbol{\varepsilon})+\exp(ikx)\boldsymbol{\varepsilon}^*a^\dagger(\mathbf{k},\boldsymbol{\varepsilon})].$$

Here, b and $d^\dagger$ are annihilation and creation operators for electrons and positrons, respectively; $\psi(\mathbf{r})$ indicates electron wave functions which are solutions of the Dirac equation $(-i\boldsymbol{\alpha}\cdot\boldsymbol{\nabla}+\beta+V(r)-E)\psi(\mathbf{r})=0$, where $V(r)=eA_0^{\rm Coul}$ is the central potential for the atomic electron in question. The α and β matrices are related to the γ matrices by $\boldsymbol{\alpha}=\gamma^0\boldsymbol{\gamma}$, $\beta=\gamma^0$. In the spinor representation we have

$$\boldsymbol{\alpha}=\begin{pmatrix}0 & \boldsymbol{\sigma}\\ \boldsymbol{\sigma} & 0\end{pmatrix},$$

with $\boldsymbol{\sigma}$ the familiar 2×2 Pauli matrices, and

$$\beta=\begin{pmatrix}1 & 0\\ 0 & -1\end{pmatrix}.$$

(We are using a compact notation for 4×4 matrices.) The destruction and creation operators for photons are denoted by a and $a^\dagger$. The photons are specified by four-momentum $(k,\mathbf{k})$ and four-polarization $(0,\boldsymbol{\varepsilon})$. Here the radiation gauge was chosen. We lose manifest Lorentz and gauge covariance, in order that only the two transverse degrees of freedom of the radiation field appear in the formalism. The cross section in our approximation is obtained from the matrix element of the S-matrix between the initial and final states S_{fi}:

$$\begin{aligned}S_{fi}&=\langle f\mid S\mid ki\rangle\\ &\approx\langle f\mid 1-ie\textstyle\int d^4x:\bar\Psi(x)A^{\rm rad}(x)\Psi(x):\mid ki\rangle\\ &=ie(2\pi/k)^{1/2}\textstyle\int d^4x\psi_f^\dagger\boldsymbol{\alpha}\cdot\boldsymbol{\varepsilon}\psi_i\exp(i\mathbf{k}\cdot\mathbf{r})\\ &\quad\times\exp[-i(k+1-\epsilon-E)t]\\ &=-i2\pi M_{fi}\delta(k+1-\epsilon-E).\end{aligned}$$

We have used

$$S=T\exp\{-ie\textstyle\int d^4x\bar\Psi(x)(\gamma_\mu A^\mu)^{\rm rad}(x)\Psi(x)\},$$

since the interaction Hamiltonian

$$H_{\rm int}=e\textstyle\int\bar\Psi(x)(\gamma_\mu A^\mu)^{\rm rad}(x)\Psi(x)\,d^3r,$$

(see for example, Berestetskii, Lifshitz, and Pitaevskii, 1971, p. 132 and p. 243). Here the matrix element is

$$M_{fi}=(2\pi\alpha/k)^{1/2}\textstyle\int d^3r\psi_f^\dagger\boldsymbol{\alpha}\cdot\boldsymbol{\varepsilon}\psi_i\exp(i\mathbf{k}\cdot\mathbf{r}). \quad (2.2.4)$$

In the matrix element, ψ_i is the initial bound-electron wave function, square-normalized to unity, with binding energy ϵ, i.e., $\int |\psi_i|^2 d^3r=1$; ψ_f is the final electron wave function, asymptotically normalized to a unit-amplitude plane wave of four-momentum $(E, \mathbf{p})$ and four-polarization $(0, \zeta)$ plus an incoming spherical wave. (See for example, Sommerfeld, 1939; Bethe, Maximon, and Low, 1953; Mott and Massey, 1965.) The transition probability per unit time between the initial and final states is then

$$W_{fi}=2\pi |M_{fi}|^2 \delta(k+1-\epsilon-E).$$

We can obtain the cross section by summing over the energies of the final state and dividing by the flux of incoming particles (in this case, the velocity of the photon is $c=1$ relative to the atom). As the density of final states is given by

$$\rho_f=\rho(\mathbf{p})\, dE,$$

with

$$\rho(\mathbf{p})=pE\, d\Omega/(2\pi)^3,$$

we obtain the cross section, after integrating over energies E of the outgoing electron, as

$$d\sigma=(2\pi)^{-2}pE |M_{fi}|^2 d\Omega, \qquad (2.2.5)$$

subject to energy conservation

$$k+1-\epsilon-E=0. \qquad (2.2.6)$$

This describes the transition between definite initial and final electron spin states, resulting from the absorption of a photon of definite polarization. To obtain the observed cross section, we must perform a suitable averaging over initial state, and summing over final-state, polarizations. In Sec. 2.2b we will choose a coordinate system for the calculations. We also briefly survey photon polarizations and electron polarizations (see, for example, Tolhoek, 1956, for a detailed discussion), and then in Sec. 2.2c discuss the polarization dependence of the cross section. A qualitative discussion of the matrix element is given in Sec. 2.3; this leads to an understanding of some properties of the photoelectric process, such as the nature of atomic-electron screening effects, the ratios for the cross sections of certain subshells, etc.

2.2b A Convenient Coordinate System, Photon and Electron Polarizations

One can calculate the matrix elements M_{fi} in any coordinate system in the laboratory frame, but a judicious choice simplifies the calculation. In this review, we take a coordinate system centered at the atomic nucleus with z axis $\hat{z}$ along $\mathbf{k}$, $\hat{y}$ along $\mathbf{k}\times\mathbf{p}$, and $\hat{x}$ in the $(\mathbf{k}, \mathbf{p})$ plane (the production plane) as shown in Fig. 2. This choice leads to substitution rules for the matrix element M_{fi}, to be discussed in Sec. 2.2c, which simplify our consideration of the polarization correlations.

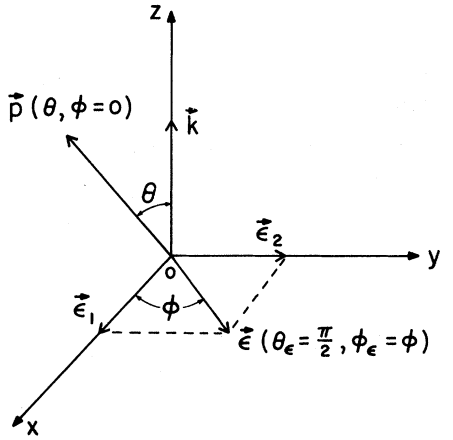

FIG. 2. A convenient coordinate system centered at the atomic nucleus with z axis z along $\mathbf{k}$, $\hat{y}$ along $\mathbf{k}\times\mathbf{p}$, and $\hat{x}$ in the $(\mathbf{k}, \mathbf{p})$ plane for atomic photoeffect.

We now consider photon polarization. The wave function of a photon with a definite momentum $\mathbf{k}$ and a definite polarization is

$$A^0=0,$$

and

$$\mathbf{A}(x)=(2\pi/k)^{1/2} \exp(-ikx)\,\boldsymbol{\varepsilon},$$

where $\boldsymbol{\varepsilon}$ is a complex unit vector describing photon polarization such that $\boldsymbol{\varepsilon}^*\cdot\boldsymbol{\varepsilon}=1$ and $\boldsymbol{\varepsilon}\cdot\mathbf{k}=0$. We describe photon polarization with Stokes parameters

$$\xi_1=\epsilon_1^*\epsilon_1-\epsilon_2^*\epsilon_2, \qquad \xi_2=\epsilon_1\epsilon_2^*+\epsilon_1^*\epsilon_2,$$
$$\xi_3=i(\epsilon_1\epsilon_2^*-\epsilon_1^*\epsilon_2), \qquad (2.2.7)$$

where $\boldsymbol{\varepsilon}=\epsilon_1\hat{x}+\epsilon_2\hat{y}$, with $|\epsilon_1|^2+|\epsilon_2|^2=1$. In order to specify the polarization completely, the three parameters $\boldsymbol{\xi}$ must be determined, e.g., by polarization measurements with respect to three linearly independent bases. For these bases we could take: (1) two states of linear polarization with perpendicular planes of polarization, (2) two other states of linear polarization making angles of $\pi/4$ with the planes of polarization in (1), (3) the two states of left and right circular polarized light.

We use the spinor representation for Dirac electron wave functions. In this representation any matrix element between four-component states can be reduced to matrix elements between two-component spinors

$$\chi=\sum_s a_s\chi^s,$$

with

$$\chi^\dagger\chi=1, \qquad \chi^{1/2}=\begin{pmatrix}1\\0\end{pmatrix}, \qquad \chi^{-1/2}=\begin{pmatrix}0\\1\end{pmatrix}.$$

The two-component spinor χ is the large component of the asymptotic constant four-component spinor corresponding to an asymptotic free particle plane wave state. The small component of the asymptotic spinor

may be written as $[\boldsymbol{\sigma}\cdot\mathbf{p}/(E+1)]\chi$. This leads to a simple way to separate out the quantities depending on polarization (see for example, Berestetskii, Lifshitz, and Pitaevskii, 1971). The polarization state of the ejected electron is specified by its spin direction $\boldsymbol{\zeta}$ in its rest system, with

$$\begin{aligned}\zeta_1&=\boldsymbol{\xi}\cdot(\mathbf{y}\times\mathbf{p})/|\,\mathbf{y}\times\mathbf{p}\,|,\\ \zeta_2&=\boldsymbol{\zeta}\cdot\hat{y},\\ \zeta_3&=\boldsymbol{\zeta}\cdot\hat{p};\end{aligned}\qquad(2.2.8)$$

here $(\zeta_1, \zeta_2, \zeta_3)$ form a right-handed set.

The spin direction $\boldsymbol{\zeta}$ is determined from χ by requiring that χ be an eigenstate of $\boldsymbol{\sigma}\cdot\boldsymbol{\zeta}$:

$$\boldsymbol{\sigma}\cdot\boldsymbol{\zeta}\chi=\chi.\qquad(2.2.9)$$

From Eq. (2.2.9) we have

$$(1-\boldsymbol{\sigma}\cdot\boldsymbol{\zeta})\chi\chi^\dagger=0.$$

For normalized χ, the solution clearly is

$$\chi\chi^\dagger=\tfrac{1}{2}(1+\boldsymbol{\sigma}\cdot\boldsymbol{\zeta}),\qquad(2.2.10)$$

permitting the determination of $\boldsymbol{\zeta}$ from χ. Alternatively, from Eq. (2.2.9) we also have $\chi^\dagger\boldsymbol{\sigma}\cdot\boldsymbol{\zeta}\chi=1$. In the rest system, $\boldsymbol{\zeta}$ is the only vector available; so that

$$\chi^\dagger\boldsymbol{\sigma}\chi=\boldsymbol{\zeta}.\qquad(2.2.11)$$

The polarization state of the bound electron is described by J_z, the z component of the total angular momentum J. However, if the bound-electron state is a $J=\frac{1}{2}$ state, then it can also be specified by a large component 2-spinor χ_i. In general, a state of complete polarization of a bound electron with total angular momentum J is described by $4J$ independent quantities, corresponding to a linear combination, with complex coefficients, of the $(2J+1)$ substates of different J_z, subject to one normalization condition and one arbitrary phase. For $J=\frac{1}{2}$, the two degrees of freedom can be taken to correspond to χ_i, but for $J>\frac{1}{2}$ there are more degrees of freedom.

2.2c Polarization Dependence of Matrix Elements and Cross Sections

In this review our main concern is with the photoeffect cross sections when initial and final polarizations are not observed. However, for completeness we give here a general discussion of all possible polarization correlations between incident photon and ejected electron, assuming that only the polarization of the bound electron is not observed. The specific formulas for these polarization correlations in partial-wave expansion are given in Sec. 5.1.

If we assume a $J=\frac{1}{2}$ bound state, then (cf. Sec. 2.2b) both the initial and final states of the electron are specified by the large component two-spinors χ_i and χ_f. The four-component wave functions ψ_i and ψ_f are linear in χ_i and χ_f, respectively. Hence, we can write the matrix element M_{fi} as

$$\begin{aligned}M_{fi}&=(2\pi\alpha/k)^{1/2}\int\psi_f^\dagger\boldsymbol{\alpha}\cdot\boldsymbol{\varepsilon}\psi_i\exp(i\mathbf{k}\cdot\mathbf{r})\,d^3r\\&=\chi_f^\dagger M(\boldsymbol{\varepsilon})\chi_i.\end{aligned}\qquad(2.2.12)$$

(Here we follow the argument of Nagel, 1960.) The 2×2 matrix $M(\boldsymbol{\varepsilon})$ is linear in $\boldsymbol{\varepsilon}$ and is some linear combination of the unit matrix and the Pauli spin matrices $\boldsymbol{\sigma}$, i.e., $M(\boldsymbol{\varepsilon})=\epsilon_1M_1+\epsilon_2M_2$, with M_1 and M_2 being linear combinations of 1 and $\boldsymbol{\sigma}$. Under the time-reversal transformation $\mathfrak{I}$ (see pp. 72–73 of Bjorken and Drell, 1964) the photoeffect matrix element M_{fi} of Eq. (2.2.4) becomes

$$\begin{aligned}\mathfrak{I}M_{fi}\mathfrak{I}^{-1}&=(2\pi\alpha/k)^{1/2}\int d^3r(T\psi_f^*)^\dagger T\boldsymbol{\alpha}^*\cdot\boldsymbol{\varepsilon}^*T^{-1}T\psi_i^*\\&\qquad\times\exp(-i\mathbf{k}\cdot\mathbf{r})\\&=M_{fi}'^*=M_{fi}^*,\end{aligned}$$

since $T=i\gamma^1\gamma^3=T^\dagger=T^{-1}=-T^*$, where the prime refers to the substitutions

$$\begin{aligned}\psi(\mathbf{r})&\to\begin{pmatrix}\sigma_y & 0\\ 0 & \sigma_y\end{pmatrix}\psi(\mathbf{r}),\\(\epsilon_1,\epsilon_2)&\to(-\epsilon_1,\epsilon_2).\end{aligned}\qquad(2.2.13a)$$

As the potential V is invariant under the time-reversal transformation, the transformed states $T\psi_f^*$ and $T\psi_i^*$ are also physical states—$T\psi_i^*$ corresponds to the bound state with the same total angular momentum J but opposite J_z, while $T\psi_f^*$ corresponds to the continuum state asymptotically with opposite space momentum $\mathbf{p}$ and opposite spin. This implies the equivalence of two matrix elements, in which the polarization properties are related by

$$\begin{aligned}\chi&\to\sigma_y\chi,\\(\epsilon_1,\epsilon_2)&\to(-\epsilon_1,+\epsilon_2).\end{aligned}\qquad(2.2.13b)$$

In terms of $\boldsymbol{\zeta}$ and $\boldsymbol{\xi}$ these become

$$\begin{aligned}(\zeta_1,\zeta_2,\zeta_3)&\to(-\zeta_1,\zeta_2,-\zeta_3)\\(\xi_1,\xi_2,\xi_3)&\to(\xi_1,-\xi_2,-\xi_3).\end{aligned}\qquad(2.2.14)$$

Thus, we have

$$\chi_f^\dagger(\epsilon_1M_1+\epsilon_2M_2)\chi_i=(\sigma_y\chi_f)^\dagger(-\epsilon_1M_1+\epsilon_2M_2)\sigma_y\chi_i,$$

or

$$\begin{aligned}M_2&=A(\theta)+iB(\theta)\boldsymbol{\sigma}\cdot\hat{y},\\M_1&=iC(\theta)\boldsymbol{\sigma}\cdot(\mathbf{y}\times\mathbf{p})/|\,\mathbf{y}\times\mathbf{p}\,|+iD(\theta)\boldsymbol{\sigma}\cdot\hat{p},\end{aligned}\qquad(2.2.15)$$

where θ is the angle between $\mathbf{k}$ and $\mathbf{p}$ and A, B, C, D are complex-valued scalar functions.

Substituting Eqs. (2.2.12) and (2.2.15) into Eq. (2.2.5) and averaging over the initial electron spin states, we find for the photoeffect cross section

$$\frac{d\sigma}{d\Omega}(\boldsymbol{\xi},\boldsymbol{\zeta})=\left(\frac{d\sigma}{d\Omega}\right)_{\text{unpol}}\{\tfrac{1}{2}\sum_{\mu,\nu=0}^{3}\xi_\mu\zeta_\nu C_{\mu\nu}(\theta)\},\qquad(2.2.16)$$

with $C_{00}\equiv1$, $\xi_0\equiv1$, and $\zeta_0\equiv1$. (Note that ξ_μ and ζ_ν are

not four-vectors.) Here $(d\sigma/d\Omega)_{\text{unpol}}$ is the differential cross section averaged over the initial photon and electron polarizations and summed over the final electron spins

$$(d\sigma/d\Omega)_{\text{unpol}}=\lambda_0 D_{00}, \quad (2.2.17)$$

with

$$\lambda_0=(2\pi)^{-2}pE, \quad (2.2.18)$$

and

$$D_{00}=\tfrac{1}{2}(|A|^2+|B|^2+|C|^2+|D|^2). \quad (2.2.19)$$

The real numbers $C_{\mu\nu}(\theta)$, satisfying $|C_{\mu\nu}|\leq 1$ since cross sections cannot be negative, are the polarization correlations between the incident photon and ejected electron. The nonvanishing polarization correlations are given $C_{00}\equiv 1$ and

$$\begin{aligned}
C_{10}&=-(2D_{00})^{-1}(|A|^2+|B|^2-|C|^2-|D|^2),\\
C_{31}&=+D_{00}^{-1}\,\text{Re}\,(AC^*-BD^*),\\
C_{33}&=+D_{00}^{-1}\,\text{Re}\,(AD^*+BC^*),\\
C_{21}&=D_{00}^{-1}\,\text{Im}\,(AC^*-BD^*),\\
C_{23}&=D_{00}^{-1}\,\text{Im}\,(AD^*+BC^*),\\
C_{02}&=D_{00}^{-1}\,\text{Im}\,(AB^*+CD^*),\\
C_{12}&=-D_{00}^{-1}\,\text{Im}\,(AB^*-CD^*). \quad (2.2.20)
\end{aligned}$$

Although Eqs. (2.2.17)–(2.2.20) were obtained assuming complete polarization of the photon, i.e., that $|\boldsymbol{\xi}|=1$, it is easy to see that they are also valid for partial polarization $|\boldsymbol{\xi}|<1$ because any statistical mixture can be obtained by incoherent superposition of two appropriately chosen pure states. That the only nonzero polarization correlations are as above follows from the application of Eqs. (2.2.14) to Eq. (2.2.16). Although the discussion here has been restricted to the case $J=\frac{1}{2}$, these conclusions regarding nonvanishing correlations are true for general J, as is Eq. (2.2.16). The specification of $C_{\mu\nu}$ in terms of amplitudes A, B, C, D depends on the assumption $J=\frac{1}{2}$. We note also that applying the time-reversal transformation to the bound wave function ψ_i is equivalent to changing the sign of M for the bound wave function, except for an arbitrary phase factor. This means that the change of the sign of the quantum number M for a given $J(\geq\frac{1}{2})$ is equivalent to the substitutions given by Eqs. (2.2.13a) or (2.2.13b). Thus, if we do not average the photoeffect cross section over initial electron spins, we have

$$C_{\mu\nu}(M)=+C_{\mu\nu}(-M)$$

for $C_{\mu\nu}=C_{00}, C_{10}, C_{31}, C_{33}, C_{21}, C_{23}, C_{02}$, and C_{12}; and

$$C_{\mu\nu}(M)=-C_{\mu\nu}(-M)$$

otherwise, where

$$J_z\psi_i=M\psi_i.$$

2.3 A Simple Model for Photoeffect and Consequences of the Dominance of Compton Wavelength Distances

The calculation of the photoeffect in first Born approximation, representing the ejected electron by a plane wave, was attempted by Hall and Oppenheimer (1931). Although this calculation gives the correct leading order of Z dependence, terms of the same order also arise from the second term in $a\equiv Z\alpha$ of the continuum wave function. The correct result in leading order of a, the Sauter formula (1931), can be obtained by iterating the plane wave; this is discussed in Sec. 6.1b. However, the simpler calculation does yield a qualitative understanding of certain features of the process.

For these qualitative purposes an even cruder nonrelativistic model suffices (Pratt, 1960a). Let us have $\boldsymbol{\alpha}\cdot\boldsymbol{\varepsilon}=\mathbf{p}\cdot\boldsymbol{\varepsilon}$, $\psi_f=\exp(i\mathbf{p}\cdot\mathbf{r})$, and approximate the s wave bound states as $\psi_i\propto\delta^{3/2}\exp(-\delta r)$, with $\delta=Z\alpha/n$, n the principal quantum number. Then the matrix element M_{fi} is characterized by the integral

$$\begin{aligned}
\delta^{3/2}\int d^3r\,\mathbf{p}\cdot\boldsymbol{\varepsilon}\exp(-i\mathbf{q}\cdot\mathbf{r}-\delta r)&\\
=8\pi\delta^{5/2}\mathbf{p}\cdot\boldsymbol{\varepsilon}/(\delta^2+q^2)^2&\\
=8\pi\delta^{5/2}p\epsilon_1\sin\theta/(\delta^2+q^2)^2, \quad (2.3.1)&
\end{aligned}$$

where $\mathbf{q}=\mathbf{k}-\mathbf{p}$ is the momentum transfer to the atom. Note that the matrix element is one order higher in δ (or a) than its integrand, essentially because energy–momentum conservation does not permit the process in the absence of the external field. It is for this reason that contributions to the lowest order matrix element can come from the order a correction to the plane-wave final state (Sauter, 1931a,b). The cross section for s state photoeffect goes as a^5, with a^3 coming from the bound-state normalization; for the same reasons the cross section for a general state of orbital angular momentum L goes as a^{5+2L}.

In addition to Z dependence, the model tells us something about angular distributions. Here $(\mathbf{p}\cdot\boldsymbol{\varepsilon})$ vanishes in the forward or backward direction, where $\mathbf{p}$ is along $\mathbf{k}$, and it peaks when $\mathbf{p}$ is perpendicular to $\mathbf{k}$. The position of the peak is shifted by the denominator $(q^2+\delta^2)^2$ if q^2 is not necessarily small compared to δ^2. This is always the case in the energy region we are discussing, so that angular distributions peak fairly sharply close to the forward direction. (The vanishing forward cross section persists in the Sauter result but is not exact; there is a nonvanishing forward component of higher order in Z which becomes important in heavy atoms.)

We can also use our simple model to estimate the important regions of configuration space for the photoeffect matrix element—this is crucial to our subsequent discussion. The integral is cut off at large distances in two different ways. The bound-state decaying exponential provides a cutoff for $r\sim 1/\delta$; the oscillating

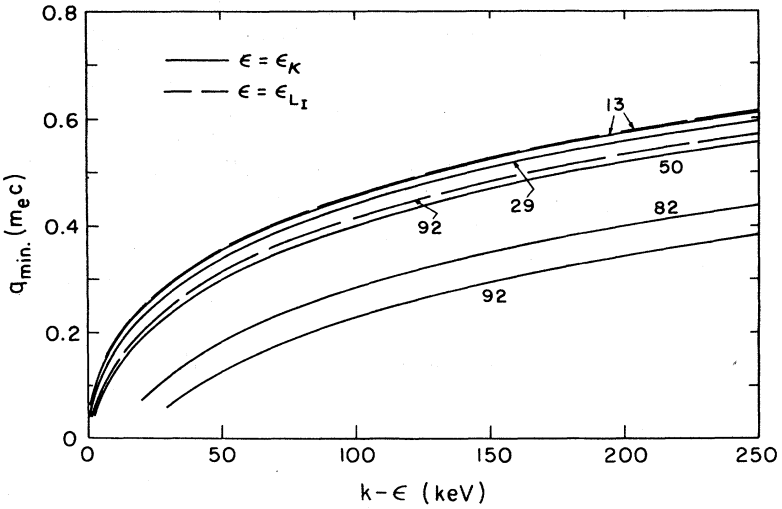

FIG. 3. Values of the minimum momentum transfer $q_{\min}$ for the K shell and the L_I subshell. The eigenvalues ϵ_K for $Z=$ 13, 29, 50, 82, and 92 are 0.0028015, 0.017122, 0.056933, 0.17469, and 0.23053 $m_e c^2$, respectively; ϵ_{L_1} for $Z=13$ and 92 are 0.0001999 and 0.04323 $m_e c^2$, respectively.

momentum transfer factor exp ($i\mathbf{q}\cdot\mathbf{r}$) provides a cutoff for $r\sim 1/q$. In the energy range we are discussing, the momentum cutoff acts first, because there is a nonzero minimum momentum transfer, $q_{\min}=p-k$ (even for forward emission), leading to a cutoff at the order of electron Compton wavelength distances, as shown in Fig. 3. *This means that the important region for the photoelectric matrix element (for energies above* 10 keV) *is large compared to nuclear sizes and small compared to atomic electron cloud dimensions.* We emphasize: the dominant contributions to photoeffect do *not* come from the regions where bound state wave functions are largest. We will discuss the consequences of this below.

A similar method has been used to predict the important regions for high-energy bremsstrahlung and pair production (Bethe and Maximon, 1954; Olsen, Maximon, and Wergeland, 1957). Bethe and Maximon found that for high energies the bremsstrahlung or pair production cross section is only significant for $q\sim 1$ and $q\sim(1/E)$. From this Olsen, Maximon, and Wergeland concluded that the important regions for these two processes are: (1) $\rho\sim E$, $|z|\sim E$, and (2) $\rho\sim 1$, $|z|\sim E$ in the cylindrical coordinates ρ, z, ϕ with z axis along $\mathbf{k}$.

Our model does not suffice to establish the energy dependence of total cross sections. These are known to decrease monotonically, falling steeply close to threshold and decreasing as $1/k$ in the high-energy limit.

The behavior of screened electron wave functions near but outside the atomic nucleus has been discussed by Pratt and Tseng (1972) and is summarized in Sec. 4. It was shown that point-Coulomb shapes persist to quite large distances ($r\approx 5\lambda\!\!\!^{-}_e$) for bound states and also for continuum states. The screening effects on continuum-state normalizations cancel the screening effects on the kinematic factor pE in the photoeffect cross sections. *Thus, at distances important for the photoeffect, the only effect of screening is a change in bound-state normalizations.* We examine the validity of this prediction in Sec. 6. A consequence of this normalization screening theory is that *shapes of angular distributions and polarization correlations are independent of screening.* Previously atomic screening was taken into account by considering cross sections as a function of Z and replacing Z by $Z_{\text{effective}}$, chosen to reproduce observed binding energies. It was pointed out by Pratt (1960a) that this "effective charge" method fits the atomic wave functions over the regions which give the main contributions to their normalization integral, but at least for energies well above threshold these are not the regions important for the photoeffect matrix element.

These ideas can also be used to predict model- and energy-independent ratios of cross sections from states having the same angular momentum. This follows (Pratt, 1960b) because in a given atom the bound-state wave functions of the same angular momentum but different principal quantum number n are proportional to each other in the important region $r\sim 1$, and for the point-Coulomb model the proportionality is nearly independent of Z. Hence, angular distributions and polarization correlations from such states are the same.

3. THE ATOMIC MODEL

3.1 Basic Atomic Model

3.1a Central-Field Approximation

A simple, solvable quantum-mechanical system is that of a hydrogen (or hydrogenlike) atom. The single electron moves in the electrostatic field of the nucleus, which is assumed to be an infinitely heavy point mass. As this is a spherically symmetric field the resulting eigenfunctions, whether in the Schrödinger or in the Dirac formulation, can be decomposed into products

of a radial function and an angular (and spin) function. Though this so-called point-Coulomb potential is the simplest possible atomic model, it turns out to be very useful both because it gives qualitative results and because through the normalization theory (see Secs. 2.3 and 4.5) such results can easily be converted into more exact predictions. For a many-electron atom, there are additional interactions among all pairs of electrons, $\sum_{i<j}(e^2/r_{ij})$. This problem can be handled in the central-field approximation, which assumes that each electron moves in a potential representing the attraction of the nucleus and the spherically averaged repulsive electrostatic interaction of the other electrons, represented by their charge distributions. The interaction $\sum_{i<j}(e^2/r_{ij})$ is replaced by a central-field potential $\sum_i U(r_i)$; the resulting eigenfunctions are products of single-electron wave functions which can be decomposed into radial and angular (and spin) parts. One simple such approximate potential is the basis of the well known Thomas–Fermi (TF) model. (The derivation can be found in most textbooks on quantum mechanics, especially Gombás, 1949, 1956.) Underlying the TF model is a semiclassical and nonrelativistic approach which statistically considers a gas that consists of free electrons at zero temperature, obeying the Pauli exclusion principle. The potential function derived from this approach is universal for all atoms. There is no exact analytic expression for this potential; its values have been tabulated (see Gombás, 1949; Kobayashi, Matsukuma, Nagai, and Umeda, 1955). The semiclassical approximation becomes invalid for very small and very large radii: for small r the charge density diverges as $(1/r)^{3/2}$ instead of being finite, and for very large r it decreases as r^{-6} instead of exponentially (Messiah, 1962, Vol. II, p. 618). The TF model describes the electrostatic potential that an infinitesimal test charge sees in a given atom. It therefore includes the redundant interaction of an electron, whose wave function we are calculating, with itself. We mention two of the variants of the TF model, aimed at correcting some of its shortcomings, which have been used in some photoeffect calculations. The first is Shalitin's FAM model, a modification of the Fermi–Amaldi model (Shalitin, 1965), which explicitly corrects for the self-energy of the electron. The second (which we denote by TFC) is Csavinsky's analytic expression for a TF model corrected for its failure to decrease exponentially at large distances (Csavinsky, 1968). Though this class of statistical models is not the best at our disposal, such models are nevertheless useful for illustrating certain features of the photoelectric process.

3.1b Self-Consistent-Field Method

The self-consistent field (SCF) method for calculating atomic orbitals suggested by Hartree (1928) is based on an iterative procedure for the numerical solution of a class of integrodifferential equations known generally as the Hartree–Fock (HF) equations. One begins with a set of trial wave functions and calculates potentials which in turn yield a new set of functions. The new wave functions serve to start a new computation. This iterative process is continued until, for example, the values of the wave function or the eigenvalue obtained agree to within a specified accuracy (typically with relative errors about 3×10^{-5} or 10^{-6}) with those of the former stage, and thus self-consistency is achieved. We now outline the derivation of the HF equation (of which Hartree's equation is a special case) which presently appears to yield the optimal description of an atom as a potential. An excellent detailed discussion is given by Slater (1960).

Before proceeding with this derivation a comment on units is in order. As is customary in calculations of atomic wave functions, atomic units are used throughout Sec. 3 unless otherwise specified. In atomic units we have, $\hbar=m_e=|e|=1$; the unit of length is the Bohr radius ($a_e=\hbar^2/m_e e^2\approx0.529$ Å); and the unit of energy is $2R_y$ (where R_y is the ionization potential of the hydrogen atom, $R_y=m_e e^4/2\hbar^2\approx13.605826$ eV).

The total energy of the atomic system in a state ϕ is $\langle\phi|H|\phi\rangle$, where the Hamiltonian H, in the nonrelativistic Schrödinger form, is

$$H=-\tfrac{1}{2}\sum_i\nabla_i^2-\sum_i(Z/r_i)+\sum_{i<j}(r_{ij})^{-1}, \quad (3.1.1)$$

and the summation extends over all electrons of the atom. We approximate ϕ by a Slater determinant constructed from single particle functions u_i. We look for functions that minimize the energy of the system, subject to orthonormalization conditions, and obtain the following set of equations:

$$\begin{aligned}-\tfrac{1}{2}\nabla_1^2u_i(r_1)-(Z/r_1)u_i(r_1)&\\+(\sum_j\int u_j^*(r_2)(r_{12})^{-1}u_j(r_2)\,d^3r_2)u_i(r_1)&\\-\sum_j\delta(m_{si}m_{sj})(\int u_j^*(r_2)(r_{12})^{-1}u_i(r_2)\,d^3r_2)u_j(r_i)&\\=-\sum_j\lambda_{ij}\delta(m_{si}m_{sj})u_j(r_1).&\quad(3.1.2)\end{aligned}$$

In some cases (e.g., for closed shells, see discussion below and in Sec. 3.2) there exists a unitary transformation which diagonalizes the matrix λ_{ij}. The only change then in Eq. (3.1.2) is that the right-hand side becomes $-\lambda_{ii}u_i(r_1)$, which we call $-\epsilon_iu_i(r_1)$. We will refer to this form as the modified Eq. (3.1.2). The terms of the modified Eq. (3.1.2) have a simple physical interpretation. The first term on the left-hand side of Eq. (3.1.2) is the kinetic energy part; the second term gives the potential energy due to the nucleus; the third term (known also as the direct interaction) represents the repulsive Coulomb interaction between *all* possible parts of electrons (the charge density of each electron being proportional to $u_i^*u_i$); the last term represents the exchange interaction. We would expect the ϵ_i on the right-hand side of the modified

Eq. (3.1.2) to be the single-particle binding energy. Indeed, Koopmans (1933) showed the ϵ_i is the energy required to remove the ith electron from the atom, provided that the orbitals of the remaining ion are the same as those of the neutral atom (this "frozen orbitals" assumption will be discussed in Sec. 3.2c). For $i=j$ in Eq. (3.1.2) the exchange term cancels the appropriate direct term and corrects the equation for the fact that an electron *does not* exert a repulsive interaction on itself. The problem of self-energy (mentioned in Sec. 3.1a) is automatically dealt with in the HF formulation. Omitting the exchange (fourth) term and the self-energy term from the left-hand side of Eq. (3.1.2) leads to Hartree's formulation of the self-consistent-field method.

Always assuming central-field-type solutions

$$u_{nlm}=[G_{nl}(r)/r]Y_{lm}(\theta,\phi),$$

we can carry out the implicit angular integrations of Eq. (3.1.2) and find the second-order integrodifferential HF (nonrelativistic) equation for the radial wave function,

$$\left(-\frac{1}{2}\frac{d^2}{dr_1^2}-\frac{Z}{r_1}+\frac{l_i(l_i+1)}{2r_1^2}+\sum_{nj lj}(4l_j+2)r_1^{-1}v_0(n_jl_j,n_jl_j;r_1)\right)G_{n_il_i}(r_1)-\sum_{nj lj}\left(\frac{2l_j+1}{2l_i+1}\right)^{1/2}\sum_k c^k(l_i0;l_j0)$$
$$\times r_1^{-1}v_k(n_il_i,n_jl_j;r_1)G_{nj lj}(r_1)=-\lambda_{ii}G_{n_il_i}(r_1)-\sum_{s\neq i,l_s=l_i}(4l_s+2)\lambda_{is}G_{n_sl_s}(r_1). \quad (3.1.3)$$

The summation $\sum_{nj lj}$ extends over all shells in the atom, each being characterized by n_j and l_j;

$$v_k(n_jl_j,n_il_i;r_1)=\frac{1}{r_1^k}\int_0^{r_1}G_{n_jl_j}(r_2)G_{n_il_i}(r_2)r_2^k\,dr_2+r_1^{k+1}\int_{r_1}^{\infty}G_{n_jl_j}(r_2)G_{n_il_i}(r_2)r_2^{-k-1}\,dr_2;$$

and the c^k are angular integrals over products of three spherical harmonics tabulated by Condon and Shortley (1935) and Slater (1960).

The full exchange term is nonlocal and so difficult (though possible) to handle, even numerically. Making a statistical approximation to this term, based upon the properties of a free-electron gas, Slater (1951) replaced it by the expression

$$V_{ex}=-r^{-1}[81rn(r)/32\pi^2]^{1/3}, \quad (3.1.4)$$

where the radial charge density

$$n(r)=4\pi r^2\sum_j u_j^*(r)u_j(r)=\sum_j G_j^2(r).$$

Thus, Slater achieved an equation of the central-field type with the advantage that all electrons see the same potential. We denote this type of potential as the (nonrelativistic) Hartree–Fock–Slater (HFS) potential. To derive this expression, Slater rewrote the exchange term in Eq. (3.1.2) as

$$-\int\sum_j\delta(m_{si}m_{sj})$$
$$\times\frac{u_i^*(r_1)u_j^*(r_2)\,(r_{12})^{-1}u_j(r_1)u_1(r_2)\,d^3r_2}{u_i^*(r_1)u_i(r_1)}u_i(r_1). \quad (3.1.5)$$

This term will correct the direct term in Eq. (3.1.2) for the interaction of the particle with itself, provided that u_i is one of the occupied orbitals (the case with which we will deal). We can regard this term as representing the potential energy at position r_1 of the electron in question, due to a charge distribution at position r_2 of magnitude

$$-\sum_j\delta(m_{si}m_{sj})\frac{u_i^*(r_1)u_j^*(r_2)u_j(r_1)u_i(r_2)}{u_i^*(r_1)u_i(r_1)}. \quad (3.1.6)$$

By integrating Eq. (3.1.6) over d^3r_2 and using the orthogonality relations of the u_i and u_j, we find that only the term $j=i$ contributes, and when integrated gives one electronic charge. Therefore, the charge distribution of electrons of the same spin adds up to one less than the total number of electrons of this spin. The net charge density of electrons of this spin, corrected for the exchange charge, goes to zero at r_1, where our electron is located, because for $r_1=r_2$ the exchange charge density just cancels the total density of all electrons of this spin [see Eq. (3.1.6) for $r_1=r_2$, and the direct term of Eq. (3.1.2)]. It is as if the electron whose wave function we were finding carried with it a hole, centered on its position r_1, such that an electronic charge of that amount (one unit) is removed from the immediate neighborhood of its position. If ρ is the density of this charge, which is equal to the total density of electronic charge of the same spin at the given point, and R is the radius of the hole, we find $(4\pi/3)R^3\rho=1$; therefore $R\propto\rho^{-1/3}$. As the potential energy at the center of a uniformly charged sphere is proportional to $R^{-1}\propto\rho^{1/3}$, one obtains the form for V_{ex} in Eq. (3.1.5). (For more details see Slater, 1968.) Slater notes that this approximation is particularly inaccurate for very small and very large radii, therefore affecting K shell and outer-shell electron wave functions calculated in such a potential.

So far, we have described the nonrelativistic case. The same steps are followed to achieve a relativistic

treatment. This relativistic HF treatment has been described by Swirles (1935) and developed by Grant (1961) and others. (An excellent review and a complete list of references are given by Grant, 1970.) One begins with the Dirac relativistic Hamiltonian which, in atomic units, has the form

$$\sum_s [-ic\boldsymbol{\alpha}_s\cdot\boldsymbol{\nabla}_s+\beta_s c^2-(Z/r_s)]+\sum_{s<t} r_{st}^{-1}, \quad (3.1.7)$$

where $\boldsymbol{\alpha}$ and β are the Dirac matrices.

The state ϕ is constructed from a determinant of single-particle wave functions of the relativistic central-field-type

$$\psi_{KM}(\mathbf{r})=\begin{pmatrix}[G_K(r)/r]\Omega_{KM}(\hat{r})\\ [iF_K(r)/r]\Omega_{-KM}(\hat{r})\end{pmatrix}, \quad (3.1.8)$$

where the quantum number K and the function $\Omega_{KM}(\hat{r})$ are as defined in Sec. 4.2b. The next step is to minimize the expectation value of this Hamiltonian, with respect to these functions, subject to the orthonormalization conditions; this leads to the relativistic HF equations (HF). Again for closed shells, one can diagonalize the matrix λ, prove Koopmans' theorem, and carry through Slater's approximation to the exchange term (HFS). A detailed description and formulas are given by Grant (1961, 1970) and Coulthard (1967). The recommended theoretical photoeffect cross sections of Sec. 6 are based on relativistic HFS potentials obtained with a computer program provided by Dr. D. Liberman [Liberman, Cromer, and Waber (1971)].

3.2 Validity of the Basic Atomic Model

3.2a. Exchange and Correlation Effects

We have described the HFS potential used for tabulations presented in this review. We now discuss alternatives to the HFS approximation which lead to a more accurate treatment of the consequences of the Hamiltonian Eq. (3.1.7). We will also subsequently discuss modifications of the Hamiltonian.

Our first remark concerns the spherical symmetry problem. Generally, except in the case of closed shells, the solutions of the HF equation (whether in the nonrelativistic or the relativistic form) *do not* yield central-field-type (or spherically symmetric) eigenfunctions, due to the nonlocal exchange term. Obviously, by omitting the exchange term and the self-energy term (and getting the Hartree equation) or by approximating it by any spherically-symmetric expression (as in the HFS case), one regains central-field-type wave functions. In Hartree's case one does not impose the antisymmetrization of the wave function ϕ required for identical particles (electrons), and ϕ is a product of single-particle functions. In the HF case, antisymmetry is imposed, and for closed shells ϕ is a single Slater determinant, whereas in the general case it is a linear combination of such determinants. In the energy range of concern in this work, the dominant contributions come from inner shells which are filled; for the inner shells, the deviations from central-field-type wave functions, due to only partially filled outer shells, are small. In the restricted HF formulation one simply assumes that the functions have the central-field form. The variation is then carried out with respect to the radial function (and not to the complete wave function). Thus, spherical symmetry is imposed. The fact that such approximations are usually not serious, combined with the difficulties of handling the general HF scheme, account for the lack of strict HF computations.

Now let us mention some modifications of the HFS potential which were examined in the course of our investigation. Gáspár (1954) and Kohn and Sham (1965) obtained an expression for the effective exchange term which is 2/3 of Slater's value. We denote this HFS2/3. In this derivation, the statistical approximation for the exchange term is made before performing the variational calculation, rather than afterwards as done by Slater. Physically, this means that the value is taken at the Fermi surface, rather than the average as in Slater's derivation. The argument supporting this procedure is that density adjustments come about by redistribution of the electrons near the Fermi surface. More recently, Rosen and Lindgren (1968) have approached this problem in a semiempirical fashion. They write the approximation to the exchange term in the form

$$V_{ex}=-(C/r)[81r^n n(r)^m/32\pi^2]^{1/3}.$$

Here C, m, and n are adjustable parameters. Slater's approximation corresponds to the choice $C=m=n=1$; the HFS2/3 case corresponds to the choice $C=\frac{2}{3}$ and $m=n=1$. Rosen and Lindgren have recommended choices of C, n, m as functions of Z. We have denoted by RL, photoeffect cross sections which we calculated using their recommended potential parameters.

The HFS-type potentials do not behave asymptotically as $-(e^2/r)$ as they should. When the potential is artificially corrected to behave properly this is usually referred to as the Latter modification or tail correction. Liberman (1970) suggested an additional correction term in the variational equation to account for this deficiency. Thus, the correct asymptotic behavior of the wave function is achieved and so are the required ionic potential forms suitable for photoelectric calculations. Whenever we refer to an ionic potential we mean this type. Comparisons of photoelectric cross sections calculated by using these alternative potentials are made in Sec. 6, but no strong case can be made for any particular choice.

The full HF procedures yield a proper treatment of exchange. However, it is generally believed that, when a full treatment of exchange effects is needed, so is a treatment of electron correlations not contained in the

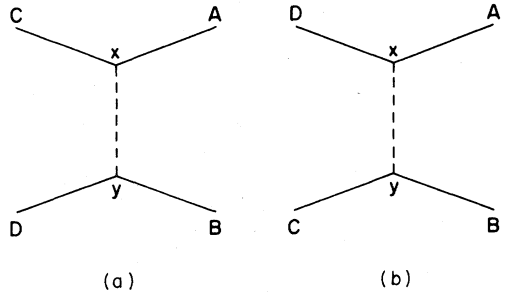

FIG. 4. Diagrams of the second-order scattering matrix $S^{(2)}$ as given by Eq. (3.2.1).

HF procedure. The electron correlations represent the difference between quantities calculated by means of the exact solutions of Eqs. (3.1.1) or (3.1.7), corresponding to the nonrelativistic or relativistic case, and the respective HF equations. The neglect of these correlations is inherent in the single-particle model which assumes that the electrons move independently of each other, even though the HF model does take into account some correlation between electrons having the same spin via their exchange interaction. It is well established by now that correlation effects play an important role in affecting photoionization cross sections at low energies close to absorption edges. Intricate methods (e.g., intrachannel effects, close-coupling, and many-body perturbations) have been suggested and applied to calculate detailed structures for such cases (e.g., Chang and McDowell, 1968; Conneely, Smith and Lipsky, 1970; Kelly, 1969; Manson and Cooper, 1968; Starace, 1970, and references therein). We do not attempt to review this subject or give a complete list of references for two reasons: (1) These calculations are still in their early stages and are not yet ready for further review (the latest review of this problem is that of Fano and Cooper, 1968); (2) These calculations deal with energies which are usually below our range of interest. Some calculations in fact were performed for higher energies (up to 30 keV) with these methods (e.g., Manson and Cooper, 1968; Kelly and Ron, 1972). In these calculations relativistic effects were neglected and the dipole approximation was used; the main purpose was to test the methods and numerical procedures. Comparison of results for aluminum and iron from these methods with the FAM results of Rakavy and Ron (1967) shows differences of 3%–6% in the 5–30-keV energy range. As noted by Kelly and Ron (1972), preliminary calculations showed that in the keV range, when the inner-shell contributions to the cross section were dominant, the correlation correction was small. This can be understood by noticing that in a perturbation treatment the relative contribution of the correlation correction, for a given matrix element, decreases roughly as $1/k$. Similarly, Rosen and Lindgren (1968) found that correlation effects are important for the higher shells but not for the inner shells. This suggests, therefore, that correlation effects tend to be small at higher energies and that we are justified in disregarding them in this review.

3.2b Magnetic and Retardation Interactions

These problems involve investigation of the complete interaction between two charges (electrons in our case) which do not lead to emission or absorption of (real) photons. The subject has primarily been investigated in the context of obtaining corrections to binding energies. The lowest nonzero order of perturbation for such a process is the second order of the scattering matrix:

$$S^{(2)}=-\tfrac{1}{2}e^2\int T[j^\mu(x)j^\nu(y)]T[A_\mu(x)A_\nu(y)]\,d^4x\,d^4y, \tag{3.2.1}$$

where T is the time-ordering operator, j_μ is the μ component of the current operator ($j_\mu=:\bar{\psi}\gamma_\mu\psi:$), and A_ν is the ν component of the radiation field vector potential. Diagramatically, the scattering matrix $S^{(2)}$ is shown in Fig. 4. [Figure 4(b) is the exchange term corresponding to Fig. 4(a).] The evaluation of $S^{(2)}$ is straightforward, and a detailed description is given in Akhiezer and Berestetskii (1965), Secs. 37, 38. Writing the time dependence as

$$\psi_A(x)=\psi_A(\mathbf{r}_1)\ \exp\ (-i\omega_A t_1),$$

where $\psi_A(x)$ is the solution of the Dirac equation and similarly for B, C, D, switching over to the transition matrix [which in our case reads $S=-2\pi iU\delta(\omega_A+\omega_B-\omega_C-\omega_D)$], and using $\omega_{AC}=\omega_A-\omega_C$, etc. one finds

$$U_{AB:CD}=\int\psi_C^*(\mathbf{r}_1)\psi_D^*(\mathbf{r}_2)[(1-\boldsymbol{\alpha}_1\cdot\boldsymbol{\alpha}_2)/|\,\mathbf{r}_1-\mathbf{r}_2\,|]$$
$$\times\exp\,(i\,|\,\omega_{AC}\,|\,|\,\mathbf{r}_1-\mathbf{r}_2\,|/c)\psi_A(\mathbf{r}_1)\psi_B(\mathbf{r}_2)\,d\mathbf{r}_1\,d\mathbf{r}_2, \tag{3.2.2}$$

where $\boldsymbol{\alpha}_1$ operates on $\psi_A(\mathbf{r}_1)$, while $\boldsymbol{\alpha}_2$ operates on $\psi_B(\mathbf{r}_2)$.

The presence of the retardation factor

$$\exp\,(i\,|\,\omega_{AC}\,|\,|\,\mathbf{r}_1-\mathbf{r}_2\,|/c)$$

prevents the introduction of a general operator for the interaction between two electrons, because Eq. (3.2.2) depends explicitly on the initial and final energies of the system. Expanding the retardation factor in powers of v/c (using $\omega=\omega_{AC}=\omega_{DB}$) we find, for an expansion up to and including v^2/c^2,

$$\frac{\exp\,(i\omega r/c)}{r}=r^{-1}+i\frac{\omega}{c}-\frac{\omega^2}{2c^2}r. \tag{3.2.3}$$

We refer the reader to Akhiezer and Berestetskii (1965) for the demonstration that $U_{AB;CD}$ is a matrix element of the operator

$$U=(r_{12})^{-1}-\tfrac{1}{2}[\boldsymbol{\alpha}_1\cdot\boldsymbol{\alpha}_2+(\boldsymbol{\alpha}_1\cdot\hat{r}_{12})(\boldsymbol{\alpha}_2\cdot\hat{r}_{12})/r_{12}]$$
$$\equiv(r_{12})^{-1}+B(1,2). \tag{3.2.4}$$

Here we have $r_{12}=|\mathbf{r}_1-\mathbf{r}_2|$ and $\hat{r}$ is the unit vector in the $\mathbf{r}$ direction, and $B(1, 2)$ is the so-called Breit operator (Breit, 1929, 1930, 1932). The leading term in the expansion is the Coulomb interaction, and the Breit correction is of order v^2/c^2 relative to the Coulomb term (as the matrix elements of $\boldsymbol{\alpha}$ are v/c). The expansion is valid when $v/c\ll 1$, which implies a light atom. For heavy atoms some use Eq. (3.2.2), which depends on the initial and final states.

An alternative way of deriving the same result is given by Bethe and Salpeter (1957), starting from the semirelativistic Dirac equation for two electrons,

$$[E-H(1)-H(2)-(r_{12})^{-1}]\psi=0, \qquad (3.2.5)$$

with

$$H(i)=\boldsymbol{\alpha}_i(c\mathbf{P}_i+\mathbf{A}(\mathbf{r}_i))+\beta_i c^2-A_0(\mathbf{r}_i),$$
$$\psi=\psi_1(\mathbf{r}_1)\psi_2(\mathbf{r}_2),$$
$$E=E_1+E_2,$$
$$(E_i-H(i))\psi_i(\mathbf{r}_i)=0, \qquad i=1, 2.$$

The calculation of the energy E, due to the exchange of a virtual photon between the two electrons, is carried out in the framework of ordinary perturbation theory. In the denominator there appears the quantity $k+E_n-E_0$, where k is the photon energy, E_n is the energy of an intermediate state, and E_0 is the given energy of the initial state. When one neglects E_n-E_0 with respect to k (which amounts to saying that $Z\alpha\ll 1$), one finds that ΔE is just the expectation value of the Breit operator over the initial state wave function. However, one obtains erroneous results by either trying to solve exactly the equation

$$[E-H(1)-H(2)-(r_{12})^{-1}]\psi=B(1, 2)\psi \qquad (3.2.6)$$

or by treating $B(1, 2)$ in perturbation calculations in orders higher than first. This stems from the fact that when both electrons in the intermediate state n are of negative energy, the quantity $k+E_n-E_0\approx -2m_e c^2$ is not small, and the result is a different operator, smaller by an order of $\hbar/m_e c r_{12}$ than the Breit operator. (For more results, the reader is referred to Bethe and Salpeter, 1957). Thus, one should use the Hamiltonian (3.1.7) with magnetic and retardation effects treated as a perturbation instead of including the Breit operator in the unperturbed Hamiltonian.

Desiderio and Johnson (1970) and Mann and Johnson (1971) (who give a detailed discussion of this problem) carried out a calculation including quantum electrodynamic corrections to binding energies of K electrons in heavy atoms ($Z=74$–90). They find that the contribution of the Breit interaction is less than 0.4%. These results suggest that, in view of our claimed accuracy, we are justified in disregarding such effects. However, if such corrections to photoelectric cross sections are carried out, one should consider carefully the consistency problems discussed above.

3.2c Atomic Rearrangements

Under this heading we include various problems which arise as a result of possible changes occurring in an atom after the removal of one of its electrons. We are thus led to questions concerning the relations existing between eigenvalues (which result from theoretical calculations) and theoretical binding energies, the interpretation of experimental data, and comparisons between theoretical and experimental binding energies. [See for example, Rosen and Lindgren (1968), Manne and Åberg (1970), Köhler and Lin (1971) and especially Meldner and Perez (1971).]

So far we have neglected any possible rearrangement effects. *Both the bound and continuum states were calculated in the same potential corresponding to the extreme case of "frozen" orbitals (method A in Rosen and Lindegren,* 1968). The binding energy is given by the difference between the total energy of the atom and that of the ion having the same orbitals (thus, only one SCF calculation is needed). Intuitively, this corresponds to the case of a long relaxation time (*sudden approximation* for the ejection of the electron). Under this assumption, the HF method yields Koopmans' theorem, identifying this binding energy with the eigenvalue. The theorem is not exactly valid for approximate HF methods, where a correction term to the one-electron eigenvalue should be added in order to find the binding energy. The other extreme assumption (method B in Rosen and Lindgren, 1968) maintains that *the relaxation time is short* and readjustment occurs. In order to find the binding energy in this case, the total energy of the ion is to be calculated in a separate SCF computation. Intermediate situations could also exist. The difference in binding energies predicted in these two modes of calculation is relatively small (though observable) for the inner shells and becomes 10%–15% for the outer shells of medium and heavy atoms. It is assumed that the eigenvalues have been corrected for the nonvalidity of Koopmans' theorem, the correction being $\sim$100 eV for K shells in medium-heavy and heavy elements. Rosen and Lindgren find that binding energies calculated by method B agree better with experiment for inner shells than those of method A (in particular for light and medium elements). For the outermost electrons on the other hand, method A seems to yield better results. Meldner and Perez (1971) refute this in their more complete analysis and indicate that detailed measurements of the spectrum are needed in order to determine rearrangement times.

This problem directly enters our calculation when we wish to determine the value of the binding energy to be used in Einstein's equation, Eq. (2.2.6). In some computations (e.g., Storm and Israel, 1970) the experimental binding energy was used. There are some advantages to this procedure. The absorption edges are exactly at the proper place and no scaling is

needed when comparing theory with experiment. Also, the kinematics of the process is well dealt with and the continuum wave function is calculated with the correct kinetic energy. A possible drawback to this procedure is the destruction of model consistency. Using the experimental binding energy might be equivalent to including implicitly various corrections without consistently making them in the bound and continuum wave functions. As we show in Sec. 6, the use of either experimental binding energies or calculated eigenvalues, for a given potential, causes the cross section to differ by about the same amount that this cross section differs from one calculated with a different potential. For high energies, the difference becomes small and unimportant. Unfortunately, we are not yet in a position to decide which procedure to follow.

The problems discussed in this section, which are important not only in atomic physics but in other fields as well (e.g., nuclear physics), still remain open.

3.2d Nuclear Effects

As stated in Sec. 3.1a, we assume the atomic nucleus to be an infinite-mass point charge. This assumption eliminates effects stemming from the finite size of the nucleus. It was shown in Sec. 2.3 that the main contribution to the photoelectric matrix element is from distances $r \sim q^{-1}$, where q is the momentum transfer. Thus, we expect that the effect of the finite size of the nucleus will be significant for momentum transfers that yield small values of r. Indeed, for heavy atoms, high photon energies, and back-angle scattering, we may anticipate some effect: A 2-MeV photon ejecting an electron in the backward direction will impart a momentum transfer of $q \sim 9m_e c$ to the nucleus, yielding $r \sim 0.1\lambda\!\!\!^{-}_e$, still large compared to the uranium nuclear radius ($\approx 0.02\lambda\!\!\!^{-}_e$). But for 20 MeV, the corresponding distance is $r \sim 0.022\lambda\!\!\!^{-}_e$, and one could begin to see nuclear effects at back angles. However, the contribution of such back-angle terms to the total photoelectric cross section is negligible in all cases (see also Sec. 2.3). Nuclear magnetic moment effects, important in back-angle bremsstrahlung at higher energies (Goldemberg and Pratt, 1966) similarly are not expected to be important here.

We have also assumed that the nucleus can absorb momentum in the photoeffect reaction without absorbing energy, yielding a recoilless process. Thus, Eq. (2.2.6) is considered to be exact. The energy of a backward scattered photoelectron ejected by a 2-MeV photon from an aluminum atom, the mass of which is considered infinite, differs from the correct result by at most 0.0015%, and the error is insignificant for heavier atoms. However, the same assumptions applied to hydrogen yield an error of 0.4%. Thus, one should be careful when applying this assumption to light elements and very high energies. But in such circumstances, photoelectric cross sections become small and unimportant in comparison with other processes. A consequence of this effect is line broadening, but this is far smaller than the natural width (which is about 0.07% in gold) and even that is always neglected compared with other causes of line broadening. Tucker, Roberts, Nestor, Carlson, and Malik (1968) and Rosen and Lindegren (1968) find that finite-nuclear-size corrections to binding energies are negligible (if corrections for the invalidity of Koopmans' theorem are considered) and also corrections to wave functions are small outside the nuclear volume. The change of the binding energy of a $1s$ electron in Hg due to the finite size of the nucleus is less than 0.1%.

4. ELECTRON WAVE FUNCTIONS

4.1 Introduction

To calculate the photoeffect matrix element and cross section under the assumptions previously outlined we need electron wave functions in the central potential V. In this review we describe electrons with solutions of the Dirac equation, as for large Z, relativistic effects can be of some importance even at low energies. However, for qualitative discussions, we will often use Schrödinger wave functions, which more simply display certain features of the process. We will discuss in Sec. 6 the circumstances in which Schrödinger wave functions can be used for quantitative photoeffect calculations.

The major computational problem is that of obtaining continuum wave functions. We note three general methods for calculating such functions in a given potential:

(1) Partial-wave series: Many terms are generally required, but with present computers numerical calculations are feasible if fewer than ~100 partial waves are required.

(2) Born approximation: Based on a perturbation expansion in V, calculations are hard to handle beyond lowest order in Z and generally converge poorly, except in the lightest elements.

(3) Approximate high-energy wave functions: These are useful for special purposes and have been used to obtain the high-energy limit of the photoeffect.

Much work has been done on the point-Coulomb potential, which is sometimes a useful approximation. Nonrelativistic bound and continuum wave functions for the point-Coulomb potential may be written in closed form. For the relativistic case the bound states can be given in closed form; for continuum states the coefficients of the partial-wave series are known and there is also an approximate high-energy wave function in closed form—the Furry–Sommerfeld–Maue wave function. (See, for example, Furry, 1934; Sommerfeld and Maue, 1935). The failure to obtain a relativistic closed-form expression is connected with the fact that

the Dirac equation for an electron in the point-Coulomb potential can be separated only in spherical coordinates.

In Sec. 4.2, we briefly summarize the general formalism for electron wave functions in central potentials which fall off more rapidly than the point-Coulomb potential at large distances. For the point-Coulomb potential, a brief discussion of the analytic expressions is also given. Section 4.2 gives the partial-wave formalism for continuum electrons used in most present photoeffect calculations. The two other methods for describing continuum electrons, the Born approximation and the high-energy approximation, are discussed in Sec. 4.3. In Sec. 4.4, we examine screening effects on bound- and continuum electron wave functions and determine radius at which deviations from the point-Coulomb shape become important. We show that point-Coulomb shapes persist to quite large distances ($r \approx 5\lambda\!\!\!^{-}_e$) for bound states and continuum states (Pratt and Tseng, 1972). We consider also the small-distance behavior of bound-state electron wave functions of different shells in the point-Coulomb potential; when combined with the screening analysis this leads to a simple prediction of ratios of photoeffect differential cross sections of given orbital angular momentum L, neglecting terms of relative order of a^2 (Pratt, 1960b).

4.2 General Formalism

4.2a Nonrelativistic Bound-State and Continuum Wave Functions

The states of an electron in a central potential are described by the Schrödinger equation with Hamiltonian

$$H=-\nabla^2/2+V(r). \tag{4.2.1}$$

Since the orbital angular momentum operator $\mathbf{L}$ commutes with the Hamiltonian H, one can construct simultaneous eigenfunctions of H, $\mathbf{L}^2$, and L_z, where L_z is the z component of $\mathbf{L}$. Such solutions of the Schrödinger equation $H\psi=T\psi$, where T is the energy of the electron, are of the form

$$\psi(\mathbf{r})=R(r)\,Y_{lm}(\hat{r}), \tag{4.2.2}$$

where the spherical harmonics $Y_{lm}(\hat{r})$ are the eigenstates of L^2 and L_z, and the radial wave functions $R(r)$ satisfy the equation

$$R''+2r^{-1}R'+2(T-V)R-l(l+1)r^{-2}R=0. \tag{4.2.3}$$

If the potential $V(r)$ is finite everywhere except at the origin and $\lim_{r\to 0} r^2V(r)=0$, we can require that the wave function ψ also be finite in all space. We choose the solution of Eq. (4.2.3) which behaves as r^l near the origin. (See for example, Secs. 32 and 35 of Landau and Lifshitz, 1965). If the potential $V(r)<0$ and $\lim_{r\to\infty} V(r)=0$, it is possible to constrain the electron to move within a limited volume of space, for discrete negative values of the energy T. For such bound states, the radial wave functions are normalized by requiring

$$\int_0^\infty R^2r^2\,dr=1. \tag{4.2.4}$$

At large distances, the radial bound-state wave function R decreases exponentially as $\exp[-(-2T)^{1/2}r]$ (apart from polynomials in the point-Coulomb case). The continuum wave functions are normalized to the asymptotic forms

$$R(r)\sim(pr)^{-1}\sin(pr-l\pi/2+\delta_l) \tag{4.2.5a}$$

for screened potentials, where the momentum $p=(2T)^{1/2}$, and δ_l is the phase shift for the lth partial wave. For the point-Coulomb potential, due to its long-range character, the asymptotic form of the continuum radial wave function is

$$R(r)\sim(pr)^{-1}\sin(pr-l\pi/2+\delta_l+ap^{-1}\ln 2pr). \tag{4.2.5b}$$

The phase shift δ_l depends on the energy T and is determined uniquely by the differential equation for R, Eq. (4.2.3), and the requirement that R be regular at the origin. For only a few potential models, such as point-Coulomb or square well, can the radial wave function R and the phase δ_l be obtained in analytic form. In general, either approximation methods or numerical methods must be used.

For the point-Coulomb potential $V(r)=-Z\alpha/r\equiv -a/r$, the solutions of Eq. (4.2.3) regular at the origin are

$$R(r)=N_l r^l\exp[-(-2T)^{1/2}r]$$
$$\times{}_1F_1[l+1-a(-2T)^{-1/2},\,2l+2,\,2(-2T)^{1/2}r], \tag{4.2.6}$$

where ${}_1F_1$ is the confluent hypergeometric function, and N_l is a normalization constant. For bound states, i.e., $T\equiv-\epsilon<0$, the requirement that R not grow at large distances requires that $[L+1-a(2\epsilon)^{-1/2}]$ be either a negative integer or zero, i.e., that

$$\epsilon=a^2/2n^2, \qquad n=1,\,2,\,3,\,\cdots. \tag{4.2.7}$$

If the radial bound-state wave function R_{nL} is normalized using Eq. (4.2.4), we have

$$R_{nL}(r)=N_{nL}r^L\exp(-ar/n)$$
$$\times{}_1F_1(L+1-n,\,2L+2,\,2ar/n), \tag{4.2.8}$$

where

$$N_{nL}=[(n+L)!/2n(n-L-1)!]^{1/2}$$
$$\times(2a/n)^{L+3/2}/(2L+1)!. \tag{4.2.9}$$

For continuum states, i.e., $T>0$, we have the normalized radial wave function regular at the origin

$$R_{pl}(r)=N_{pl}r^l\exp(-ipr)$$
$$\times{}_1F_1(l+1+ia/p,\,2l+2,\,2ipr), \tag{4.2.10}$$

with

$$N_{pl}=(2p)^l \exp(a\pi/2p)\,|\,\Gamma(l+1-ia/p)\,|/(2l+1)!. \tag{4.2.11}$$

The phase in this case is

$$\delta_l=\arg\Gamma(l+1-ia/p). \tag{4.2.12}$$

Instead of the continuum state wave functions, Eq. (4.2.2), which correspond to stationary states with definite energy $T=p^2/2$, orbital angular momentum l, and projection thereof m, we often use for the continuum states another system of functions which describes states with a definite energy and a definite linear momentum $\mathbf{p}$ rather than a definite orbital angular momentum. These states can be written as superpositions of the partial wave states:

$$\begin{Bmatrix}\psi_{\rm in}(\mathbf{r})\\ \psi_{\rm out}(\mathbf{r})\end{Bmatrix}=\sum_{l=0}^{\infty}(2l+1)i^l\exp[\{\mp\}i\delta_l]R(r)P_l(\mathbf{p}\cdot\mathbf{r}/pr), \tag{4.2.13}$$

where $\psi_{\rm in}$ and $\psi_{\rm out}$ are asymptotically normalized to unit amplitude plane waves (or distorted plane waves in the point-Coulomb case) plus an incoming or outgoing spherical wave. (See, for example, Sec. 134 of Landau and Lifshitz, 1965). If we are interested in only the total photoelectric cross sections, we can use either set of continuum wave functions. (Also one can use either $\psi_{\rm in}$ or $\psi_{\rm out}$.) However, if we are also interested in angular distributions (i.e., dependence on momentum direction of the outgoing electrons), we should use Eqs. (4.2.13) for the continuum electron wave functions, and for the photoeffect case we should use $\psi_{\rm in}$ in Eqs. (4.2.13) for the final-electron wave function.

For the point-Coulomb potential, the electron wave functions ψ_i and ψ_f needed for the photoelectric matrix element are thus given by the analytic expressions

$$\psi_i=N_{nL}r^L\exp(-ar/n)\times{}_1F_1(L+1-n,2L+2,2ar/n)Y_{LM}(\hat{r}), \tag{4.2.14}$$

$$\psi_f=\sum_{l=0}^{\infty}(2l+1)i^l\exp(-i\delta_l)N_{pl}r^l\exp(-ipr)\times{}_1F_1(l+1+ia/p,2l+2,2ipr)P_l(\mathbf{p}\cdot\mathbf{r}/pr),$$
$$=\exp(\pi a/2p)\Gamma(1+ia/p)\exp(i\mathbf{p}\cdot\mathbf{r})\times{}_1F_1(-ia/p,1,-ipr-i\mathbf{p}\cdot\mathbf{r}), \tag{4.2.15}$$

where N_{nL}, N_{pl}, and δ_l are given by Eqs. (4.2.9), (4.2.11), and (4.2.12). Note that in this nonrelativistic case the partial-wave series for the continuum wave function may be summed in closed form.

4.2b Relativistic Bound-State and Continuum Wave Functions

For the relativistic electron case the angular-momentum operator $\mathbf{J}=\mathbf{L}+\mathbf{s}$, where $\mathbf{L}=\mathbf{r}\times\mathbf{p}$ is the orbital angular-momentum operator and $\mathbf{s}=\boldsymbol{\sigma}/2$ the spin operator, commutes with the Dirac Hamiltonian

$$H=-i\boldsymbol{\alpha}\cdot\nabla+\beta+V(r).$$

Here we have

$$\boldsymbol{\alpha}=\begin{pmatrix}0&\boldsymbol{\sigma}\\ \boldsymbol{\sigma}&0\end{pmatrix}\quad\text{and}\quad\beta=\begin{pmatrix}1&0\\ 0&-1\end{pmatrix}$$

in the spinor representation ($\boldsymbol{\sigma}$ stands for the familiar 2×2 Pauli matrices). Therefore, one can construct simultaneous eigenfunctions of H, $\mathbf{J}^2$, J_z, and parity. Such solutions of the Dirac equation $H\psi=E\psi$, where $E=1+T$ is the total energy of the electron, can be written as

$$\psi_{\kappa m}(\mathbf{r})=r^{-1}\begin{pmatrix}g_\kappa(r)&\Omega_{\kappa m}(\hat{r})\\ if_\kappa(r)&\Omega_{-\kappa m}(\hat{r})\end{pmatrix}, \tag{4.2.16}$$

where the symbol κ is a quantum number which combines j and parity:

$$\kappa=\mp(j+\tfrac{1}{2})\quad\text{as}\quad j=l\pm\tfrac{1}{2}\qquad(\text{or } j=l'\mp\tfrac{1}{2}). \tag{4.2.17}$$

In spectroscopic notation, l (not an eigenvalue) is used instead of parity: $\kappa=-1,+1,-2,+2,-3,\cdots$ corresponds to $s_{1/2}$ (abbreviation s), $p_{1/2}(p)$, $p_{3/2}(\bar{p})$, $d_{3/2}(d)$, $d_{5/2}(\bar{d})$, $\cdots$ states. The spherical spinor

$$\Omega_{\kappa m}(\hat{r})=\sum_{s=\pm1/2}C(l\tfrac{1}{2}j;m-s,s)Y_{l,m-s}(\hat{r})\chi^s \tag{4.2.18}$$

is an eigenstate of $\mathbf{J}^2$ and $\mathbf{L}^2$:

$$\begin{pmatrix}\mathbf{J}^2\\ J_z\\ \mathbf{L}^2\end{pmatrix}\Omega_{\kappa m}=\begin{pmatrix}j(j+1)\\ m\\ l(l+1)\end{pmatrix}\Omega_{\kappa m}. \tag{4.2.19}$$

(We see that the relativistic wave function ψ is not an eigenstate of $\mathbf{L}^2$; the l used in spectroscopic notation is the eigenstate of the large component and actually indicates the parity of ψ.) The quantity $C(j_1j_2j;m_1m_2)$ is the Clebsch–Gordan coefficient [we choose the Condon–Shortley (1935) phase convention]. The radial wave functions g and f satisfy the equations

$$dg_\kappa(r)/dr=(E+1-V(r))f_\kappa(r)-\kappa g_\kappa(r)/r,$$
$$df_\kappa(r)/dr=-(E-1-V(r))g_\kappa(r)+\kappa f_\kappa(r)/r. \tag{4.2.20}$$

(See for example, Sec. 35 of Berestetskii, Lifshitz, and Pitaevskii, 1971.) We will consider only $V(r)<0$, and $V\to-a/r$ as $r\to0$, where $a\equiv Z\alpha$. In order to interpret $|\psi|^2$ as a probability density, one chooses the solutions of the Dirac equation $H\psi=E\psi$ for which $\psi\propto r^{\gamma-1}$ near the origin, with $\gamma=(\kappa^2-a^2)^{1/2}$. If $a^2>\kappa^2$ the wave functions oscillate when $r\to0$. However, because of the finite size of the nucleus, the existence of atoms with larger values of $Z(>137)$ is possible. The problem has been investigated by Popov (1971).

We next consider normalization of the radial wave

functions. The bound-state wave functions are normalized by requiring

$$\int_0^\infty (G_K^2+F_K^2)\,dr=1, \tag{4.2.21}$$

where we replace g_κ and f_κ by G_K and F_K for bound states. The wave functions of the discrete spectrum ($E<1$) again decrease exponentially as $r\to\infty$. The continuum wave functions are normalized such that at large distances

$$g_\kappa\sim[(E+1)^{1/2}/2E]p^{-1}\sin(pr-l\pi/2+\delta_\kappa+Q(r)),$$
$$f_\kappa\sim[(E-1)^{1/2}/2E]p^{-1}\cos(pr-l\pi/2+\delta_\kappa+Q(r)). \tag{4.2.22}$$

Here $Q(r)\sim0$ for screened potentials, and $Q(r)=\nu\ln 2pr$ with $\nu=aE/p$ for the point-Coulomb potential, again due to its long-range character (see Sec. 5.2b for more detailed discussion). Now $p=(E^2-1)^{1/2}$ is the momentum of the electron; δ_κ is the phase shift for the partial wave κ. The phase shift depends on the energy E and is determined uniquely by the differential equations for g and f, Eqs. (4.2.20), and the requirement of small-distance behavior. In general, the radial wave functions g and f and the phase δ_κ cannot be obtained in analytic form. Either approximation methods or numerical methods are required. The analytic approximations will be discussed in Sec. 4.3 and the numerical methods in Sec. 5.2.

For the point-Coulomb potential, there are analytic expressions for the radial wave functions. For bound states, i.e., for $E=1-\epsilon<1$, the condition that the wave functions not grow at infinity requires that $\gamma_B-aE(1-E^2)^{-1/2}$ be either a negative integer or zero, i.e., that

$$1-\epsilon=[1+a^2(\gamma_B+n')^{-2}]^{-1/2}. \tag{4.2.23}$$

Here we have $\gamma_B=(K^2-a^2)^{1/2}$, $n'=n-|K|$, and n is the principal quantum number. If the radial wave functions G_K and F_K are normalized according to Eq. (4.2.21), then we have the normalized radial Dirac eigenfunctions (see for example, Sec. 14 of Bethe and Salpeter, 1957)

$$G_K=W(x)[-n'{}_1F_1(-n'+1, 2\gamma_B+1, x)+(N-K)\,{}_1F_1(-n', 2\gamma_B+1, x)],$$
$$F_K=-[\epsilon/(2-\epsilon)]^{1/2}W(x)[n'{}_1F_1(-n'+1, 2\gamma_B+1, x)+(N-K)\,{}_1F_1(-n', 2\gamma_B+1, x)], \tag{4.2.24}$$

with

$$W(x)=[\Gamma(2\gamma_B+1)]^{-1}\times[(2-\epsilon)\Gamma(2\gamma_B+n'+1)/4N(N-K)(n'!)]^{1/2}\times(2a/N)^{1/2}\exp(-x/2)x^{\gamma_B}, \tag{4.2.25}$$
$$x=2ar/N,$$
$$N=[n^2-2n'(|K|-\gamma_B)]^{1/2}, \tag{4.2.26}$$

and

$$1-(1-\epsilon)^2=a^2/N^2. \tag{4.2.27}$$

For continuum states, i.e., for $E=1+T>1$, the normalized radial wave functions g_κ and f_κ can be written (see for example, Perlman and Robson, 1959)

$$g=[(E+1)/2E]^{1/2}(R+R^*),$$
$$f=i[(E-1)/2E]^{1/2}(R-R^*), \tag{4.2.28}$$

with

$$R=\frac{(\gamma+i\nu)|\,\Gamma(\gamma+i\nu)|\,e^{\pi\nu/2}}{2p\Gamma(2\gamma+1)}\times e^{i\xi}(2pr)^\gamma e^{-ipr}F(\gamma+1+i\nu, 2\gamma+1, 2ipr),$$
$$\gamma=(\kappa^2-a^2)^{1/2},\qquad \nu=aE/p,$$
$$e^{i\xi}=[(\gamma-\kappa)p+ia(1-E)]/[2(E-1)(E\kappa-\gamma)(\kappa-\gamma)]^{1/2}, \tag{4.2.29}$$

and

$$\eta_\kappa=-\kappa/|\kappa|.$$

The asymptotic forms of the radial wave functions for the point-Coulomb potential are given by Eq. (4.2.22) with $Q(r)=\nu\ln 2pr$ and

$$\delta_\kappa=\xi-\arg\Gamma(\gamma+i\nu)+(l+1-\gamma)\pi/2. \tag{4.2.30}$$

We may use for the continuum states another set of functions which describes states with definite energy and definite momentum $\mathbf{p}$, just as in the nonrelativistic case, instead of the system of continuum state wave functions, Eq. (4.2.16) corresponding to stationary states with definite energy $E=(1+p^2)^{1/2}$, total angular momentum j, projection thereof m, and parity. The states with definite energy and definite momentum can be written as superpositions of partial waves,

$$\begin{Bmatrix}\psi_{\rm in}(\mathbf{r})\\ \psi_{\rm out}(\mathbf{r})\end{Bmatrix}=4\pi\sum_{\kappa m}[\Omega_{\kappa m}{}^\dagger(\hat p)\chi(\zeta)]i^l\times\exp(\{\mp\}i\delta_\kappa)\psi_{\kappa m}(\mathbf{r}), \tag{4.2.31}$$

where $\psi_{\kappa m}(r)$ is given by Eq. (4.2.16). We have

$$\chi=\sum_s a_s\chi^s\quad\text{with}\quad\chi^\dagger\chi=1,$$
$$\chi^{1/2}=\begin{pmatrix}1\\0\end{pmatrix},\qquad \chi^{-1/2}=\begin{pmatrix}0\\1\end{pmatrix}.$$

The wave functions $\psi_{\rm in}$ and $\psi_{\rm out}$ are asymptotically normalized to unit-amplitude plane waves (or distorted plane waves for the point-Coulomb case) plus an incoming or outgoing spherical wave. [See for example, p. 207 of Rose, 1961. If we choose $\mathbf{p}$ along the z axis, then Eq. (4.2.31) gives Darwin's solutions (Darwin, 1928) of the Dirac equation.] The relativistic electron

wave functions needed for photoeffect calculations are

$$\psi_i = r^{-1}\begin{pmatrix} G_K\Omega_{KM}(\hat{r}) \\ iF_K\Omega_{-KM}(\hat{r}) \end{pmatrix} \tag{4.2.32}$$

for the initial bound state and

$$\psi_f = 4\pi r^{-1}\sum_{\kappa m}[\Omega_{\kappa m}^{\dagger}(\hat{p})\chi(\zeta)]i^l \exp(-i\delta_\kappa) \times \begin{pmatrix} g_\kappa\Omega_{\kappa m}(\hat{r}) \\ if_\kappa\Omega_{-\kappa m}(\hat{r}) \end{pmatrix} \tag{4.2.33}$$

for the final continuum state, i.e., the ψ_{in} of Eqs. (4.2.31). (However, if one is interested in only the total cross section, the ψ_{out} of Eqs. (4.2.31) can also be used.) The boundary conditions are given by Eqs. (4.2.21) and (4.2.22), which say that

$$\int |\psi_i|^2 d^3r = 1, \tag{4.2.34}$$

and ψ_f is asymptotically normalized to a unit-amplitude plane wave (or distorted plane wave for the point-Coulomb case) plus an incoming spherical wave with a definite momentum $\mathbf{p}$.

4.3 Approximate Wave Functions

4.3a Relativistic Born Approximation

The Born approximation method is a series expansion of the wave function in powers of the interaction potential. Beyond lowest order, this method cannot be directly applied to the point-Coulomb potential because each term of the Born series contains infrared divergences arising from the long-range character of the point-Coulomb potential. The difficulty can be avoided by replacing the point-Coulomb potential by a screened one, for example, $V(r) = -a\exp(-\lambda r)/r$, for which the successive Born series terms are covergent. The higher order terms in a matrix element remain singular in the limit $\lambda \to 0$, but correspond only to an infinite phase factor, so that the square modulus of a matrix element remains finite in the limit. (See for example, Dalitz, 1951; Gavrila, 1959, 1961; Gorshkov, 1961; Weinberg, 1965.)

The Born approximation has been studied both in configuration space and in momentum space. We can simply Fourier transform to get one result from the other, but the momentum space form is often a more convenient starting point.

The configuration space approach is described in detail by Mott and Massey (1965). The wave function ψ is expanded in powers of a, namely, $\psi = \psi_0 + a\psi_1 + a^2\psi_2 + \cdots$, where ψ_0 represents the electron undisturbed by the field, i.e., the plane wave, and $\psi_1, \psi_2, \cdots$ consist only of incoming or outgoing waves at infinity. For an electron of energy E in the potential $V(r)$, the Dirac equation has the form

$$(E - V - \beta + i\boldsymbol{\alpha}\cdot\boldsymbol{\nabla})\psi = 0. \tag{4.3.1}$$

Multiplying Eq. (4.3.1) on the left with the operator $(E - V + \beta - i\boldsymbol{\alpha}\cdot\boldsymbol{\nabla})$ we obtain the iterated equation

$$[\nabla^2 + p^2 - 2EV + i\boldsymbol{\alpha}\cdot(\boldsymbol{\nabla}V) + V^2]\psi = 0. \tag{4.3.2}$$

Linearizing Eq. (4.3.2) in the expansion parameter a, we have (using $V(r) = -a\exp(-\lambda\mathbf{r})/r$, letting $\lambda \to 0$, and suppressing the infinite phase factor) the Born series of the wave function ψ to first order in a as (see Scheck and Stingl, 1968)

$$\psi_{\text{out}} = \{\exp(i\mathbf{p}\cdot\mathbf{r}) + a[F_1(\mathbf{r},\mathbf{p}) + \boldsymbol{\alpha}\cdot(\hat{r} - \hat{p})F_2(\mathbf{r},\mathbf{p})]\}u,$$

and

$$\psi_{\text{in}} = \{\exp[i\mathbf{p}\cdot\mathbf{r}] + a[F_1^*(\mathbf{r},-\mathbf{p}) - \boldsymbol{\alpha}\cdot(\hat{r} + \hat{p})F_2(\mathbf{r},-\mathbf{p})\}u, \tag{4.3.3}$$

with

$$F_1(\mathbf{r},\mathbf{p}) = (iE/p)\exp(i\mathbf{p}\cdot\mathbf{r})[Ei(iw) - \ln w],$$
$$F_2(\mathbf{r},\mathbf{p}) = \exp(i\mathbf{p}\cdot\mathbf{r})(e^{iw} - 1)/2w,$$
$$w \equiv pr - \mathbf{p}\cdot\mathbf{r}, \tag{4.3.4}$$

$Ei(x)$ denoting the exponential integral function (Erdélyi, Magnus, Oberhettinger, and Tricomi, 1953, and u the free-particle Dirac spinor.

Now let us consider the momentum space approach. The wave function with a definite momentum $\mathbf{p}$ in momentum space $\mathbf{q}$, $\psi_{\text{p}}(\mathbf{q})$, is defined as the Fourier transform of the wave function with a definite momentum $\mathbf{p}$ in configuration space $\mathbf{r}$, $\psi_{\text{p}}(\mathbf{r})$. That is, we have

$$\psi_{\text{p}}(\mathbf{q}) = (2\pi)^{-3}\int d^3r \exp(-i\mathbf{q}\cdot\mathbf{r})\psi_{\text{p}}(\mathbf{r}). \tag{4.3.5}$$

In configuration space the Dirac equation for an electron in the central potential $V(r)$ has the form

$$(i\gamma_\mu\nabla^\mu - \gamma_0 V(r) - 1)\psi_{\text{p}}(\mathbf{r})e^{-iEt} = 0, \tag{4.3.6}$$

with $\gamma_\mu\nabla^\mu = \gamma_0(\partial/\partial t) + \boldsymbol{\gamma}\cdot\boldsymbol{\nabla}$, $E = (1 + \mathbf{p}^2)^{1/2}$ the energy of the electron. Fourier transformation of Eq. (4.3.6) gives

$$(\gamma_\mu q^\mu - 1)\psi_{\text{p}}(\mathbf{q}) = -\int d^3q' V(\mathbf{q} - \mathbf{q}')\gamma_0\psi_{\text{p}}(\mathbf{q}'), \tag{4.3.7}$$

with

$$\gamma_\mu q^\mu = \gamma_0 q_0 - \boldsymbol{\gamma}\cdot\mathbf{q}, \qquad q_0 = E,$$

and

$$V(\mathbf{q} - \mathbf{q}') \equiv (2\pi)^{-3}\int d^3r \exp[-i(\mathbf{q} - \mathbf{q}')\cdot\mathbf{r}]V(r). \tag{4.3.8}$$

Expanding $\psi_{\text{p}}(\mathbf{q})$ in power series in a for $V(r) = -a\exp(-\lambda r)/r$, just as we did in the configuration space case, we have the wave function in momentum space to first order in a

$$\begin{Bmatrix} \psi_{\text{p}}^{\text{out}}(\mathbf{q}) \\ \psi_{\text{p}}^{\text{in}}(\mathbf{q}) \end{Bmatrix} = \left[\delta(\mathbf{q} - \mathbf{p}) + \frac{a}{2\pi^2}\frac{\gamma_\mu q^\mu + 1}{\mathbf{p}^2 - \mathbf{q}^2\{\pm\}i\eta} \times \frac{\gamma_0}{|\mathbf{q} - \mathbf{p}|^2 + \lambda^2}\right]u(\mathbf{p}). \tag{4.3.9}$$

Here $u(\mathbf{p})$ is the momentum space spinor of a free electron of momentum $\mathbf{p}$, and η is an infinitesimal positive real quantity introduced to circumvent the poles. (See for example, Sec. 9β of Bethe and Salpeter, 1957.)

4.3b Approximate High-Energy Wave Functions for Continuum States

For an electron of energy E in the potential $V(r)$ we have the iterated equation (4.3.2). Substituting $\psi=\exp(i\mathbf{p}\cdot\mathbf{r})Fu$, where u is taken as a free spinor, we have

$$[\nabla^2+2i\mathbf{p}\cdot\nabla-2EV+i\alpha\cdot(\nabla V)+V^2]Fu=0, \quad (4.3.10)$$

which is still exact. When E is large, F may be chosen as a solution of the differential equation

$$[2i\mathbf{p}\cdot\nabla+\nabla^2-2EV]F=0. \quad (4.3.11)$$

This choice leads to the Furry–Sommerfeld–Maue wave functions for $V=-a/r$,

$$\psi_{\text{in}}=\Gamma(1+i\nu)\exp(\pi\nu/2)\exp(i\mathbf{p}\cdot\mathbf{r})[1-(i/2E)\alpha\cdot\nabla]\times{}_1F_1(-i\nu;1;-ipr-i\mathbf{p}\cdot\mathbf{r})u(\mathbf{p}),$$
$$\psi_{\text{out}}=\Gamma(1-i\nu)\exp(\pi\nu/2)\exp(i\mathbf{p}\cdot\mathbf{r})\times[1-(i/2E)\alpha\cdot\nabla]{}_1F_1(i\nu;1;ipr-i\mathbf{p}\cdot\mathbf{r})u(\mathbf{p}), \quad (4.3.12)$$

where $\nu=aE/p$, and $u(\mathbf{p})$ is the spinor of a free electron with momentum $\mathbf{p}$. The Furry-Sommerfeld-Maue wave function can also be obtained by approximating $\gamma\equiv(\kappa^2-a^2)^{1/2}$ by $|\kappa|$ in the partial wave series. (See for example, Bethe and Maximon, 1954; Johnson and Deck, 1962.) The Furry–Sommerfeld–Maue wave function is thus a good approximation for all energies provided $a^2/|\kappa|\ll 1$ and screening is small.

For some high-energy problems, such as the photoeffect, an even simpler function sufficies. This is obtained by solving Eq. (4.3.11) without the factor ∇^2 (Pratt, 1960a)

$$(i\mathbf{p}\cdot\nabla-EV)F=0. \quad (4.3.13)$$

Let the z axis be along the direction of the momentum $\mathbf{p}$, then Eq. (4.3.13) becomes

$$ip\partial F/\partial z=EVF, \quad (4.3.14)$$

which leads to the modified plane wave approximation

$$F=\exp\left(\frac{-E}{p}\int_{z_0}^{z}V(\rho,z')\,dz'\right), \quad (4.3.15)$$

where z_0 can be determined from the boundary conditions. For short-range potentials the boundary conditions require that $F=1$ at $-\infty$ or $+\infty$, giving the solutions

$$\begin{pmatrix}F_{\text{out}}\\F_{\text{in}}\end{pmatrix}=\exp\left(\frac{-E}{p}\int_{\mp\infty}^{z}V(\rho,z')\,dz'\right). \quad (4.3.16)$$

F_{in} is the solution needed for the photoeffect.

For a point-Coulomb field, $V(r)=-a/r$, the integrals in Eq. (4.3.16) diverge at $\pm\infty$, corresponding to the well-known fact that for such a long-range field it is not correct to impose plane waves as a boundary condition. Instead, the incoming (outgoing) electron near $-\infty$ $(+\infty)$ should be described by the distorted plane wave

$$\exp[i\mathbf{p}\cdot\mathbf{r}\mp i\nu\ln(pr\mp\mathbf{p}\cdot\mathbf{r})], \quad (4.3.17)$$

with $\nu=aE/p$. In other words, for a point-Coulomb field the desired solutions are

$$\begin{pmatrix}F_{\text{out}}\\F_{\text{in}}\end{pmatrix}=\exp[\mp\nu\ln(pr\mp\mathbf{p}\cdot\mathbf{r})]. \quad (4.3.18)$$

Computing ∇^2F/EVF at high energies, the additional condition for the validity of these wave functions is that $pr\pm\mathbf{p}\cdot\mathbf{r}$ be large. Indeed, Eq. (4.3.18) may be obtained as the limit of the confluent hypergeometric functions of the Furry–Sommerfeld–Maue solution for $pr\pm\mathbf{p}\cdot\mathbf{r}$ large. (Prange and Pratt, 1957.) For the atomic photoeffect at high energies we need a wave function valid in the region for which both $\rho\sim 1$, $z\sim 1$ (Pratt, 1960a). The modified plane wave Eq. (4.3.18) is accurate in these regions, as well as in the region $\rho\sim E$ and $z\sim E$, one of two important regions in high-energy bremsstrahlung (Olsen, Maximon, and Wergeland, 1957).

4.4 Behavior of Electron Wave Functions at Compton Wavelength Distances

We have argued that small distances $r\sim 1$ are important for the photoeffect. Let us see what we can say about the behavior of electron wave functions at such distances. In the small r region let us describe bound and continuum wave functions, apart from normalizations, by the first few terms of a power series in r, and examine the dependence of these series on screening by a potential with a similar expansion.

Consider the Schrödinger radial equation, Eq. (4.2.3). Taking out a function r^l with $R=r^lS$ gives

$$\tfrac{1}{2}S''+(l+1)r^{-1}S'+(T-V)S=0. \quad (4.4.1)$$

For the central potential $V=-(a/r+V_0+V_R)$, with V_0 a constant and $V_R(r=0)=0$, the expansion of S in r begins

$$S=1-[a/(l+1)]r+\cdots. \quad (4.4.2)$$

The r^2 term is dependent on T and V_0 but not on V_R where we normalize S such that $S(0)=1$. Hence until the r^2 term becomes significant S is the same as in the point-Coulomb case. This also shows that for a given l the shape of the wave function is independent of n for bound states or of the energy E for continuum states. We find that

$$\psi=(N/N_c)\psi_c[1+[\langle i\,|\,V_R\,|\,i\rangle/(2l+3)]r^2+\cdots], \quad (4.4.3)$$

where N/N_c is the ratio of screened to point-Coulomb normalizations. (The definition of the normalization is

TABLE 4.1. Square of the ratio Ξ of screened to point-Coulomb bound-state normalizations for states K, $L_{\rm I}$, $L_{\rm II}$, and $L_{\rm III}$, where $\Xi \equiv \lim_{r\to 0} G^s(r)/G^c(r) = \lim_{r\to 0} F^s(r)/F^c(r)$. (Here G and F are the normalized bound-state wave functions.)

Z	Potentials	K	$L_{\rm I}$	$L_{\rm II}$	$L_{\rm III}$
	Ionic	0.9659	0.5257	0.3319	0.3306
	HFS2/3	0.9286	0.4996	0.3025	0.3012
13	HFS	0.9479	0.5260	0.3360	0.3346
	TFC	0.9065	0.4546	0.2355	0.2346
	TF	0.8823	0.4633	0.2461	0.2452
	Ionic	0.9905	0.8895	0.8370	0.7999
	HFS2/3	0.9819	0.8829	0.8251	0.7899
92	HFS	0.9868	0.8905	0.8378	0.8011
	TFC	0.9915	0.9127	0.8860	0.8508
	TF	0.9897	0.8866	0.8344	0.8019

given in Sec. 5.2.) Further terms can be obtained (Pratt and Tseng, 1972). The magnitude of deviation from point-Coulomb shape can be estimated using the exponential model $V=-ae^{-\lambda r}/r$, with $\lambda=1.13\alpha Z^{1/3}$, to be approximately $\frac{1}{4}[(3n^2-l(l+1))/(2l+1)]\alpha^2Z^{2/3}r^2$. Thus for small distances, $r\sim 1$, the shape is indeed close to point-Coulomb and screening enters only in N/N_c.

How is this analysis modified for continuum states? For the low-energy case we may use our previous analysis. The only difference is how we specify $\delta T \equiv T-T_c$, the change in kinetic energy between point-Coulomb and screened calculations. Since T is no longer calculated from the expectation value of $\delta V \equiv V-V_c$ for continuum states, one would expect $\delta T=0$. (For a bound state, δT can be calculated from the expectation value of δV with perturbation techniques: $\delta T \approx -\langle i \mid \delta V \mid i\rangle = -V_0 - \langle i \mid V_R \mid i\rangle$.) But in fact this is not the correct physical choice. For example, in atomic photoeffect with a given incident photon energy, if the bound-state energy is shifted δT_B due to screening, the ejected continuum electron will also have an energy shift $\delta T=\delta T_B$ and in fact its wave function will have a shape considerably closer to the Coulomb shape at small distances than for $\delta T=0$. A shape even closer to point-Coulomb results from the choice $\delta T=-V_0$, for the r^2 term in ψ/ψ_c then vanishes. (Numerical results show that these features persist to higher energies.)

We may summarize the lowest order results for ψ/ψ_c in these three cases for $V=-(a/r)[1+V_1\lambda r+V_2(\lambda r)^2+\cdots]$:

(1) $\delta T=0$,

$$\psi/\psi_c \approx (N/N_c)\{1-[V_0/(2l+3)]r^2\} = (N/N_c)\{1-[V_1 a\lambda/(2l+3)]r^2\}; \quad (4.4.4)$$

(2) $\delta T=\delta T_B$,

$$\psi/\psi_c \approx (N/N_c)\{1+[\langle i \mid V_R \mid i\rangle/(2l+3)]r^2\} \approx (N/N_c)\{1+[(3n^2-L(L+1))/2(2l+3)]V_2\lambda^2 r^2\}, \quad (4.4.5)$$

with l, L continuum, and bound orbital quantum numbers;

(3) $\delta T=-V_0$,

$$\psi/\psi_c \approx (N/N_c)\{1-[V_2 a\lambda^2/3(l+2)]r^3\}. \quad (4.4.6)$$

The relative orders of the deviations are as a, λ, and $a\lambda r$, respectively.

Our conclusion is that *deviations from point-Coulomb shapes remain rather small out to several Compton wavelengths because they are characterized not by ar or $(ar)^2$ but by $(\alpha^2Z^{2/3}r^2)$*. A similar analysis for the coupled radial wavefunctions of the Dirac equation verified that relativistic effects do not change the conclusion that deviations from point-Coulomb shape are small at these distances. The algebra is considerably more complicated and we shall not reproduce it here.

So far we have discussed the shape of electron wave functions. A second related question concerns the normalization of electron wave functions. Although we shall not discuss the theory of these normalization constants, for completeness we will make a few comments. For continuum wave functions at high energies the deviations of N/N_c from 1 is small. For low-κ partial waves, except at very low energies, $\tilde{N}\equiv(pE)^{1/2}N$ is equal to $\tilde{N}_c\equiv(p_cE_c)^{1/2}N_c$ for the case with energy shift, where N and N_c are the normalizations of the wave functions for screened and point-Coulomb potentials, respectively (Pratt and Tseng, 1972). At high energies even for high-κ partial waves we have $\tilde{N}=\tilde{N}_c$ with or without energy shift. The worst cases are for high κ at low energies, which are not of concern in most processes. For photoeffect, the low-κ partial waves dominate the cross section for low

TABLE 4.2. Values of $(\Xi^2)_{\rm HFS}$ for $Z=13$–92.

Z	K	$L_{\rm I}$	$L_{\rm II}$	$L_{\rm III}$
13	0.9479	0.5260	0.3360	0.3346
20	0.9615	0.6509	0.4928	0.4899
26	0.9686	0.7133	0.5790	0.5745
29	0.9713	0.7354	0.6112	0.6058
42	0.9784	0.7968	0.7016	0.6915
47	0.9801	0.8128	0.7254	0.7134
50	0.9810	0.8211	0.7377	0.7244
60	0.9832	0.8443	0.7717	0.7540
74	0.9853	0.8689	0.8072	0.7824
79	0.9859	0.8757	0.8170	0.7892
82	0.9861	0.8794	0.8223	0.7927
92	0.9868	0.8905	0.8378	0.8011

photon energies. Therefore, we may conclude that for photoeffect $\tilde{N}$ is equal to $\tilde{N}_c$. This is important since in photoeffect and other similar processes the matrix element is multiplied by $(pE)^{1/2}$ for each continuum electron. Consequently, except at very low energies screening effects on continuum wave functions may be neglected.

For bound states, we present values of the square of the ratio of screened (s) to point-Coulomb (c) bound-state normalization for states K, $L_{\rm I}$, $L_{\rm II}$, and $L_{\rm III}$ in Table 4.1 in five different potentials, i.e., the ionic HFS2/3 (ionic), the Kohn–Sham (HFS2/3), the Hartree–Fock–Slater (HFS), the modified Thomas–Fermi (TFC), and the Thomas–Fermi (TF) potential models. This shows that for low Z the choice of the model is quite important. For high Z the difference is less than 1% for the K shell, less than 3.5% for the $L_{\rm I}$ shell, and less than 8% for the $L_{\rm II}$, and $L_{\rm III}$ shells. Finally we tabulate values of the square of the ratio Ξ of the HFS to point-Coulomb bound-state normalizations for K, $L_{\rm I}$, $L_{\rm II}$, and $L_{\rm III}$ shells in Table 4.2 for elements $Z=13$–92. We see that the screening effect is more important for low Z and much more important for higher, shells—1% to 4% for the K shell over the same range of Z, and 10%–70% for the L-shell.

So far we have considered the deviation of screened electron wave functions from the point-Coulomb wave functions at small distances. Now we will consider the small distance behavior of electron point-Coulomb wave functions of the same L but different n. (See Pratt, 1960b). For simplicity let us again examine the nonrelativistic case. For bound states, on expansion, the radial wave functions for general (n, L), Eq. (4.2.8) to relative order a is, as already shown,

$$C(n, L)\,(2ar)^L[1-ar/(L+1)], \tag{4.4.7}$$

where

$$C(n, L)=[(2L+1)!]^{-1}[(n+L)!/2n(n-L-1)!]^{1/2} \times(2a)^{3/2}n^{-(3/2+L)}, \tag{4.4.8}$$

the n dependence appears only as a constant of proportionality. Thus at small distances, wave functions of the same L but different n are similar in shape.

The same conclusion is obtained for the Dirac wave function. Direct expansion of the radial parts, neglecting relative order of a^2, gives

$$r^{-1}\begin{pmatrix}G\\F\end{pmatrix}=C(n, L)\,(2ar)^L\begin{pmatrix}1-ar/(L+1)\\-a/2(L+1)\end{pmatrix} \tag{4.4.9}$$

for $K<0$, [i.e., $J=L+\frac{1}{2}$, $L=-(K+1)$], and

$$r^{-1}\begin{pmatrix}G\\F\end{pmatrix}=C(n, L)\,(2ar)^{L-1} \times\begin{pmatrix}a^2(2L+1)/2L+2ar-2(ar)^2/(L+1)\\a(2L+1)-2a^2r\end{pmatrix} \tag{4.4.10}$$

for $K>0$ (i.e., $J=L-\frac{1}{2}$, $L=K$), where Eqs. (4.2.24) have been used. This property of the wave function may be demonstrated directly from the coupled differential equations for G and F, Eqs. (4.2.20).

5. NUMERICAL FORMULATION AND METHODS

5.1 Numerical Formulation

Consider calculation of the matrix element M_{fi} defined by Eq. (2.2.4). By inserting the expressions for ψ_i and ψ_f from Eqs. (4.2.32)–(4.2.33), we may obtain M_{fi} in terms of the integrals over initial and final radial wave functions G_K, F_K, g_κ, f_κ:

$$M_{fi}(M)=4\pi(2\pi\alpha/k)^{1/2}i^L\sum_{\kappa m}[\Omega_{\kappa m}{}^\dagger(\hat{p})\chi]^\dagger\exp(i\delta_\kappa)[\epsilon_-R_+(m)+\epsilon_+R_-(m)], \tag{5.1.1}$$

where $\epsilon_\pm=\epsilon_1\pm i\epsilon_2$, and

$$R_\pm(m)=(-i)^{l+L-1}\int d^3r e^{ikz}r^{-2}[g_\kappa F_K C_{jlm}{}^\pm C_{JL'M}{}^\mp Y_{l,m\mp1/2}{}^*(\hat{r})\,Y_{L',M\pm1/2}(\hat{r}) -G_K f_\kappa C_{jl'm}{}^\pm C_{JLM}{}^\mp Y_{l';m\mp1/2}{}^*(\hat{r})\,Y_{L,M\pm1/2}(\hat{r})]. \tag{5.1.2}$$

Here we have $C_{jlm}{}^\pm\equiv C(l1/2j;\ m\mp1/2,\ \pm1/2)$, i.e.,

$$C_{jlm}{}^+=\eta_\kappa[(l+\eta_\kappa m+\tfrac{1}{2})/(2l+1)]^{1/2},$$
$$C_{jlm}{}^-=[(l-\eta_\kappa m+\tfrac{1}{2})/(2l+1)]^{1/2},$$
$$\eta_\kappa\equiv-\kappa/|\kappa|. \tag{5.1.3}$$

If we use the Wigner–Eckart theorem, the only nonvanishing terms require $m=M\pm1$ for $R_\pm$. Since (see for example, p. 63 and 81 of Edmonds, 1957)

$$e^{ikz}=\sum_{\lambda=0}^{\infty}[4\pi(2\lambda+1)]^{1/2}i^\lambda j_\lambda(kr)\,Y_{\lambda,0}(\hat{r}),$$

and

$$\int Y_{l_2,u}^*(\hat{r})\,Y_{l_1,u}(\hat{r})\,Y_{l,0}(\hat{r})\,d\Omega=(-)^u[(2l_2+1)(2l_1+1)(2l+1)/4\pi]^{1/2}\begin{pmatrix}l_2 & l_1 & l\\ 0 & 0 & 0\end{pmatrix}\begin{pmatrix}l_2 & l_1 & l\\ -u & u & 0\end{pmatrix},$$

we have

$$R_\pm(m)=\sum_{\lambda=0}^{\infty}(-i)^{l+L-\lambda-1}\delta_{m,M\pm1}(-)^{M\pm1/2}\int_0^\infty dr j_\lambda(kr)$$
$$\times\{g_\kappa F_K C_{jlm}{}^{\pm}C_{JL'M}{}^{\mp}[(2l+1)(2L'+1)]^{1/2}T(l,L',\lambda;M\pm1/2)$$
$$-G_K f_\kappa C_{jl'm}{}^{\pm}C_{JLM}{}^{\mp}[(2l'+1)(2L+1)]^{1/2}T(l',L,\lambda;M\pm1/2)\},$$

where

$$T(l_2,l_1,l;u)\equiv(2l+1)\begin{pmatrix}l_2 & l_1 & l\\ 0 & 0 & 0\end{pmatrix}\begin{pmatrix}l_2 & l_1 & l\\ -u & u & 0\end{pmatrix}. \tag{5.1.4}$$

From the definition and the symmetry properties of the 3-j symbol of Wigner (see Edmonds, 1957, p. 46) we have $T(l,L',\lambda;M\pm\frac{1}{2})=0$ unless $|l-L'|\leq\lambda\leq l+L'$ and $l+L'+\lambda$ is even. This restricts λ to the values $|l-L'|$, $|l-L'|+2,\cdots,l+L'$. Similarly, we have $T(l',L,\lambda;M\pm\frac{1}{2})=0$ unless $|l'-L|\leq\lambda\leq l'+L$ and $l'+L+\lambda$ is even. Changing the summation index from λ to n by defining $h(n)=l+L'-2n$ for $n=0,1,2,\cdots,n_{\max}=(l+L'-|l-L'|)/2$, and $u(n)=l'+L-2n$ for $n=0,1,2,\cdots,n_{\max}=(l'+L-|l'-L|)/2$, we have

$$\sum_{\lambda=0}^{\infty}(-i)^{l+L-\lambda-1}j_\lambda(kr)\,T(l,L',\lambda;M\pm1/2)=-\eta_\kappa\sum_{\lambda=|l-L'|}^{(l+L')}{}'\,j_\lambda(kr)P_2{}^{\pm}(M),$$

$$\sum_{\lambda=0}^{\infty}(-i)^{l+L-\lambda-1}j_\lambda(kr)\,T(l',L,\lambda;M\pm1/2)=-\eta_\kappa\sum_{\lambda=|l'-L|}^{(l'+L)}{}'\,j_\lambda(kr)P_1{}^{\pm}(M),$$

where $\sum'$ denotes a summation index running in steps of 2, $\eta_K=-K/|K|$, $\eta_\kappa=-\kappa/|\kappa|$; and

$$P_1{}^{\pm}(M)=(-)^{(l'+L-\lambda)/2}T(l',L,\lambda;M\pm1/2),$$
$$P_2{}^{\pm}(M)=(-)^{(l+L'-\lambda)/2}T(l,L',\lambda;M\pm1/2). \tag{5.1.5}$$

Define

$$Q_1{}^{\pm}(M)=\eta_\kappa(-)^{M\pm1/2}[(2l'+1)(2L+1)]^{1/2}C_{jl'M\pm1}{}^{\pm}C_{JLM}{}^{\mp},$$
$$Q_2{}^{\pm}(M)=-\eta_K(-)^{M\pm1/2}[(2l+1)(2L'+1)]^{1/2}C_{jlM\pm1}{}^{\pm}C_{JL'M}{}^{\mp}, \tag{5.1.6}$$

and

$$s_1=\int_0^\infty dr j_\lambda(kr)G_K f_\kappa,$$
$$s_2=\int_0^\infty dr j_\lambda(kr)g_\kappa F_K. \tag{5.1.7}$$

Then we have

$$R_\pm(m)=\delta_{m,M\pm1}\sum_{J=1}^{2}Q_n{}^{\pm}\sum_{\lambda}{}'P_n{}^{\pm}s_n. \tag{5.1.8}$$

The index λ runs from $|l'-L|$ to $(l'+L)$ in steps of two for $n=1$, and from $|l-L'|$ to $(l+L')$ in steps of two for $n=2$. The s integrals s_1 and s_2 are the basic integrals to be obtained numerically, and we discuss their calculation in Sec. 5.2.

To obtain the photoeffect cross section it is necessary to calculate the absolute square of the matrix element M_{fi} given by Eq. (5.1.1):

$$|M_{fi}(M)|^2=16\pi^2(2\pi\alpha/k)\sum_{\bar{\kappa}\bar{m}m}\Omega_{\bar{\kappa}\bar{m}}{}^{\pm}(\hat{p})\tfrac{1}{2}(1+\boldsymbol{\zeta}\cdot\boldsymbol{\sigma})\Omega_{\kappa m}(\hat{p})\exp[i(\delta_\kappa-\delta_{\bar{\kappa}})]$$
$$\times[(1+\xi_3)R_+(\bar{m})R_+(m)+(\xi_1+i\xi_2)R_+(\bar{m})R_-(m)+(\xi_1-i\xi_2)R_-(\bar{m})R_+(m)+(1-\xi_3)R_-(\bar{m})R_-(m)]. \tag{5.1.9}$$

In terms of the polarization parameters discussed in Sec. 2.2b, the photoeffect differential cross section has the form

$$d\sigma(M,\boldsymbol{\xi},\boldsymbol{\zeta})/d\Omega=(d\sigma/d\Omega)_{\text{unpol}}\{\tfrac{1}{4}\sum_{\mu,\nu=0}^{3}\xi_\mu\zeta_\nu B_{\mu\nu}(M)\}, \tag{5.1.10}$$

where

$$\xi_0=1, \qquad \tfrac{1}{2}\sum_{M=-J}^{J}B_{00}(M)=1,$$

and $(d\sigma/d\Omega)_{\text{unpol}}$ is the differential cross section from unpolarized photons, summed over all allowed values of M for the given subshell, and summed over final electron spins. Our interest is in the cross section summed over all allowed values of M for the given subshell. Thus we have the photoeffect cross section

$$d\sigma(\boldsymbol{\xi},\boldsymbol{\zeta})/d\Omega=(d\sigma/d\Omega)_{\text{unpol}}\{\tfrac{1}{2}\sum_{\mu,\nu=0}^{3}\xi_\mu\zeta_\nu C_{\mu\nu}(\theta)\}, \tag{2.2.16}$$

with $C_{00}\equiv 1$. As mentioned in Sec. 2.2c, the matrix element M_{fi} is invariant under the substitutions of Eqs. (2.2.14) and consequently the only nonzero polarization correlations are C_{10}, C_{31}, C_{33}, C_{21}, C_{23}, C_{02}, C_{12}; and $C_{00}\equiv 1$.

Define

$$A_\pm{}^+(M)=C_{jl,M+1}{}^{\pm}Y_{l,M+1\mp 1/2}(\hat{p})R_\kappa{}^+(M),$$
$$A_\pm{}^-(M)=C_{jl,M-1}{}^{\pm}Y_{l,M-1\mp 1/2}(\hat{p})R_\kappa{}^-(M), \tag{5.1.11}$$

where

$$R_\kappa{}^\pm(M)=\sum_{n=1}^{2}Q_n{}^\pm\sum_{\lambda}{}'P_n{}^\pm s_n. \tag{5.1.12}$$

Then by using the symmetry of 3-j symbol $T(j_1, j_2, j_3; -\mu)=(-)^{j_1+j_2+j_3}T(j_1, j_2, j_3; \mu)$ and Eqs. (5.1.3), we have

$$P_n{}^\pm(-M)=P_n{}^\mp(M),$$
$$Q_n{}^\pm(-M)=-\eta_\kappa\eta_K Q_n{}^\mp(M), \tag{5.1.13}$$

which leads to

$$R_\kappa{}^\pm(-M)=-\eta_\kappa\eta_K R_\kappa{}^\mp(M). \tag{5.1.14}$$

Since $Y_{lm}(\theta,\phi=0)=(-)^m[(2l+1)(l-m)!/4\pi(l+m)!]^{1/2}\times P_l{}^m(\cos\theta)$, we have $Y_{l,-m}(\theta,\phi=0)=(-)^m Y_{l,m}(\theta,\phi=0)$. Then from Eqs. (5.1.11) we have

$$A_\pm{}^+(-M)=(-)^{M\pm 1/2}\eta_K A_\mp{}^-(M). \tag{5.1.15}$$

Using Eqs. (2.2.5), (5.1.9), (2.2.15), and (5.1.15) we obtain the unpolarized photoeffect differential cross sections and the photoeffect polarization correlations as follows:

$$(d\sigma/d\Omega)_{\text{unpol.}}=\lambda_0 D_{00}, \tag{5.1.16}$$

where

$$\lambda_0=16\pi pE\alpha/k, \tag{5.1.17}$$

and

$$D_{00}=\sum_{\kappa,\bar{\kappa}}\cos\delta\sum_{M=1/2}^{J}\{A_+{}^+\bar{A}_+{}^+ + A_-{}^+\bar{A}_-{}^+ + A_+{}^-\bar{A}_+{}^- + A_-{}^-\bar{A}_-{}^-\}. \tag{5.1.18}$$

$\bar{A}_\pm{}^\pm$ is obtained from $A_\pm{}^\pm$ in Eqs. (5.1.11) by replacing κ by $\bar{\kappa}$; $\delta\equiv\delta_\kappa-\delta_{\bar{\kappa}}$. The nonvanishing polarization correlations between the incident photon and the ejected electron are $C_{00}\equiv 1$,

$$C_{10}=D_{00}{}^{-1}\sum_{\kappa\bar{\kappa}}\cos\delta\sum_{M=1/2}^{J}\{A_+{}^+\bar{A}_+{}^- + A_-{}^+\bar{A}_-{}^- + A_+{}^-\bar{A}_+{}^+ + A_-{}^-\bar{A}_-{}^+\},$$

$$C_{31}=D_{00}{}^{-1}\sum_{\kappa\bar{\kappa}}\cos\delta\sum_{M=1/2}^{J}\{A_{21}\cos\theta+A_{22}\sin\theta\},$$

$$C_{33}=D_{00}{}^{-1}\sum_{\kappa\bar{\kappa}}\cos\delta\sum_{M=1/2}^{J}\{A_{21}\sin\theta-A_{22}\cos\theta\},$$

$$C_{21}=D_{00}{}^{-1}\sum_{\kappa\bar{\kappa}}\sin\delta\sum_{M=1/2}^{J}\{A_{11}\cos\theta+A_{12}\sin\theta\},$$

$$C_{23}=D_{00}{}^{-1}\sum_{\kappa\bar{\kappa}}\sin\delta\sum_{M=1/2}^{J}\{A_{11}\sin\theta-A_{12}\cos\theta\},$$

$$C_{02}=D_{00}{}^{-1}\sum_{\kappa\bar{\kappa}}\sin\delta\sum_{M=1/2}^{J}\{A_-{}^+\bar{A}_+{}^+ + A_-{}^-\bar{A}_+{}^- - A_+{}^+\bar{A}_-{}^+ - A_+{}^-\bar{A}_-{}^-\}, \tag{5.1.19}$$

and

$$C_{12}=D_{00}{}^{-1}\sum_{\kappa\bar{\kappa}}\sin\theta\sum_{M=1/2}^{J}\{A_-{}^-\bar{A}_+{}^+ + A_-{}^+\bar{A}_+{}^- - A_+{}^-\bar{A}_-{}^+ - A_+{}^+\bar{A}_-{}^-\},$$

with

$$A_{21}=A_+{}^+\bar{A}_-{}^+ + A_-{}^+\bar{A}_+{}^+ - A_+{}^-\bar{A}_-{}^- - A_-{}^-\bar{A}_+{}^-,$$
$$A_{22}=A_+{}^-\bar{A}_+{}^- + A_-{}^+\bar{A}_-{}^+ - A_-{}^-\bar{A}_-{}^- - A_+{}^+\bar{A}_+{}^+,$$
$$A_{11}=A_+{}^+\bar{A}_-{}^- + A_-{}^+\bar{A}_+{}^- - A_+{}^-\bar{A}_-{}^+ - A_-{}^-A_+{}^+,$$
$$A_{12}=A_+{}^-\bar{A}_+{}^+ + A_-{}^+\bar{A}_-{}^- - A_-{}^-\bar{A}_-{}^+ - A_+{}^+\bar{A}_+{}^-. \tag{5.1.20}$$

To obtain the unpolarized total photoeffect cross section for a given subshell, average Eq. (5.1.9) over the incident photon polarizations, sum it over the final electron spins and all allowed values of M for the given subshell, and integrate it over $d\Omega$, to find

$$\sigma_{\text{unpol}}=\lambda_0\sum_{\kappa}\sum_{M=1/2}^{J}\{[R_\kappa{}^+(M)]^2+[R_\kappa{}^-(M)]^2\}, \tag{5.1.21}$$

where $R_\kappa{}^\pm(M)$ is given by Eq. (5.1.12).

The final form of these formulas has consequences for the programming of the numerical calculations. In the formulation just described, which was used by Pratt, Levee, Pexton, and Aron (1964) and Schmickley

and Pratt (1967), the summations left are over κ and M. This way it is easier to correct results for truncation errors in case too few κ values have been considered. However, the computation of angular distributions is more complicated. In other formulations (Alling and Johnson, 1965; Rakavy and Ron, 1967; Byrsk and Zerby, 1968) the final result is given in the form

$$(d\sigma/d\Omega)_{\text{unpol}}=\sum_{n=0}^{\infty} B_n P_n(\cos\theta). \tag{5.1.22}$$

(P_n is the Legendre polynomial and $n=0$ corresponds to the case of a total cross section). Here we have

$$\begin{aligned}B_n=(8\pi\alpha PE/k)&\sum_{\lambda,\bar{\lambda},\kappa,\bar{\kappa},\Lambda,\bar{\Lambda}}(-1)^{J-1/2+\Lambda+\bar{\Lambda}+j+\bar{j}}\\
&\times\cos\left[\delta_\kappa-\delta_{\bar{\kappa}}+\tfrac{1}{2}\pi(\bar{l}-l+\lambda-\bar{\lambda})\right]\\
&\times\left[(2\lambda+1)(2\bar{\lambda}+1)(2\bar{l}+1)(2l+1)(2j+1)(2\bar{j}+1)\right]^{1/2}\\
&\times C(l\bar{l}n;00)C(\lambda 1\Lambda;01)C(\bar{\lambda}1\bar{\Lambda};01)\\
&\times C(\Lambda\bar{\Lambda}n;1-1)W(\Lambda\bar{\Lambda}j\bar{j};nJ)W(l\bar{l}j\bar{j};n\tfrac{1}{2})\\
&\times\{(-\kappa\,||\,S_\Lambda^\lambda\,||\,K)\int G_K j_\lambda(kr)f_{-\kappa}\,dr\\
&-(\kappa\,||\,S_\Lambda^\lambda\,||\,-K)\int F_{-K}j_\lambda(kr)g_\kappa\,dr\}\\
&\times\{(-\bar{\kappa}\,||\,S_\Lambda^{\bar{\lambda}}\,||\,K)\int G_K j_{\bar{\lambda}}(kr)f_{-\bar{\kappa}}\,dr\\
&-(\bar{\kappa}\,||\,S_\Lambda^{\bar{\lambda}}\,||\,-K)\int F_{-K}j_{\bar{\lambda}}(kr)g_{\bar{\kappa}}\,dr\},\end{aligned}$$

where

$$\begin{aligned}(-\kappa\,||\,S_\Lambda^\lambda\,||\,K)=(-1)^L&\left[(3/8\pi)(2j+1)\right.\\
&\left.\times(2J+1)(2\Lambda+1)(2l+1)(2L+1)\right]^{1/2}\\
&\times C(lL\lambda;00)X\begin{pmatrix}\lambda & 1 & \Lambda\\ l & \frac{1}{2} & j\\ L & \frac{1}{2} & J\end{pmatrix}.\end{aligned}$$

[See Eq. (4.2.17) for the relations between κ, l, and j.] With this second formulation the computation of angular distributions is easier, but to correct for truncation errors requires repeating the entire calculation. Also, the truncation in n of Eq. (5.1.22) should be handled carefully, especially for forward and backward photon angles where more terms are needed (assuming that the needed B_n's can be calculated with sufficient accuracy).

5.2 Numerical Methods

As discussed in Sec. 5.1, the problem of computing photoelectric cross sections has been reduced essentially to the numerical evaluation of the s-integrals [given by Eqs. (5.1.7)]. These integrals involve threefold products of a bound wave function, a continuum wave function, and a spherical Bessel function. Both the bound and continuum wave functions are solutions of the radial Dirac equation (4.2.20). Other factors are combined with the radial integrals to obtain matrix elements and cross sections, such as Legendre polynomials, Clebsch–Gordan coefficients, etc. We will describe the numerical methods employed for each component.

5.2a The Bound-State Wave Function

Putting $E=E_b=1-\epsilon$ in Eqs. (4.2.20) gives the equation for the bound state, where E_b is the total energy of the bound electron, and $\epsilon>0$ is the binding energy. These two coupled differential equations constitute an eigenvalue problem. The standard procedure for solving this system of equations is based upon "outward" and "inward" integrations which are then matched. This method utilizes certain boundary conditions, which the solutions must satisfy, and we will discuss these before describing the method in detail.

Making the substitution

$$\begin{aligned}F&=\bar{G}r^{\gamma_B},\\ F&=\bar{F}r^{\gamma_B},\end{aligned}\tag{5.2.1}$$

and assuming that our potentials have a point-Coulomb-like behavior near $r=0$, we find

$$\begin{aligned}a\bar{F}(0)-(\gamma_B+K)\bar{G}(0)&=0,\\ a\bar{G}(0)+(\gamma_B-K)\bar{F}(0)&=0.\end{aligned}\tag{5.2.2}$$

A necessary and sufficient condition for the existence of a nontrivial solution is that the determinant of the coefficients in Eqs. (5.2.2) be zero, yielding

$$\gamma_B=+(K^2-a^2)^{1/2}. \tag{5.2.3}$$

The positive sign is chosen in order to obtain a physically acceptable wave function.

The asymptotic behavior of Eq. (4.4.20) is

$$\begin{aligned}(E_b+1)F-(dG/dr)&=0,\\ (E_b-1)G+(dF/dr)&=0.\end{aligned}\tag{5.2.4}$$

If we disregard the physically unacceptable solution corresponding to a growing exponential, the asymptotic solution of Eqs. (4.2.20) is

$$\begin{aligned}G(r)&\sim C_1(r)\,\exp(-\lambda r),\\ F(r)&\sim C_2(r)\,\exp(-\lambda r),\end{aligned}\tag{5.2.5}$$

where $\lambda=+(1-E_b^2)^{1/2}$, $E_b<1$. $C_1(r)$, $C_2(r)$ have generally the form of finite powers of r; for point-Coulomb and screened potentials (which we assume to be falling faster than $1/r$) we have

$$C_2(r)/C_1(r)\sim-\left[(1-E_b)/(1+E_b)\right]^{1/2}. \tag{5.2.6}$$

(See Rose, 1961, Secs. 28 and 29.)

Since the equations are linear and homogeneous, one can choose $\bar{G}(0)$ arbitrarily, and $\bar{F}(0)$ is then determined by either of Eqs. (5.2.2). One assumes that this ratio of $\bar{F}(0)/\bar{G}(0)$ holds for small r_0 (e.g., $r_0\approx10^{-3}$. In practice we have $r_0=r_0(Z)$ which is larger the lower the atomic number Z.). This was checked numerically

for values in the range 10^{-3}–10^{-6} and no appreciable difference was found. Making a first rough guess for ϵ, one can begin integrating the differential equations from this value of r_0 and for any given potential $V(r)$. The Runge–Kutta–Gill [e.g., Ralston and Wilf (1962)] integration scheme was used; comment on it will be made in the next subsection. The "outward" integration is continued until a radius R is reached (generally a distance at which the correct number of maxima and minima of the wave function have already occurred). Then choosing a point $R_f > R$ [large enough so that the asymptotic conditions (5.2.5–6) can be assumed to be satisfied—a numerical criterion is given later] one can begin integrating "inward" from R_f to R with an arbitrary choice of G [F is taken from the ratio F/G given by Figs. (5.2.5–6)]. The next step is to match these two solutions, which we label "out" and "in", respectively. This is achieved by a method analogous to that described by Hartree (1957) for the Schrödinger equation. Varying the electron energy by a small amount δE_b will cause a small change δG and δF in the wave functions. Imposing the condition

$$F/G\,|_{\text{out}}+\delta(F/G)|_{\text{out}}=F/G|_{\text{in}}+\delta(F/G)\,|_{\text{in}}$$

to insure the continuity of the functions and their derivatives yields the following interative scheme

$$E_b^{(P+1)}=E_b^{(P)}+\left(\frac{F}{G}\bigg|_{\text{out}}-\frac{F}{G}\bigg|_{\text{in}}\right)\times\left(\frac{1}{G_{\text{out}}^2}\int_0^R (F^2+G^2)\,dr+\frac{1}{G_{\text{in}}^2}\int_R^\infty (F^2+G^2)\,dr\right)^{-1}. \tag{5.2.7}$$

Here G_{in}, G_{out}, F_{in}, F_{out} are the values of the (unnormalized) Dirac functions at the matching point R and P is the iteration number. The iterations are considered to have converged if

$$(\epsilon^{(P+1)}-\epsilon^{(P)})/\epsilon^{(P+1)}<10^{-3}\ \text{(or, better, } 10^{-5}). \tag{5.2.8}$$

In order to insure that R_f was chosen large enough, the ratio $|G(R_f)/G_{\max}|$ (where $G_{\max}$ is the maximal value of the function) is checked. If it is bigger than 10^{-6} then R_f is increased and the inward integration is repeated until this and criterion (5.2.8) are met. When the solution is accepted, it is normalized by

$$\begin{pmatrix}G\\F\end{pmatrix}=\frac{N}{G_{\text{out}}}\begin{pmatrix}G\\F\end{pmatrix}\qquad \text{for } r\leq R,$$

$$=\frac{N}{G_{\text{in}}}\begin{pmatrix}G\\F\end{pmatrix}\qquad \text{for } r>R, \tag{5.2.9}$$

where

$$N^{-2}=\frac{1}{G_{\text{out}}^2}\int_0^R (F^2+G^2)\,dr+\frac{1}{G_{\text{in}}^2}\int_R^{R_f} (F^2+G^2)\,dr.$$

This method is very stable even if the first guess for ϵ is rough. The convergence is rapid and few iterations are needed.

5.2b The Continuum Wave Function

The differential equations to be solved in this case are Eqs. (4.2.20) with $1+T=E>1$. They then constitute an initial value problem and E is determined by Eq. (2.2.6). The same boundary conditions (5.2.2) exist at the origin. The continuum wave functions $g_\kappa(r)$ and $f_\kappa(r)$ are normalized by requiring that asymptotically they are given by Eqs. (4.2.22) as we discussed in Sec. 4.2b, which correspond to modified phase-shifted free-field solutions. The exact free-field solutions are given in terms of spherical Bessel functions (see Rose, 1961, Chapt. V). Outside the range of the potential (which need not require asymptotic values of r) the functions (unnormalized) are therefore linear combinations of the regular and irregular solutions

$$g_\kappa(r)=r[(E+1)/2E]^{1/2}[A_\kappa^+(\rho)j_\kappa(\rho)-A_\kappa^-(\rho)y_\kappa(\rho)],$$
$$f_\kappa(r)=r[(E-1)/2E]^{1/2}\times[A_\kappa^+(\rho)j_{\kappa-1}(\rho)-A_\kappa^-(\rho)y_{\kappa-1}(\rho)], \tag{5.2.10}$$

with

$$\rho\equiv pr;$$

or

$$g=r[(E+1)/2E]^{1/2}A_\kappa(\rho)\times[\cos\delta_\kappa(\rho)j_\kappa(\rho)-\sin\delta_\kappa(\rho)y_\kappa(\rho)]$$
$$f=r[(E-1)/2E]^{1/2}A_\kappa(\rho)\times\cos\delta_\kappa(\rho)j_{\kappa-1}(\rho)-\sin\delta_\kappa(\rho)y_{\kappa-1}(\rho)], \tag{5.2.11}$$

with

$$A_\kappa(\rho)=\{[A_\kappa^+(\rho)]^2+[A_\kappa^-(\rho)]^2\}^{1/2},$$
$$\delta_\kappa(\rho)=\tan^{-1}[A_\kappa^-(\rho)/A_\kappa^+(\rho)]\quad \text{if } A_\kappa^+(\rho)>0;$$
$$=\tan^{-1}[A_\kappa^-(\rho)/A_\kappa^+(\rho)]+\pi\quad \text{if } A_\kappa^+(\rho)<0,\quad A_\kappa^-(\rho)>0;$$
$$=\tan^{-1}[A_\kappa^-(\rho)/A_\kappa^+(\rho)]-\pi\quad \text{if } A_\kappa^+(\rho)<0,\quad A_\kappa^-(\rho)<0. \tag{5.2.12}$$

Here j_κ and y_κ are spherical Bessel functions of the first and second kind. Using the asymptotic expressions for j_κ and y_κ in Eqs. (5.2.11) we obtain the unnormalized wave functions asymptotically as follows:

$$g_\kappa(r)\sim A_\kappa p^{-1}[(E+1)/2E]^{1/2}\sin(pr-\kappa\tfrac{1}{2}\pi+\bar{\delta}_\kappa),$$
$$f_\kappa(r)\sim A_\kappa p^{-1}[(E-1)/2E]^{1/2}\cos(pr-\kappa\tfrac{1}{2}\pi+\bar{\delta}_\kappa), \tag{5.2.13}$$

with

$$\delta(\rho)\sim\bar{\delta}_\kappa.$$

Comparing Eqs. (5.2.13) with Eqs. (4.2.22), we see that the solutions should be multiplied by a normalization constant $N_\kappa = A_\kappa^{-1}$, and that the phase shift δ_κ can be determined by

$$\bar{\delta}_\kappa = \delta_\kappa - (l-\kappa)\tfrac{1}{2}\pi. \tag{5.2.14}$$

The numerical calculation proceeds as follows: Assigning any nonzero value to $\bar{g}_\kappa(0)$, one fixes the value of $\bar{f}_\kappa(0)$ by the choice

$$\lim_{r\to 0}[\bar{f}_\kappa(r)/\bar{g}_\kappa(r)] = (\gamma+\kappa)/a, \tag{5.2.15}$$

with

$$\bar{g}(r) \equiv r^{-\gamma} g(r) \quad \text{and} \quad \bar{f}(r) \equiv r^{-\gamma} f(r).$$

Assuming that Eq. (5.2.15) holds also for small values of r (e.g., $r_0 = 10^{-3}$) one can proceed from r_0 with the Runge–Kutta–Gill method. This version contains an automatic error control so that the steps are not constant but vary according to preassigned error limits that we impose. Such types of computations were carried out by Rakavy and Ron (1967). A difficulty arises when trying to solve numerically these differential equations with a constant step grid utilizing the Euler or Runge–Kutta schemes. As Pratt, Levee, Pexton, and Aron (1964) show, unless the integration starts at a radius $r_n = nh$ (h is the constant step) such that $n \geq \gamma$, errors will propagate and increase. In order to avoid the singularity exhibited at $r=0$, they employed power-series solutions for values $n \leq j \approx \gamma$ and used the functions thus determined to start the integration by the Runge–Kutta method at r_j. When the potential is not given analytically it is approximated by a power-series expansion of the form $V(r) \approx -(a/r) + b_0 + b_1 r + b_2 r^2 + \cdots$ which usually gives good results for the values of $V(r)$. However one should avoid applying this method in the quite rare cases when the result is sensitive to the choice of the coefficients b_i, which cannot be made uniquely. Both procedures yield functions with the proper shapes. The over-all normalization must still be set and the phase shifts determined. We can calculate them from Eqs. (5.2.10) and (5.2.12), where g and f are the unnormalized values at $r = R_n$, and we denote the normalization constant and the phase shift by $[A_\kappa(\rho_n)]^{-1}$ and $\delta_\kappa(\rho_n) + (l-\kappa)\frac{1}{2}\pi$ with $\rho_n \equiv pR_n$. This assumes that the normalization radius R_n is sufficiently large so that we are in the free-field region. Physically no such region exists for the ejected electron since it since it leaves a singly ionized atom. Similarly, in some of the mathematical models there is no true free-field region. For computational purposes such a R_n generally exists, but often it is too large, thus consuming much computer time in integration of the wave function and therefore making the method impractical.

In order to devise a better procedure let us first investigate the behavior of the exact solutions. It is well known [e.g. Rose (1961)] that the point-Coulomb potential causes a distortion in the phase-shift with a r-dependent term $(aE/p)\ln 2pr$. Similarly we introduce the r-dependent functions $A(\rho)$ and $\delta(\rho)$ such that the unnormalized wave functions g and f are given by

$$g = p^{-1}[(E+1)/2E]^{1/2} A_\kappa(\rho) \sin[\rho - \kappa\tfrac{1}{2}\pi + \delta_\kappa(\rho) + Q(\rho)],$$
$$f = p^{-1}[(E-1)/2E]^{1/2} A_\kappa(\rho) \times \cos[\rho - \kappa\tfrac{1}{2}\pi + \delta_\kappa(\rho) + Q(\rho)], \tag{5.2.16}$$

where $\rho = pr$, and $Q(\rho)$ is the phase correction integral defined by

$$dQ(\rho)/d\rho = -V(r)E/p^2. \tag{5.2.17}$$

The boundary conditions imposed on this function are that for a point-Coulomb potential

$$Q = (aE/p)\ln 2\rho. \tag{5.2.18}$$

For screened potentials asymptotically we have

$$Q(\rho) \sim 0, \tag{5.2.19}$$

so that

$$Q(\rho) = \frac{E}{p^2}\int_\rho^\infty V(s)\, ds,$$

and $Q=0$ for free fields (see further discussion below). We have asymptotically the unnormalized solutions:

$$g \sim p^{-1}[(E+1)/2E]^{1/2} A_\kappa \sin(\rho - \kappa\tfrac{1}{2}\pi + \bar{\delta}_\kappa),$$
$$f \sim p^{-1}[(E-1)/2E]^{1/2} A_\kappa \cos(\rho - \kappa\tfrac{1}{2}\pi + \bar{\delta}_\kappa). \tag{5.2.20}$$

[Note that in the point-Coulomb case one would add Q as defined in Eq. (5.2.18).] Thus we have asymptotically

$$A_\kappa(\rho) \sim A_\kappa \qquad \delta_\kappa(\rho) \sim \bar{\delta}_\kappa.$$

Inserting Eqs. (5.2.16) into Eqs. (4.2.20) will yield two first-order differential equations for $\delta_\kappa(\rho)$ and $A_\kappa(\rho)$. Denoting the argument of the trigonometric functions in Eqs. (5.2.16) by $\theta(\rho)$, recalling Eq. (5.2.17), and using the definitions

$$\tilde{\kappa}(\rho) = \kappa\{1 + [rV(r)/\kappa p]^2\}^{1/2},$$

and

$$\tilde{\theta}(\rho) = \theta(\rho) + (\kappa/2\,|\,\kappa\,|)\tan^{-1}|\,rV(r)/\kappa p\,|,$$

we get the following equations:

$$d\delta_\kappa(\rho)/d\rho = -[\tilde{\kappa}(\rho)/\rho]\sin 2\tilde{\theta}(\rho),$$
$$\frac{dA_\kappa(\rho)/d\rho}{A_\kappa(\rho)} = \frac{\tilde{\kappa}(\rho)}{\rho}\cos 2\tilde{\theta}(\rho).$$

For large values of ρ, we expect $\delta_\kappa(\rho) + Q(\rho)$ to vary insignificantly with respect to ρ. Therefore we may assume $\tilde{\theta}(\rho) \approx \rho +$ slowly varying functions of ρ. Then $\sin 2\tilde{\theta}(\rho)$ is almost periodic with a period π/p on the

r axis. Likewise $\tilde{\kappa}(\rho)$ is almost constant over short intervals of ρ. Thus for large values of ρ we have

$$d\delta_\kappa(\rho)/d\rho \approx -(\kappa/\rho)\sin 2\rho,$$

$$\frac{dA_\kappa(\rho)/d\rho}{A_\kappa(\rho)} \approx \frac{\kappa}{\rho}\cos 2\rho,$$

which yields asymptotically

$$\delta_\kappa(\rho) \sim \bar{\delta}_\kappa + (\kappa/2\rho)\cos 2\rho,$$

$$\ln A_\kappa(\rho) \sim \ln A_\kappa + (\kappa/2\rho)\sin 2\rho. \qquad (5.2.21)$$

These functions oscillate with a period π about the asymptotic limit and with an envelope which decreases as $1/\rho$. Averaging over one period gives

$$\langle \delta_\kappa(\rho) \rangle_{\text{av}} \approx \bar{\delta}_\kappa - (\kappa/4\rho^2)\sin 2\rho + \text{order of } \rho^{-3},$$

$$\langle \ln A_\kappa(\rho) \rangle_{\text{av}} \approx \ln A_\kappa - (\kappa/4\rho^2)\cos 2\rho + \text{order of } \rho^{-3};$$

that is, by averaging over a period we reduce the error of approximating the limit values by a factor of $(2\rho)^{-1}$.

This investigation of the character of the asymptotic behavior of the exact functions $A(\rho)$ and $\delta(p)$ suggests the following improved procedure for calculating the numerical coefficients $A_\kappa(\rho_n)$ and $\delta_\kappa(\rho_n)$ with $\rho_n \equiv pR_n$: starting at R_n one calculates, as shown above, $A_\kappa(\rho_n)$ and $\delta_\kappa(\rho_n)$ but also for a series of points $R_n + \delta R_n$ over one period. The resulting values are then averaged over this period by means of a tenth order Newton–Cotes formula (Abramowitz and Stegun, 1965). The point R_n is chosen from the semiempirical formula

$$R_n = 57.6(ZE/p)^{2/3}E^{1/2}\ (\text{MeV})[0.5 + (|\kappa|^{1/2}/Z]],$$

$$\text{for } E\ (\text{MeV}) < 0.95\ \text{MeV};$$

$$= 40.(|\kappa|^{1/2}Z^{1/4}/p)[1 + (0.6Z^{1/3}/|\kappa|\ E\ (\text{MeV})^{1/4}],$$

$$\text{for } E\ (\text{MeV}) \geq 0.95\ \text{MeV},$$

which has been estimated by Tseng (1970) to be valid for the point-Coulomb potential. It may be used for kinetic energies of the electron down to 1 keV for low-Z elements and to 20 keV for heavy elements. Obviously it is an overestimate for screened potentials.

Before concluding this subsection let us mention some other methods of normalizing the continuum wave functions. One way is to use Eqs. (5.2.16), which we call the trigonometric method, rather than using Eqs. (5.2.10) or (5.2.11), the spherical Bessel function method which we have described. Schmickley (1966) demonstrated that the latter method yields more accurate results for a given R_n. Another method was followed by Brysk and Zerby (1968) who normalized the continuum wave function by utilizing the WKB method. Though better known for the Schrödinger equation (e.g., Messiah, 1961) it can be applied straightforwardly to the Dirac equation (Rose, 1961). We will not reproduce the standard formulas but note two steps in the derivation of Brysk and Zerby which are particular to photoeffect cases: (1) They noted that the normalization factor is in practice not constant but varies with R_n. Considering its exact r dependence they imposed the condition that the extra terms which appear as a consequence in the newly derived r-dependent expression and cause it to deviate from its original r-independent form should cancel. (2) In the final expression for the normalization factor there appears the third derivative of the potential. For potentials known only numerically this type of computation is unreliable. Brysk and Zerby overcame this problem by taking the ratio of the screened to the nonscreened potential, which is nearly exponential, and differentiated the analytic result they fitted. Finally let us point to another possibility that, to our knowledge, no one has applied to photoelectric computations. That is to normalize the continuum wave functions by matching them to point-Coulomb wave functions with $Z=1$. This fits the physical situation as the process results in a singly ionized atom; it is also the correct approach for some of the mathematical models. In view of the remarks that have been made above we would not expect this method to yield appreciable changes in total cross sections calculated by the standard methods.

5.2c Other Related Quantities

The bound and continuum states are needed for computing the s integrals (5.1.7). These integrals were calculated with Simpson's rule due to the fact that the mesh used was not an equidistant one. (More sophisticated methods are probably available.) Another set of quantities which appear in these integrals, as well as in the expressions for the normalization factors and phase shifts, are the spherical Bessel functions. These functions can be computed utilizing their standard recursion formulas (e.g., Morse and Feshbach, 1953). In order to avoid numerical divergencies, one has to compute the spherical Bessel function, e.g., $j_l(x)$, from a large value $l=\Lambda$ and downwards to $l=0$ and then normalize the results when $x<l+\frac{1}{2}$. A similar method using recursion formulas for ratios of spherical Bessel functions is described in detail by Corbató and Uretsky (1959). It is suitable for use in computers for which the exponent cannot be taken sufficiently large. The use of recursion formulas is very desirable in our case as it yields simultaneously the functions at a desired radius r for all needed l values.

Usually the other required quantities in the photoeffect calculation do not pose numerical difficulties. The Legendre functions are calculated by using their standard recursion relations (e.g., Morse and Feshbach, 1953). The Clebsch–Gordon and Racah coefficients are calculated by using standard explicit formulas (see e.g., Edmonds, 1957; Rotenberg, Bivins, Metropolis, and Wooten, 1959).

TABLE 5.1. Relative error of continuum normalizations. The number ρ represents the radius at which the normalization is calculated numerically.

	$p(m_e c)$	$\rho(\hbar)$	$\kappa=-1$	$+1$	-20	$+20$
$Z=13$	0.5	50	0.008	0.007	0.004	0.031
	0.5	235	0.008	0.013	0.008	0.026
	5.0	50	0.002	<0.001	0.002	0.038
	5.0	235	0.009	0.009	0.007	0.029
$Z=26$	0.5	50	<0.003	0.002	<0.004	0.016
	0.5	235	0.012	0.010	0.007	<0.004
$Z=92$	0.5	50	0.011	0.032	0.025	0.002
	0.5	235	0.006	0.005	0.008	0.012
	5.0	50	0.008	<0.001	<0.004	0.005
	5.0	235	0.008	0.009	0.007	0.011

5.3 Accuracy of the Numerical Computations

There are two complementary methods for estimating the errors in the final result obtained in photoeffect calculations. One method is to use estimates of errors in the various numerical methods employed in calculating the various components and in some reasonable way combine these into a single estimate of an over-all error. The second method is to compare some analytic formulas with final numerical results which can be reproduced by the computer program. We illustrate the first method with the error analysis of Pratt, Levee, Pexton, and Aron (1964), Schmickley (1966), and Schmickley and Pratt (1967) and the second method with the analysis of Ron (1966) and Rakavy and Ron (1965, 1967).

The accuracy of the program which calculates the bound-state wave function can be tested for the point-Coulomb potential by comparison with analytic results. The relative accuracy obtained is better than 10^{-4}–10^{-6}, depending on the type of calculation and the tolerance demanded.

The major errors involved in the numerical computation of the continuum wave functions arise from inaccurate normalization. The numerical results can be compared with the analytical results of the point-Coulomb potential. As Table 5.1 taken from Schmickley (1966) shows, these errors are less than 5×10^{-4}. They depend on E, κ, and Z and are higher for large κ, small E, and high Z. They vary also with the radius of normalization if it has been chosen to be too small. The error in the normalization also increases rapidly as the threshold energy is approached. However, this type of error is insensitive to the grid size and may be attributed to the very long periods of low-energy continuum states. Errors in Bessel functions, Legendre polynomials, Clebsch–Gordan coefficients, etc. are completely negligible as these functions are computed with an accuracy better than 10^{-8}–10^{-10}.

The errors in the partial wave radial integrals, which are calculated by Simpson's rule, are due first to the errors of the component programs and second to the errors of the integration procedures. More refined methods might reduce this kind of error. The errors which arise from the choice of R, the upper limit of the integration, are summarized in Table 5.2 reproduced from Pratt, Levee, Pexton, and Aron (1964). It indicates the distance in r which it was necessary

TABLE 5.2. Regions contributing to partial-wave integrals.

		κ			
Z	k (MeV)	$+1$	$+5$	$+9$	$+15$
26	0.354	84	80	108	(does not contribute)
	1.131	58.5	63	78.5	89.5
50	0.354	41	45	50	(does not contribute)
92	0.208	19	28.5	35	(does not contribute)
84	0.354	20	26	31.5	(does not contribute)
	1.131	22	25	27	31
82	1.1368	21.5	23	27	28.5
	2.0	19.5	25	26	27
	2.754	22.5	24.5	25	25.5

TABLE 5.3. Values of $|\kappa|$ needed for accuracy to one part in 10^n.

	n					
k (MeV)	1	2	3	4	5	6
0.140	2	3	4	4	5	5
0.200	3	4	5	6	7	8
0.279	3	4	6	7	8	9
0.354	4	5	7	9	10	12
0.400	4	6	8	9	11	13
0.662	5	8	10	13	14	
1.131	7	12	15			
1.1368	8	13	16			
2.0	11	≈17				
2.754	14					

to integrate to in order to reduce the residual contribution to less than one part in 10^6. Various grid sizes were used to check the accuracy of the final integration. The errors of the results generally fluctuated by about 0.1% for the grids tested ($h=0.005$ to 0.10). For a few cases they were higher ($\sim$1%). One may say that most of the integrations are accurate to $\lesssim$1%, probably $\sim$0.5%.

The other source of errors is the so called truncation errors caused by the fact that the number of partial waves which are taken into account is limited for various practical reasons. Table 5.3 of Pratt, Levee, Pexton, and Aron (1964) gives the number of partial waves needed to calculate the total cross section to a specified accuracy. However subsequent experience indicates that the numbers cited in Table 5.3 for the higher energies should be slightly higher. In most calculations the truncation error was $\lesssim$0.1%. For high energies, expecially when a limit of $|k|=20$ was in effect, the error increased to $\gtrsim$0.5%.

The combined effects of all errors yield the following: Errors associated with the magnitude h, the grid step, are small ($\sim$0.1%) except for a few cases. The estimate of the errors in the radial integration and the information on the contribution of each κ to the cross section enable us to estimate the total error in the cross section. This estimate varies with Z and k; (for details see Pratt, Levee, Pexton, and Aron, 1964). The main conclusion is that the total cross sections are accurate to $\lesssim$0.8% (with most of them accurate to $\lesssim$0.5%) and the angular distributions and polarization correlations are accurate to $\sim$1%.

The checks according to the second method were as follows: Making no approximation beyond replacing the final electron state by a plane wave and the bound state by an eigenstate in a point-Coulomb field, a closed formula was derived for the angular distribution (for details see Ron, 1966). This analytic formula could be reproduced by the computer program by taking the bound state in a point-Coulomb field while the potential for the calculation of the free wave function was set to zero. The plane wave was written as an expansion in partial series and 26 partial waves were taken so that truncation errors were negligible. The check was performed at $k=354$ keV for uranium. The difference between the two sets of results never exceeded 0.5%. The error in total cross sections was even better than 0.5%. Additional checks were performed for a low photon energy of 100 eV for one electron in the $1s$, $2s$, $2p$ subshells of hydrogen. This choice of the energy and element was made in order to eliminate relativistic effects. The numerical results for the total cross sections were compared with analytic expressions using the nonrelativistic, dipole, and Born approximations. The deviations were about 0.2%. Also, all the results of Hulme, McDougall, Buckingham, and Fowler (1935) were reproduced, thus covering the energy range in which we are interested. We see that both methods yield about the same estimate for the errors. All studies agree also as to the main sources of error: the numerical integration of the radial integrals by Simpson's rule and the normalization error. No effort to reduce the errors seems to be needed at this stage of the art in view of the approximate nature of the potential model for wave functions used. The use of different models changes the cross sections by more than the numerical uncertainties. We may conclude that improved wave functions and atomic models are needed, and that when these are available more careful integration schemes should be used.

6. RESULTS AND DISCUSSION

In this section we will review analytic and numerical predictions for photoelectric cross sections and discuss their validity and properties. This will lead us to a recommended set of theoretical cross sections. We will compare theory with experiment and will comment on the accuracies of the various tabulations.

6.1 Analytic Results and Their Validity

Analytic results require various approximations (expansions in a, use of the point-Coulomb field, etc.). Therefore they have a limited range of validity (results are restricted to light atoms, neglect screening effects, etc.). In spite of such limitations they have the advantage of giving insight into the process. They also yield a roughly correct dependence of cross sections on the atomic number and photon energy. Thus such formulas still remain useful even with the present ability to carry out much more exact numerical calculations. We have previously (Sec. 4) discussed the approximate wave functions needed for such calculations and presented the relativistic and nonrelativistic forms of the matrix elements. Here we describe some of the analytic results which have been obtained, selected in view of their continued usefulness. In all these analytic formulas screening is neglected.

6.1a The Nonrelativistic Formula

In deriving this formula one uses exact nonrelativistic hydrogen-like wave functions for both the bound and continuum states, together with the nonrelativistic form of the matrix element [Eqs. (4.2.14), (4.2.15), and (2.2.4) with $\boldsymbol{\alpha}\cdot\boldsymbol{\varepsilon}$ replaced by $\mathbf{p}\cdot\boldsymbol{\varepsilon}$]. If in addition one makes the dipole approximation, replacing $\exp(i\mathbf{k}\cdot\mathbf{r})$ by 1 (neglect of retardation), selection rules reduce the infinite sum over continuum l, m values to a few terms. (Sommerfeld and Schur, 1930; see also Bethe and Salpeter, 1957). In this way Stobbe (1930) derived the formula for the total cross section from the K shell

$$\sigma_{1s}=\left\{\frac{4\sqrt{2}Z^5\alpha^4}{k^{7/2}}\phi_0\right\}\left[2\pi\left(\frac{\epsilon_K}{k}\right)^{1/2}\frac{\exp\left(-4n_1\cot^{-1}n_1\right)}{1-\exp(-2\pi n_1)}\right], \tag{6.1.1}$$

TABLE 6.1. Values of $R(a)$ [as defined in Eqs. (6.1.7–8)] together with the high-energy limit of the $1s$, $2s$, $2p$, and $2\bar{p}$ cross sections and their ratios with respect to $1s$ cross section. (Symbols $1s$, $2s$, $2p$, and $2\bar{p}$ refer to K, L_{I}, L_{II}, and L_{III} subshells, respectively.)

Z	$R(a)$	$1s$	$2s$	$2p$	$2\bar{p}$	$2s/1s$	$2p/1s$	$2\bar{p}/1s$	σ_L/σ_K
6	−0.0001349	0.8477	0.1057	0.00004202	0.0001353	0.1247	0.00004957	0.0001596	0.1249
13	−0.0003656	0.7103	0.08857	0.0001862	0.0005271	0.1247	0.0002621	0.0007421	0.1257
29	−0.0003348	0.4974	0.06201	0.0008599	0.001744	0.1247	0.001729	0.003506	0.1299
50	−0.01241	0.3391	0.04234	0.002558	0.003133	0.1249	0.007543	0.009239	0.1417
60	−0.02302	0.2914	0.03654	0.003816	0.003591	0.1254	0.01310	0.01232	0.1508
74	−0.04223	0.2433	0.03084	0.006327	0.004023	0.1268	0.02600	0.01654	0.1693
82	−0.05397	0.2229	0.02851	0.008326	0.004179	0.1279	0.03735	0.01875	0.1840
92	−0.06868	0.2029	0.02628	0.01169	0.004303	0.1295	0.05761	0.02121	0.2083

where

$$n_1 = a/\beta = [\epsilon_K/(k-\epsilon_K)]^{1/2},$$

and $\phi_0 = \frac{8}{3}\pi r_e^2 = \frac{8}{3}\pi\alpha^2$ is the Thomson scattering cross section. Stobbe obtained similar expressions for the L shell; results for higher shells are also available (Hall, 1936; Lewis, 1953; and Harriman, 1956). The first factor of Eq. (6.1.1) (in curly brackets) is the cross section which is obtained if the continuum wave function is replaced by a plane wave. It is invalid near threshold as the condition for using the Born approximation, $n_1 \ll 1$, cannot then be met. The second factor, in square brackets, represents the correction to the Born approximation.

We should note that there exist so called exact nonrelativistic cross sections which do not neglect retardation (Fischer, 1931a,b; and Sauter, 1931). However they differ from Stobbe's result only by quantities of order β^2, and corrections of this order also result from the use of the relativistic Dirac formulation. One may consider Stobbe's cross sections as the pure nonrelativistic result (see Bethe and Salpeter, 1957, p. 311).

The nonrelativistic formula is expected to be valid, apart from screening corrections, for light atoms and low energies. Indeed the predictions for low photon energies close to the K absorption edge, when compared with the exact relativistic Coulomb results, are very good for aluminum ($k \leq 5$–10 keV) through tin ($k \leq 40$ keV) and within 10% for heavy elements (e.g. uranium for $k = 200$ keV). However the agreement disappears rapidly as the photon energy increases, even for light elements.

6.1b The Relativistic Born Approximation Formulas

The first-order relativistic Born approximation result was obtained by Sauter (1931 a,b). In order to sum the infinite partial-wave series which appears in the matrix element he made the following approximations: (1) Replacement of γ_B by $|K|$ and of γ by $|\kappa|$, thus neglecting terms of order a^2; (2) Expansion of the resulting expression in a/β, the expansion parameter of the Born approximation. Though he did not follow the usual Born approximation method, the results are equivalent. (For an illuminating discussion of this problem see Fano, McVoy, and Albers, 1959). Here we face one peculiar feature of the photoeffect mentioned in Sec. 2.3: to get a correct expression of order n in a for the cross section one must carry out a calculation in which the wave functions and other quantities involved are correct to order $n+1$. Sauter's result for the first nonvanishing order in a is

$$\sigma_{1s} = \frac{3Z^5\alpha^4}{2k^5}\phi_0(\gamma_\beta^2-1)^{3/2}\left[\frac{4}{3}+\frac{\gamma_\beta(\gamma_\beta-2)}{\gamma_\beta+1}\times\left(1-\frac{1}{2\gamma_\beta(\gamma_\beta^2-1)^{1/2}}\ln\frac{\gamma_\beta+(\gamma_\beta^2-1)^{1/2}}{\gamma_\beta-(\gamma_\beta^2-1)^{1/2}}\right)\right], \quad (6.1.2)$$

where

$$\gamma_\beta = (1-\beta^2)^{-1/2}.$$

In the nonrelativistic limit this formula reduces to the expression in curly brackets of Eq. (6.1.1) as it should; in the extreme relativistic limit it becomes

$$\sigma_{1s} = (3Z^5\alpha^4/2k)\phi_0. \quad (6.1.3)$$

We see that for very high energies the decrease of the cross section with energy becomes slower [compared with $k^{-7/2}$ in Eq. (6.1.1) for the nonrelativistic case]. This explains the experimental fact that the photoelectric process still contributes to the total attentuation coefficient at fairly high energies. Though the nature of the approximations involved suggests that this formula should be valid for light elements and high photon energies we find on comparison with numerical calculations that in the case of Al the Sauter cross sections are high by 30%–70% in the energy range 300–2000 keV and are double the correct values for $k = 1$–100 keV. For heavier elements and high energies the error is even larger. The effective expansion parameter appears to be πa, and consequently the Sauter formula is not too useful in practice.

Gavrilla (1959) performed the next order Born approximation calculation. His result, correct to one higher order in a, is

$$\sigma_{1s} = \tfrac{1}{2}(3Z^5\alpha^4)\phi_0[\beta^3\gamma_\beta^3/(\gamma_\beta-1)^5] \times\{M(\beta)[1-(\pi a/\beta)]+\pi a N(\beta)\}, \quad (6.1.4)$$

TABLE 6.2. Error of the normalization screening theory (NT) based on the K-shell atomic-field photoeffect cross sections of Scofield with HFS potential and of HNO with point-Coulomb potential (NE$\equiv[\sigma(\mathrm{NT})-\sigma(\mathrm{Scofield})]/\sigma(\mathrm{Scofield})$).

k (keV)\NE\Z	4	13	29	50	82	92
1	0.030	...	...	...	...	...
2	−0.002	...	...	...	...	...
3	−0.01	...	...	...	...	...
5	−0.01	0.030	...	...	...	...
6	−0.01	0.023	...	...	...	...
8	−0.01	0.015	...	...	...	...
10	−0.01	0.010	...	...	...	...
15	−0.009	0.004	...	...	...	...
20	−0.008	0.001	...	...	...	...
30	...	−0.002	0.013	...	...	...
40	−0.004	−0.003	0.008	...	...	...
50	...	−0.005	0.003	0.11	...	...
60	...	−0.004	0.002	0.01	...	...
80	...	−0.005	0.002	0.01	...	...
100	...	−0.004	0.002	0.01	...	...
150	...	−0.004	−0.001	0.005	...	0.020
200	...	−0.003	−0.001	0.004	0.008	0.007
300	...	−0.003	−0.001	0.002	0.006	0.007
400	...	−0.002	−0.002	0.001	0.006	0.006

where $M(\beta)$ is the expression in the square brackets of (6.1.2), and

$$N(\beta)=\frac{1}{\beta^3}\left\{-\frac{4}{15}\gamma_\beta+\frac{34}{15}-\frac{63}{15}\gamma_\beta^{-1}+\frac{25}{15}\gamma_\beta^{-2}+\frac{8}{15}\gamma_\beta^{-3}+\frac{\gamma_\beta^2-3\gamma_\beta+2}{2\beta\gamma_\beta^3}\ln\frac{1-\beta}{1+\beta}\right\}. \quad (6.1.5)$$

This result is only directly useful for $\pi a/\beta\ll 1$.

6.1c The High-Energy Limit Formula

The Born series techniques described above give the energy dependence in the limit of small Z. By using a distorted plane wave, Eq. (4.3.18), (Pratt, 1960a) obtained the Z dependence in the limit of high energies as

$$\sigma_{1s}=\sigma_0 F(a), \quad (6.1.6)$$

where σ_0 is the high-energy limit of Sauter's formula Eq. (6.1.3). $F(a)$ is the following double integral, which was calculated numerically (see Column 3 of Table 6.1):

$$F(a)=-[(2\xi+3)/2\xi]a^{2\xi}\cdot\frac{1}{4}\int_{-1}^{1}dx\int_{-1}^{1}dy\left(\frac{1-x}{1+x}\right)^{ia}\times[a+i(1-a^2)^{1/2}x]^{-(4+2\xi)}\cdot\left\{(1-x^2y^2)^{\xi+1}[1+(\xi/a)^2]+2(1-y^2)(1-x^2y^2)^{\xi}\left[\frac{i\xi}{a}x-\left(\frac{\xi}{a}\right)^2x^2\right]\right\}, \quad (6.1.6a)$$

where

$$\xi=-1+(1-a^2)^{1/2}.$$

Expanding the integrand in powers of a gives the cross section

$$\sigma_{1s}=\sigma_0 a^{2\xi}[\exp(-2a\cos^{-1}a)][1-(4\pi a/15)+R(a)], \quad (6.1.7)$$

where $R(a)$ is defined by equating the right-hand sides of Eqs. (6.1.6) and (6.1.7). The values of $R(a)$ are given in Table 6.1. Pratt combined his formula, the correct Z dependence, with Gavrila's Eq. (6.1.4), giving the correct energy dependence, to obtain a composite formula which has been a basis for high-energy cross section predictions:

$$\sigma_{1s}=\sigma_0(\beta^3\gamma_\beta^3/k^4)a^{2\xi}M(\beta)\exp[-2(a/\beta)\cos^{-1}a]\times\{1+\pi a[N(\beta)/M(\beta)]+R(a)\}. \quad (6.1.8)$$

As $\lim_{\beta\to 1}[N(\beta)/M(\beta)]=-\frac{4}{15}$ we see that in the high-energy limit this reduces to the form (6.1.7).

We should mention that the first high-energy limit formula was derived by Hall (1934, 1936), who obtained a closed expression by writing an approximation to a double integral equivalent to, though more complicated than, (6.1.6a) (see Pratt, 1960a). However his approximate formula missed the term $-4\pi a/15$, which is not small.

6.2 Screening Effects and Shell Ratios

6.2a Range of Validity of Normalization Theory

The normalization screening theory predicts that the only effect of atomic-electron screening on photoeffect cross sections results from the change in normalization of the bound-state wave function. The

TABLE 6.3. Values of ratios $R(i/1s) \equiv (\sigma_i/\sigma_{1s})/(\sigma_i/\sigma_{1s})_{k\to\infty}$, with $i=2s$, $2p$, $2\bar{p}$, and σ_a/σ_K for the HFS potential for $Z=13$. (Symbols $1s$, $2s$, $2p$, and $2\bar{p}$ refer to K, $L_{\rm I}$, $L_{\rm II}$, and $L_{\rm III}$ subshells, respectively.)

k (keV)	$R(2s/1s)$	$R(2p/1s)$	$R(2\bar{p}/1s)$	$(\sigma_a/\sigma_K)_{\rm HFS}$
5	0.862	48.1	33.2	1.077
10	0.917	26.6	18.1	
20	0.952	14.5	9.71	
40	0.971	8.13	5.29	
60	0.980	5.92	3.79	
100	0.990	4.15	2.56	
200	1.000	2.82	1.66	1.075
300	1.002	2.38	1.31	
500	1.004	2.00	1.20	
1000	1.003	1.60	1.10	
1500	1.003	1.39	1.08	
∞	1.000	1.00	1.00	(1.075)
∞	σ_{2s}/σ_{1s} $=0.0692$	σ_{2p}/σ_{1s} $=0.0000929$	$\sigma_{2\bar{p}}/\sigma_{1s}$ $=0.000262$	

theory applies for photon energies not too near threshold, because above threshold the minimum possible momentum transfer to the nucleus $q_{\rm min}$ is of order one and the most important regions of configuration space for the photoeffect matrix element are of the order of the electron Compton wavelength. Contributions from larger distances are cut off fairly sharply, perhaps reaching the 1% level by 3 to $5r_{\rm max}$, where $r_{\rm max}=q_{\rm min}^{-1}$. Using the properties of electron wave function shapes at small distances discussed in Sec. 4, Pratt and Tseng (1972) estimated the lowest energies for which the normalization screening theory should be believed. They concluded that the normalization screening theory can be good to 1% for photon energies more than 2.5 keV above the K-shell threshold in Be, 10 keV in Al, 30 keV in Cu, 60 keV in Sn, 150 keV in Pb, and 200 keV in U.

These order of magnitude estimates are in good agreement with actual numerical calculations. Using the recent results of Scofield for the Hartree–Fock–Slater (HFS) potential and the point-Coulomb results of Hultberg, Nagel, and Olsson (HNO) (1962, 1968), we show the error of the normalization screening theory (NT) in Table 6.2 for the K shell. We find that the normalization screening theory is good to 1% for the K shell for photon energies more than 2 keV above the K-shell threshold in Be, 8 keV in Al, 25 keV in Cu, 30 keV in Sn, and 80 keV in U. For the $L_{\rm I}$ subshell the normalization screening theory was also verified in calculations using the computer code of Rakavy and Ron (1967).

6.2b Energy Dependence of Shell Ratios

Another consequence of the dominance of electron Compton wavelength distances in atomic photoeffect is that cross sections from bound states of the same orbital angular momentum L but different principal quantum number n are related. This follows from our previous remark that dependence on ϵ (i.e., n) only enters beginning with the r^2 term of a wave function expansion for small r. Thus at small distances the dependence on n only enters through the wave function normalization. (The agreement in shape between wave functions of different subshells in the same potential is not as close as between point-Coulomb and screened wave functions for the same subshell. The magnitude of deviation of the ns ($n\neq 1$) wave function from the $1s$ wave function shape is of order of $Z^2\alpha^2r^2$, compared with a $Z^{2/3}\alpha^2r^2$ deviation of screened wave functions from the point-Coulomb shape. It should also be noted that for low photon energies the important values of r for different subshells for the photoeffect matrix element are different.) This agreement in shape explains why nearly energy independent ratios of cross sections are observed for photon energies well above the threshold. As an example we show the ratio $(\sigma_{2s}/\sigma_{1s})/(\sigma_{2s}/\sigma_{1s})_{k\to\infty}\equiv R(2s/1s)$ in Tables 6.3 and 6.4 for the HFS potential, where the normalization screening theory has been used to obtain the high-energy limit $(\sigma_{2s}/\sigma_{1s})_{k\to\infty}$ for the HFS potential. The effect of the energy dependence is less than 5% for photon energies more than 2 keV above the threshold in Be, 20 keV in Al, 140 keV in Sn, and 150 keV in U. This is to be contrasted with the behavior of $R(2p/1s)$ and $R(2\bar{p}/1s)$, also shown in Tables 6.3–6.4 (symbols $2p$ and $2\bar{p}$ refer to $L_{\rm II}$ and $L_{\rm III}$ subshells), which approach their high-energy limits more slowly. As further shown in Table 6.4, although the $2p$ and $2\bar{p}$ cross sections are smaller, for high-Z elements their deviations from high-energy values are such that the ratio σ_a/σ_K is nearly energy independent. One does not see this combined effect of cancellations for low-Z elements for which $2p$ and $2\bar{p}$ are almost negligible,

TABLE 6.4. Same as Table 6.3 except for $Z=82$.

k (keV)	$R(2s/1s)$	$R(2p/1s)$	$R(2\bar{p}/1s)$	$(\sigma_a/\sigma_K)_{\rm HFS}$
100	0.893	1.63	3.17	1.262
150	0.935	1.39	2.44	1.244
200	0.971	1.27	2.08	1.237
300	1.01	1.14	1.70	1.224
400	1.03	1.07	1.51	1.226
500	1.04	1.02	1.38	1.223
600	1.04	0.980	1.30	1.221
800	1.05	0.935	1.19	1.217
1000	1.05	0.901	1.13	1.215
1500	1.04	0.869	1.05	1.211
2754	1.03	0.873	1.003	1.209
∞	1.00	1.00	1.00	(1.21)
∞	σ_{2s}/σ_{1s} $=0.114$	σ_{2p}/σ_{1s} $=0.0311$	$\sigma_{2\bar{p}}/\sigma_{1s}$ $=0.0151$	

TABLE 6.5. Photoelectric cross sections σ of aluminum for $k=5$ keV (in b/atom). Experimental value: 8814. (Symbols $1s$, $2s$, $2p$, $2\bar{p}$, $3s$, and $3p$ refer to K, $L_{\rm I}$, $L_{\rm II}$, $L_{\rm III}$, $M_{\rm I}$, and $M_{\rm II}$, respectively.)

	Potential								
σ	Ionic	Ionic–expt	HFS	HFS2/3	RL	HFS2/3–expt	B2/3–ionic[a]	TF	FAM
σ_{1s}	8261.	7996.	7995.	7725.	7698.	7880.	7344.	7162.	7862.
σ_{2s}	471.8	468.9		449.0	451.9	450.2	443.0	409.5	430.2
σ_{2p}	34.80	34.30		31.74	32.23	31.83	31.12	25.52	27.96
$\sigma_{2\bar{p}}$	67.58	66.62		62.00	62.59	61.81	60.44	49.60	54.65
σ_L	(574.2)	(569.8)	(581.4)	(542.7)	(546.7)	(543.8)	(534.6)	(484.6)	(512.8)
σ_{3s}	36.94	36.78			31.89	32.13	32.03	19.71	
σ_{3p}	1.784	1.780			1.410	1.363	1.355		
$\sigma_{3s}+\sigma_{3p}$	(38.72)	(38.56)	(33.87)	(33.55)	(33.30)	(33.49)	(33.39)	(19.71)	(~28)
Atom σ_a	8874.	8604.	8611.	8301.	8278.	8457.	7912.	7666.	~8400
Ratio σ_a/σ_K	1.074	1.076	1.077	1.075	1.075	1.073	1.077	1.070	~1.069

[a] Bound wave function calculated with HFS2/3 potential whereas the continuum function is calculated with an ionic potential.

but the ratio σ_a/σ_K reaches the high-energy limit at even lower photon energies than in high Z cases.

6.2c Potential Model Dependence of Shell Ratios

As relativistic calculations gave only the cross section for the K shell (until the 1960's), and experiments generally did not resolve the contributions of higher shells, the traditional practice has been to estimate the contribution of all higher shells by using a certain ratio σ_a/σ_K, thus getting σ_a from the calculated value σ_K. When an experiment was carried out, usually yielding σ_a, the result was reduced by this ratio to σ_K in order to compare experiment with theory. The famous "law of five fourths" simply claimed that $\sigma_a/\sigma_K=5/4$. An improvement was introduced by Davisson (1965) (see Sec. 6.5) who used Kirschner's (1930) experimental ratios measured at the K-shell thresholds. The Z dependence of this ratio was found to vary monotonically from 1.09 for Al to 1.235 for U. Later calculations by Rakavy and Ron (1965, 1967) showed that the ratio is slightly energy dependent, especially for lower energies. The analysis of Sec. 6.2b gives some theoretical support for the empirical use of this ratio and indicates to some extent the reason for its success. We note that although σ_a/σ_K is slightly energy dependent, it is almost independent of the atomic model used in the calculation. We emphasize that this model independence is *not* rigorously correct but exists within the numerical accuracies with which we are dealing. (This may be another consequence of normalization theory, for the difference in shape of the screened wave functions is still smaller than the difference between screened and Coulomb functions, so that the theory is still applicable at lower energies where larger distances contribute.) We performed a series of computations to check numerically this assertion. A sample of our results is given in Tables 6.5–6.7. We also found that the assertion holds even when energies are below the threshold of the K shell and the ratio $\sigma_a/\sigma_{\rm domin}$ (where $\sigma_{\rm domin}$ is the cross section of the dominant subshell) is considered. Whereas the cross sections themselves differ by 3%–8% depending on choice of model (see Tables 6.5–6.9), the ratios do not differ by more than ~1%, which is close to the claimed numerical accuracy of the cal-

TABLE 6.6. Same as Table 6.5 except for copper with $k=2$ keV (in b/atom). Experimental value: 247 400. (Symbols $3\bar{p}$, $3d$, $3\bar{d}$, and $4s$ refer to $M_{\rm III}$, $M_{\rm IV}$, $M_{\rm V}$, and $N_{\rm I}$, respectively.)

	Potential			
σ	TF	RL	HFS2/3	HFS
σ_{2s}	42 220	44 420	44 350	
σ_{2p}	47 160	50 930	51 050	
$\sigma_{2\bar{p}}$	90 150	97 420	97 710	
σ_L	(179 530)	(192 800)	(193 110)	(200 400)
σ_{3s}	6 618	7 197	7 225	
σ_{3p}	4 780	5 309	5 344	
$\sigma_{3\bar{p}}$	9 135	10 120	10 180	
$\sigma_{3s}+\sigma_{3p}+\sigma_{3\bar{p}}$	(20 533)	(22 630)	(22 750)	
Atom σ_a	200 000	215 400	215 860	
Ratio σ_a/σ_L	1.114	1.117	1.118	
σ_{3d}			981.2	
$\sigma_{3\bar{d}}$			1 421	
σ_M			(25 152)	(26 090)
σ_{4s}				171
Atom σ_a			218 262	226 700
Ratio σ_a/σ_L			1.130	1.131

TABLE 6.7. Cross sections (in b/atom) of various atomic models for the $M_{IV}-Q_I$ subshells of uranium and the ratios σ_a/σ_M.

$Z=92$	HFS		HFS2/3		TFC	
k	3.5793 keV	4.0000 keV	3.5793 keV	4.0000 keV	3.5793 keV	4.0000 keV
M_{IV}	0	...	0	151 762	0	149 936
M_V	286 670	...	284 056	208 458	247 847	205 036
M	2.8667×10^5	3.6714×10^5	2.8406×10^5	3.6022×10^5	2.4785×10^5	3.5497×10^5
N_I	...	...	8 589	7 287	8 659	7 310
N_{II}	...	...	10 797	9 324	10 315	8 918
N_{III}	...	...	27 622	22 684	27 445	22 550
N_{IV}	...	...	32 222	25 103	32 266	25 238
N_V	...	...	44 337	34 318	44 903	34 767
N_{VI}	...	...	18 531	12 588	16 203	11 046
N_{VII}	...	...	22 957	15 571	20 138	13 683
N	...	...	1.6506×10^5	1.2688×10^5	1.5993×10^5	1.2351×10^5
O_I	...	...	2 503	2 087	2 943	2 440
O_{II}	...	...	2 877	2 433	3 327	2 811
O_{III}	...	...	6 743	5 492	8 141	6 625
O_{IV}	...	...	5 971	4 657	7 928	6 192
O_V	...	...	8 120	6 280	10 911	8 445
O_{VI}	...	...	1 421	981	3 000	2 079
O	...	...	0.2764×10^5	0.2193×10^5	0.3625×10^5	0.2859×10^5
P_I	...	...	517.8	429.7	701.8	579.3
P_{II}	...	...	500.7	421.6	663.9	557.9
P_{III}	...	...	1 057.6	860.2	1 274.4	1 034.6
P_{IV}	...	...	~800.	~600.	~1 000.	~800.
P	...	...	0.0288×10^5	0.0231×10^5	0.0364×10^5	0.0297×10^5
Q_I	...	...	~50.	~40.	~100.	~100.
σ_a	4.8678×10^5	5.2174×10^5	4.7969×10^5	5.1139×10^5	4.478×10^5	5.101×10^5
σ_a/σ_M	1.698	1.421	1.689	1.420	1.807	1.437

culations. We chose cases (low energies and light atoms) for which the results are most sensitive to the choice of potential.

6.3 Recommended Theoretical Cross Sections

6.3a Cross Sections for the Range $k=1$–1500 keV

We consider here tabulations based on theoretical calculations. Tabulations which include a mixture of theoretical and experimental data will be discussed in Sec. 6.5. To judge given tabulations and choose among them, there are several criteria available. What are the merits of the atomic models used? How well do theory and experiment agree? How complete and how available are the data? How much effort would improvements require?

By now sufficient data is available in HFS-type atomic models that we will not consider older tabulations based on point-Coulomb or cruder screening models. The different plausible atomic models give results which differ by 3%–8% and for those models which we consider most suitable (of the HFS type), the difference is closer to the lower limit, as can be seen in Tables 6.5–6.9 and other Tables in this section. These particular calculations were carried out at energies for which there exist the most accurate experimental data (e.g., Deslattes, 1958) and where the errors in photoelectric cross sections are within 2%–3%. We observe that the difference of cross sections originating from different models is about the same as the experimental errors. Therefore no strong case can be made as to which potential model to prefer based upon the data for which $Z\gtrsim13$ and $k\gtrsim10$ keV. However we observe that for lower energies and lighter atoms the difference between cross sections calculated with different atomic models exceeds 3%–8%, whereas the experimental accuracy remains unchanged. It is therefore probable that further theoretical and experimental investigations of this type will enable one to

TABLE 6.8. Cross sections (in b/atom) of Al for different atomic models, with their deviation (percentage deviation given in parenthesis) from experimental results [Deslattes (1958)].

($Z=13$) k (keV)	Expt[a] total	σ_{expt}[b]	σ_{HFS}	$\sigma_{HFS2/3}$	σ_{Ionic}[c]	$\sigma_{HFS-expt}$[d]	$\sigma_{HFS2/3-expt}$	$\sigma_{Ionic-expt}$
8.047	2252	2214	2181 (−1.5)	2112 (−4.6)	2237 (1.0)	2187 (−1.2)	2141 (−3.3)	2194 (−0.9)
8.904	1662	1628	1619 (−0.6)	1568 (−3.7)	1660 (2.0)	1623 (−0.3)	1588 (−2.5)	1630 (0.1)
9.885	1215	1184	1186 (0.2)	1150 (−2.9)	1216 (2.7)	1189 (0.4)	1164 (−1.7)	1194 (0.8)
10.98	898.8	870.9	865.7 (−0.6)	839.9 (−3.6)	886.0 (1.7)	867.5 (−0.4)	848.8 (−2.5)	872.6 (0.2)
11.22	840.6	813.2	811.6 (−0.2)	787.7 (−3.1)	831.5 (2.3)	813.2 (0.0)	795.7 (−2.2)	818.7 (0.7)
12.49	610.8	585.8	587.9 (0.4)	570.8 (−2.6)	601.6 (2.7)	589.0 (0.5)	576.3 (−1.6)	593.1 (1.2)
14.96	362.0	341.4	339.3 (−0.6)	329.9 (−3.4)	346.7 (1.6)	339.9 (−0.4)	332.6 (−2.6)	342.5 (0.3)
17.48	228.6	210.9	210.6 (−0.1)	205.0 (−2.8)	215.0 (1.9)	210.9 (0.0)	206.4 (−2.1)	212.7 (0.9)
17.67	221.7	204.2	203.8 (−0.2)	198.3 (−2.9)	208.0 (1.9)	204.1 (−0.1)	199.7 (−2.2)	205.9 (0.8)
19.61	163.5	147.4	147.6 (0.1)	143.7 (−2.5)	150.6 (2.2)	147.8 (0.3)	144.7 (−1.8)	149.1 (1.2)
20.21	149.7	133.7	134.5 (0.6)	131.0 (−2.0)	137.3 (2.7)	134.7 (0.7)	131.8 (−1.4)	136.0 (1.7)
22.16	115.7	100.5	101.0 (0.5)	98.39 (−2.1)	103.0 (2.5)	101.0 (0.6)	98.96 (−1.5)	102.1 (1.6)

[a] Total attenuation cross section.
[b] Total photoelectric cross section.
[c] For explanation of the ionic (here based on HFS2/3) model see Secs. 3.2a and 4.4.
[d] Expt. means that the experimental value of the binding energy was inserted in Eq. (2.2.6).

distinguish between the various models. In view of the remarks of Sec. 3.2a one should be careful not to attempt this for energies so low that the HFS-type models are no longer adequate.

We know of two comprehensive theoretical tabulations of photoelectric cross sections which are based on the HFS-type atomic models. One has been given by Storm and Israel (1970) (which we denote SI). It is composed of cross sections derived from various sources using a number of atomic models. In the range of 1–100 keV (or 1–150 keV for $Z=13$) they used the Brysk and Zerby (1968) computer code with the HFS2/3 potential (and for $Z=2$–13 they used a factor between 2/3 and 1 to multiply the Slater exchange term). Experimental binding energies were inserted in place of the calculated eigenvalues. For the energy range 150–3000 keV (or 200–3000 keV for $Z=13$) they used the results of Schmickley and Pratt (1967) and Rakavy and Ron (1967), and for energies above 3 MeV an application of the Gavrila–Pratt formula (Pratt, 1960a; and Sec. 6.1c). The cross sections were not calculated for all elements and interpolations were made in order to tabulate values for $Z=1$–100.

The second tabulation, by Scofield (1972), is a complete calculation for $Z=1$–100 in the energy range 1–1500 keV using throughout the HFS potential. In view of the discussion in Sec. 6.2, Scofield's data can be easily converted into an improved Table if some other atomic model is established as superior, at least for photon energies well above absorption edges. One would have to recalculate only the bound K-shell wave functions (which is very easy to do). However, comparing Scofield's results with the SI Table for $Z=13$, 50, and 92 (see Tables 6.10–6.12) we find that the

TABLE 6.9. Same as Table 6.8 except for Cu.

($Z=29$) k (keV)	Expt.[a] Total	σ_{expt}[b]	σ_{HFS}	$\sigma_{HFS2/3}$	σ_{Ionic}[c]	Expt.[d] b.e. σ_{HFS}	Expt. b.e. $\sigma_{HFS2/3}$	Expt. b.e. σ_{Ionic}
9.670	25 740	25 570	24 640 (−3.6)	24 300 (−5.0)	25 260 (−1.1)	24 770 (−3.1)	24 880 (−2.7)	24 580 (−4.1)
9.885	23 950	23 780	23 290 (−2.1)	22 950 (−3.5)	23 960 (0.7)	23 420 (−1.5)	23 490 (−1.2)	23 180 (−2.5)
10.55	19 940	19 780	19 670 (−0.6)	19 370 (−2.1)	20 190 (2.1)	19 770 (0.0)	19 800 (0.1)	19 550 (−1.1)
10.98	18 190	18 040	17 720 (−1.8)	17 450 (−3.3)	18 150 (0.6)	17 810 (−1.3)	17 830 (−1.2)	17 640 (−2.2)
24.94	1 933	1 870	1 874 (0.2)	1 845 (−1.3)	1 903 (1.8)	1 879 (0.5)	1 867 (−0.2)	1 874 (0.2)
25.27	1 866	1 804	1 805 (0.1)	1 778 (−1.4)	1 833 (1.6)	1 810 (0.3)	1 798 (−0.3)	1 806 (0.1)
28.48	1 325	1 271	1 282 (0.9)	1 263 (−0.6)	1 301 (2.4)	1 285 (1.1)	1 276 (0.4)	1 283 (1.0)
29.19	1 237	1 185	1 195 (0.8)	1 177 (−0.7)	1 212 (2.3)	1 198 (1.1)	1 189 (0.3)	1 196 (0.9)

[a] Total attenuation cross section.
[b] Total photoelectric cross section.
[c] For explanation of the ionic (here based on HFS2/3) model see Secs. 3.2a and 4.4.
[d] Expt. means that the experimental value of the binding energy was inserted in Eq. (2.2.6).

difference is within the experimental errors (we mention in passing that the bigger error for Al at $k=$ 150 keV in Table 6.10 stems from the fact that the Brysk and Zerby computer code, designed for lower energies, begins to fail for energies higher than about 100 keV). In view of space limitations and the general agreement with the SI values, we will not reproduce the full Scofield tables here. For purposes of illustration we present in Tables 6.18–6.20 data for three selected atoms, not only for comparison purposes but also to show the contributions from the various subshells, information which is usually not given.

6.3b Cross Sections for the Range $k>1500$ keV

The calculation of cross sections for very high photon energies consumes a great amount of computer time, and large and fast computers are needed to carry out such a program. The photoelectric cross sections for such energies are small and the photoelectric process forms a tiny part of the processes occurring at such energies. Therefore it is unclear whether such an effort (and obviously experimental work) is justified, at least at the present time. Thus we resort to a semiempirical method in order to establish cross sections in this energy range.

As outlined in previous sections such a formula will consist of three factors:

(1) The correct Coulomb K-shell behavior
(2) The right choice of the ratio σ_a/σ_K
(3) The normalization effect factor which corrects for screening.

The normalization factor has been previously discussed and presents no problem. We must deal with the first two factors.

(1) *Coulomb K-shell behavior.* Although there exist quite extensive exact numerical K-shell Coulomb cross sections due to Hultberg, Nagel, and Olsson (1968) the data is insufficient for the construction of a complete tabulation for all Z's and energies up to 100 MeV. Therefore one must result to some analytic approximation. The best available formula for predicting Coulomb K-shell cross sections at high photon energies is the Gavrila–Pratt formula (Pratt, 1960a; and Sec. 6.1c). Let us mention again that this formula (6.1.8) is a combination of the high-energy formula (believed to be correct to order a^2/k and giving the right Z dependence of the cross section) and the second-order Born approximation (believed to give the right energy dependence for the limit $a\rightarrow 0$). Comparison with the

exact Hultberg, Nagel, and Olsson (1968) results shows this formula gives values which are 15%–20% high for photon energies 1.5–10 MeV and heavy elements. For light and medium elements (up to about $Z=50$) the agreement is much better. Looking for an empirical correction, we put

$$\sigma_{GP}(\text{corrected}) = (\beta^3\gamma_\beta^3/k^4)a^{2\xi}M(\beta) \times \exp\{-2(a/\beta)\cos^{-1}a\}\{1+\pi a[N(\beta)/M(\beta)] +R(a)[1-c(a,k)(a/k)]\}\sigma_0, \quad (6.3.1)$$

where $c(a, k)$ was chosen to match the Hultberg, Nagel, and Olsson (1968) results and extrapolated for other energies and elements. The results become insensitive to the exact choice of $c(a, k)$ the higher the energy and the lower the Z. For low Z ($Z \lesssim 50$), we can put $c(a, k)=0$, but the correction becomes important for the heavier elements and lower energies in the few MeV region.

TABLE 6.10. Comparison between aluminum cross sections of SI Tables and this work (Scofield's values for $k \leq 1500$ keV, and ours for $k > 1500$ keV). Here $a(\pm n)$ shall mean $a \times 10^{\pm n}$.

$Z=13$ k (keV)	SI Tables (b/atom)	This work (b/atom)	(SI Tables/ this work) (in %)
1.0	5.250(4)	5.300(4)	−0.9
1.5	1.780(4)	1.793(4)	−0.7
2.00	1.020(5)	1.013(4)	0.7
3.00	3.540(4)	3.524(4)	0.5
4.00	1.600(4)	1.609(4)	−0.6
5.00	8.460(3)	8.612(3)	−1.8
6.00	5.020(3)	5.120(3)	−2.0
8.00	2.170(3)	2.218(3)	−2.2
10.0	1.150(3)	1.146(3)	0.3
15.0	329.	336.7	−2.3
20.0	137	138.9	−1.4
30.0	38.2	39.08	−2.3
40.0	15.4	15.70	−1.9
50.0	7.58	7.697	−1.5
60.0	4.23	4.286	−1.3
80.0	1.68	1.695	−0.9
100.0	0.808	0.8245	−2.0
150.0	0.215	0.2236	−3.8
200.	0.0881	0.08970	−1.8
300.	0.0254	0.02574	−1.3
400.	0.0108	0.01112	−2.9
500.	0.00585	0.006021	−2.8
600.	0.00365	0.003764	−3.0
800.	0.00189	0.001905	−0.8
1000.	0.00117	0.001184	−1.2
1.5(3)	···	5.562(−4)	···
2. (3)	···	3.48(−4)	···
3. (3)	···	1.94(−4)	···
4. (3)	···	1.32(−4)	···
5. (3)	···	1.00(−4)	···
6. (3)	···	8.02(−5)	···
8. (3)	···	5.72(−5)	···
10. (3)	···	4.44(−5)	···

TABLE 6.11. Same as Table 6.10 except for Sn.

$Z=50$ k (keV)	SI Tables (b/atom)	This work (b/atom)	(SI Tables/ this work) (in %)
1.0	1.590(6)	1.606(6)	−1.0
1.5	6.430(5)	6.483(5)	−0.8
2.0	3.210(5)	3.268(5)	−1.8
3.0	1.180(5)	1.199(5)	−1.6
4.0	1.840(5)	1.841(5)	−0.1
5.0	1.650(5)	1.661(5)	−0.7
6.0	1.030(5)	1.035(5)	−0.5
8.0	4.810(4)	4.864(4)	−1.1
10.	2.640(4)	2.675(4)	−1.3
15.	8.690(3)	8.835(3)	−1.6
20.	3.910(3)	3.971(3)	−1.5
30.	7.870(3)	7.968(3)	−1.2
40.	3.700(3)	3.719(3)	−0.5
50.	2.010(3)	2.025(3)	−0.7
60.	1.220(3)	1.225(3)	−0.4
80.	543.	546.0	−0.5
100.	287.	289.1	−0.7
150.	89.7	89.97	−0.3
200.	39.2	39.33	−0.3
300.	12.5	12.52	−0.2
400.	5.71	5.746	−0.6
500.	3.21	3.231	−0.6
600.	2.06	2.065	−0.2
800.	1.06	1.068	−0.7
1000.	0.663	0.6664	−0.5
1500.	0.305	0.3081	−1.0
2. (3)	0.187	0.189	−1.1
3. (3)	9.97(−2)	10.1(−2)	−1.3
4. (3)	6.65(−2)	6.70(−2)	−0.7
5. (3)	4.98(−2)	4.95(−2)	0.6
6. (3)	3.89(−2)	3.92(−2)	−0.8
8. (3)	2.72(−2)	2.74(−2)	−0.7
10. (3)	2.10(−2)	2.10(−2)	0.0
15. (3)	1.32(−2)	1.32(−2)	0.0
20. (3)	9.55(−3)	9.57(−3)	−0.2
30. (3)	6.14(−3)	6.17(−3)	−0.5
40. (3)	4.55(−3)	4.55(−3)	0.0
50. (3)	3.61(−3)	3.60(−3)	0.3
60. (3)	2.98(−3)	2.98(−3)	0.0
80. (3)	2.23(−3)	2.21(−3)	0.9
100. (3)	1.77(−3)	1.76(−3)	0.6

(2) *Choice of the ratio* σ_a/σ_K. The next step is to check for what energies and atomic numbers the Coulomb results approach the high-energy limit. We have already shown in Sec. 6.2b and Table 6.3 that the separate ratios σ_i/σ_{1s} (where $i=2s, 2p, 2\bar{p}$) coverge relatively slowly (especially for higher Z's) to the high-energy limit. However the ratio σ_L/σ_{1s} converges more rapidly, for high Z due to a cancellation, because the ratios σ_{2s}/σ_{1s} and σ_{2p}/σ_{1s} approach the limit from opposite directions, and for low Z because the main

TABLE 6.12. Same as Table 6.10 except for uranium.

$Z=92$ k (keV)	SI Tables (b/atom)	This work (b/atom)	(SI Tables/ this work) (in %)
1.0	2.590(6)	2.614	−0.9
1.5	1.310(6)	1.332(6)	−1.7
2.0	7.170(5)	7.323(5)	−2.1
3.0	2.920(5)	2.997(5)	−2.6
4.0	5.190(5)	5.213(5)	−0.4
5.0	3.430(5)	3.479(5)	−1.4
6.0	2.430(5)	2.452(5)	−0.9
8.0	1.180(5)	1.202(5)	−1.8
10.	6.710(4)	6.860(4)	−2.2
15.	2.360(4)	2.430(4)	−2.9
20.	2.690(4)	2.700(4)	−0.4
30.	1.540(4)	1.566(4)	−1.7
40.	7.270(3)	7.383(3)	−1.5
50.	4.020(3)	4.092(3)	−1.8
60.	2.460(3)	2.515(3)	−2.2
80.	1.130(3)	1.161(3)	−2.7
100.	620.	635.4	−2.4
150.	941.	938.1	0.3
200.	449.	448.9	0.0
300.	160.	160.1	−0.1
400.	78.9	78.99	−0.1
500.	46.6	46.67	−0.1
600.	30.8	30.86	−0.2
800.	16.5	16.57	−0.4
1000.	10.5	10.49	0.1
1500.	4.79	4.830	−0.8
2. (3)	2.88	2.91	−1.0
3. (3)	1.48	1.50	−1.3
4. (3)	0.968	0.968	0.0
5. (3)	0.716	0.705	1.6
6. (3)	0.557	0.551	1.1
8. (3)	0.383	0.380	0.8
10. (3)	0.295	0.289	2.1
15. (3)	0.179	0.180	−0.6
20. (3)	0.129	0.130	−0.8
30. (3)	0.0830	0.0835	−0.6
40. (3)	0.0603	0.0615	−2.0
50. (3)	0.0485	0.0486	−0.2
60. (3)	0.0402	0.0402	0.0
80. (3)	0.0291	0.0299	−2.7
100. (3)	0.0232	0.0238	−2.5

contribution of higher subshells stems from the $2s$ subshell. Thus σ_a/σ_{1s} approaches the high-energy limit relatively rapidly, since at these energies the main contribution to the total cross section comes from the K and L shells. (Also note that the M shell is expected to behave as the L shell.) Even for the heavier elements (e.g., U) only about 5% of the contribution comes from the other subshells. Examining Schofield's and other results, we see that σ_a/σ_K is slowly varying as a function of energy. In view of this, we can say that choosing Scofield's σ_a/σ_K ratio for his high-energy values will cause an error of at most ~2%–3% for the heavy elements and much less for the light elements.

Our final result is

$$\sigma=\sigma_{GP}(\text{corrected})\Xi_K^2(\sigma_a/\sigma_K). \qquad (6.3.2)$$

Values of Ξ_K^2 are given in Table 4.2, and σ_a/σ_K for aluminum, tin, and uranium can be computed from values given in Tables 6.18–6.20. The $c(a, k)$'s used are zero except for uranium for which it has the value of -7.5 for $k=2$ MeV and decreases monotonically to -80 for $k=100$ MeV. We believe our final high-energy estimate to be valid within 10%, resulting from the estimated errors in σ_{GP}, Ξ_K^2, and σ_a/σ_K. Comparison of our high-energy results, based on the method just described, with those of the SI tables (see Tables 6.11–12) shows that for high energies the difference between the two sets of calculations is also small.

6.4 Comparison Between Theory and Experiment

6.4a Scope and Types of Experimental Data

Most of the experimental photoelectric data available is found in the range of 3–100 keV. The reason for this is that at high energies (hundreds and a few thousands of keV) measurements become more difficult. Also, there is less motivation to do these experiments because photoelectric cross sections in this region constitute a small fraction of the total attenuation cross section. Below 10 keV the measurements are more difficult to carry out due to the dominance of secondary effects such as emission of Auger electrons. At still lower energies good resolution is needed in order to examine the complex structures which go beyond the description of an isolated atom with the atomic field treated as a central potential (e.g. correlation effects, molecular effects, etc.); however these are outside the scope of this review.

As we do not attempt to review the experimental aspects of the process, we refer the reader who is interested in experimental techniques and more details to the references we mention and the literature quoted therein. We will just state the facts which are pertinent to our discussion. Traditionally the experiments are divided into two classes: (1) the total attenuation experiments, (2) the "direct" experiments. In experiments of the first class one uses a narrowly collimated beam source of radiation and the detector is also narrowly collimated. This way one can assume the exponential law for the intensity transmitted through the thin target slab

$$I(x)=I_0\exp(-\mu x),$$

where I_0 is the intensity of the source, x is the slab's thickness, $I(x)$ is the intensity detected, and μ is the "narrow beam" linear attenuation coefficient. When conditions for "narrow beam thin slab" do not apply

one has to consider corrections due to the geometry of the experiment (depending essentially on the source geometry) and the "build up factor" which takes into account secondary photons produced in the absorber which reach the detector. [For more details see Fano, Spencer, and Berger (1959) and Colgate (1952); references to such experiments are given by Veigele, Briggs, Bates, Henry, and Bracewell, 1971.] From the measured total absorption cross section one subtracts the calculated cross sections of the competing processes (coherent and incoherent scattering and pair production for energies above $2m_ec^2$). This so-called subtraction method thus yields results which depend on the theoretical knowledge of cross sections for other processes. At present we believe the theoretical knowledge of photoelectric cross sections to be better than for scattering. We will give some estimates in the next section.

In the second class of experiments, the photoeffect cross section (photoelectrons) are directly measured. The early experiments of this type (1920–1935) were usually performed by tracing the photoelectrons in a cloud chamber. This direct and visual method is inadequate because of the lack of sufficient statistics. Latyshev (1947) suggested the use of β-spectrometers and the method was later developed by Hedgran (1952), Hedgran and Hultberg (1954), and Hultberg (1955) (to which we refer the reader for technical details). In order to obtain the true angular distribution the experimental curves must be corrected for geometrical distortion and for multiple scattering in the converter, using Molière's (1947, 1948) theory. The shapes of the angular distributions were determined and from these ratios of cross sections of the various subshells. Absolute values could not be obtained because of the difficulty in determining the absolute radiation intensity. To solve this problem Hultberg and Stockendal (1958) and Hultberg (1959) devised a method giving a relation between the source intensity, the photoelectric cross section, and the internal conversion coefficient. By assuming knowledge of the internal conversion coefficients, which have been calculated by Sliv and Band (1956), Rose (1958), and more recently by Hager and Sletzer (1968) and Raman, Gunnick, Walkiewicz and Martin (1972), one could obtain absolute cross sections. Another approach was attempted by Titus (1959). Directly determining the incoherent flux with a photomultiplier, he measured the total intensity of the photoelectrons produced. The resolution was not good enough to distinguish the photoeffect from incoherent scattering. Therefore he subtracted the theoretical value for the latter in order to get the photoelectric cross section. Clearly the so called direct experiments depend on some theoretical knowledge. However they have important advantages over the total attenuation procedure: (1) One can distinguish contributions from the different subshells. (2) One can get angular distributions. (3) For some energy regions these types of experiments yield more accurate results than the subtraction method. Also they serve as an independent check on values of cross sections given by the total attenuation measurements. Generally speaking the accuracies claimed for both methods are in the range 2%–10%. The new total attenuation experiments claim the highest accuracy, but this cannot be entirely extended to the photoelectric cross sections themselves.

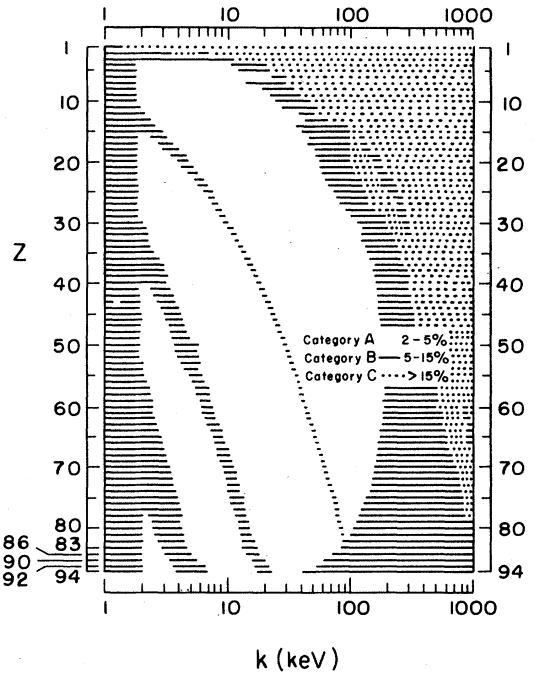

FIG. 5. Error estimates for experimental photoelectric cross sections determined by the subtraction method. The ranges of the error are designated as follows: Category $A=2\%$–5% (white area), Category $B=5\%$–15% (solid line) and Category $C>15\%$ (dotted line).

6.4b Comparison of Theory with Total Absorption and 'Direct' Measurements

The claimed accuracy of a total attenuation experiment cannot be considered the claimed accuracy of the photoelectric cross section. One must consider what share of the total attenuation coefficient is due to the photoeffect and what share to the competing processes: coherent and incoherent scattering and, for energies above $2m_ec^2$, pair production. Uncertainties in cross sections for competing processes will result in uncertainties for photoelectric cross sections deduced from attenuation experiments with subtraction methods. From the data of McMaster, Del Grande, Mallett, and Hubbell (1970) Sec. II, revision 1, one can get a good estimate of the percentage contributions of the

TABLE 6.13. Percentage contributions to the total attenuation coefficient.

	Z											
	13			29			50			92		
k (keV)	Coh.	Incoh.	Photo-effect	Coh.	Incoh.	Photo-effect	Coh.	Incoh.	Photo-effect	Coh.	Incoh.	Photo-effect
20	6.3	4.0	89.7	1.8	0.3	97.9	5.9	0.4	93.7	3.9	0.1	96
29.199							9.7	1.3	89			
30	10	13	77				1.7	0.2	98.1	4.0	0.2	95.8
40	13	27	60	4.6	2.7	92.7						
50	14	40	46				2.8	1.0	96.2	6.6	0.8	92.6
60	14	53	37	7.0	8.3	84.7						
80	11	71	18	8.6	17	74.4						
100	8.5	80	11.5	9.4	28	62.6	5.1	6.8	88.1	11	5.0	84
150				8.9	53	38.1	6.5	18	75.5	3.8	3.6	92.6
200	3.2	95	1.8	7.1	70	22.9	6.9	31	62.1	4.4	7.0	88.6
300				4.5	86	9.5	6.1	54	39.9	5.0	15	80
400							4.9	69	26.1	5.0	25	70
600							3.1	84	12.9	4.4	42	53.6
1000										2.9	63	34.1

various processes to the total attenuation cross section. In Table 6.13 we reproduce the results for a sample of elements (Al, Cu, Sn, and U) in an energy range of 20–1000 keV. This estimate utilizes results for the scattering processes obtained with the approximate form-factor approach. We have attempted to estimate the accuracy of such theoretical cross sections by comparing them with exact results of Brenner, Brown, and Woodward (1954), Brown, Peierls, and Woodward (1954), and Brown and Mayers (1955, 1957) and also with an approximate expression which they give. The form factor approach is best for low Z or for high energies. The biggest possible error in the total attenuation coefficient appears to be of the order of 4% for 50-keV photons scattered off uranium. Thus a more accurate determination of photoeffect cross sections in this region will require a better calculation of coherent and incoherent scattering. In Fig. 5 we present what we believe to be the errors in the experimental determination of photoelectric cross sections obtained by the subtraction method, taking into account both experimental and estimated theoretical inaccuracies involved in their determination. Estimates are given for all elements up to Pu and in the energy range of 1–1000 keV.

Except for a very limited number of results which perhaps may claim a slightly better accuracy (see Sec. 6.3a) we see that the accuracy is in the range of 2%–15%. The larger errors are in the high-energy region of each given atom (where "high energy" is relative to the atomic number), as in these regions the photoelectric effect constitutes a small fraction of the total process (cf. Table 6.13). In such cases the subtraction method gives large errors and should be avoided. This

TABLE 6.14. Comparison between theory (Scofield's HFS results) and experiment.

Z	Photon energy (keV)	Subshell	Experimental cross section (b/atom)	Theoretical cross section (b/atom)	Reference to experiment
92	1332	K	5.4±0.3	6.020	c
	1173	K	7.2±0.5	7.670	c
	122	L	360.±40.	279.8	d
	122	M	79.1±7.0[a]	67.71	d
	122	N_+	31.6±3.5[a]	23.48	d
82	2754	K	0.93±0.03	0.8450	e
	1332	K	3.24±0.13	2.943	e
	662	a[b]	13.8±0.8	12.23	f
	320	a	76.5±4.6	85.42	g

TABLE 6.14 (*Continued*)

Z	Photon energy (keV)	Subshell	Experimental cross section (b/atom)	Theoretical cross section (b/atom)	Reference to experiment
79	2620	*a*	0.74±0.06	0.9371	h
	662	*a*	11.62±0.16	12.64	i
78	662	*a*	11.3±0.7	11.94	f
	412	*a*	34.8±1.5	36.65	j
	320	*a*	62.8±3.8	69.51	k
	208	*a*	215.±6.	216.1	j
	158	*a*	434.±10.	451.4	j
	145	*a*	519.±52.	568.3	l
	123	*a*	848.±19.	880.9	j
	105	*a*	1286.±28.	1339.	j
	50	*a*	1983.±45.	2024.	j
73	2620	*a*	0.47±0.05	0.661	h
	662	*a*	8.55±0.14	8.90	i
	662	*a*	8.25±0.5		f
	320	*a*	76.5±4.6	52.77	k
	145	*a*	421.±42.	443.5	l
50	2620	*a*	0.11±0.03	0.123	h
	662	*a*	1.5±0.09	1.64	f
	320	*a*	1.02±0.6	10.48	f
	145	*a*	102.±8.	99.21	m
47	662	*a*	1.198±0.028	1.237	i
	662	*a*	1.12±0.07		f
	320	*a*	10.2±0.6	7.998	g
	208	*a*	27.8±1.0	27.03	j
	158	*a*	60.2±1.7	59.90	j
	145	*a*	80.±6.	76.88	m
	123	*a*	123.±3.	124.0	j
	105	*a*	198.±4.	196.0	j
	50	*a*	1646.±34.	1617	j
46	662	*a*	1.070±0.060	1.122	n
42	662	*a*	0.700±0.016	0.7425	i
29	662	*a*	0.125±0.009	0.1348	i
	208	*a*	3.43±0.3	3.271	j
	158	*a*	7.53±0.4	7.517	j
	145	*a*	10.5±0.8	9.764	m
	123	*a*	16.07±0.6	16.14	j
	105	*a*	26.7±0.8	26.16	j
	50	*a*	239.±5.	246.4	j

[a] Value computed from the experimental value of σ_L and the experimental ratios σ_L/σ_M and σ_M/σ_{N+}. (Here $N+$ means the N shell and all the higher shells.)

[b] *a* means total atomic cross section.

[c] Hultberg and Stockendal (1959).

[d] Boyd, Brantley, and Hamilton (1965).

[e] Bleeker, Goudsmit, and DeVries (1962).

[f] Parthasaradhi, Lakshminarayana, and Jnanananda (1964a).

[g] Parthasaradhi, Lakshminarayana, and Jnanananda (1966a).

[h] Titus (1965).

[i] Titus (1959).

[j] Parthasaradhi (1968).

[k] Parthasaradhi, Lakshminarayana, and Jnanananda (1966b).

[l] Parthasaradhi, Lakshminarayana, and Jnanananda (1965).

[m] Parthasaradhi, Lakshminarayana, and Jnanananda (1964b).

[n] Rao, Parthasaradhi, and Jnanananda (1969).

TABLE 6.15. Comparison between theory (Scofield's HFS results) and experiment. ($M+$ means the M shell and all the higher shells).

Z	Photon energy (keV)	Type of ratio	Experimental ratio	Theoretical ratio	Reference to experiment
92	1332	K/L	5.3±0.2	5.47	b
	1332	K/M_+	13.9±0.7	16.99	b
	1332	L/M_+	2.6±0.15	3.105	b
	1332	[a]a/K	1.26±0.02	1.242	b
	662	K/L	5.3±0.2	5.254	b
	662	K/M_+	13.9±0.7	16.24	b
	662	L/M_+	2.6±0.15	3.090	b
	662	a/K	1.26±0.02	1.252	b
	412	K/L	5.3±0.2	5.06	b
	412	K/M_+	13.9±0.7	15.57	b
	412	L/M_+	2.6±0.15	3.080	b
	412	a/K	1.26±0.02	1.262	b
	411	K/L	3.2±0.2	5.058	e
	167	$(L_I+L_{II})/L_{III}$	3.9±0.5	3.932	f
	159	$(L_I+L_{II})/L_{III}$	3.8±0.4	3.824	g
	159	M_+/M	1.4±0.4	1.348	g
	158	K/L	5.0±0.4	4.572	h
	158	$K/(L_I+L_{II})$	6.3±0.5	5.772	h
	158	$(L_I+L_{II})/L_{III}$	3.9±0.4	3.810	h
	135	$(L_I+L_{II})/L_{III}$	3.3±0.6	3.477	f
	122	$(L_I+L_{II})/L_{III}$	3.1±0.35	3.274	c
	122	L/M	4.55±0.44	4.133	c
	122	M/N_+	2.5±0.3	2.884	c
	103	$(L_I+L_{II})/L_{III}$	3.03±0.15	2.956	i
	103	L/M	3.70±0.20	4.126	i
	84	$(L_I+L_{II})/L_{III}$	2.3±0.1	2.608	d
	81	L_{II}/L_{III}	0.92±0.15	1.127	i
83	265	$(L_I+L_{II})/L_{III}$	5.0±0.5	5.460	j
	136.2	$(L_I+L_{II})/L_{III}$	3.9±0.3	3.803	j
	121.2	$(L_I+L_{II})/L_{III}$	3.8±0.8	3.548	j
	86.6	$(L_I+L_{II})/L_{III}$	2.6±0.5	2.874	j
82	411	K/L	3.70±0.27	5.784	e
79	878	K/L	5.7±1.0	6.247	j
	412	K/L	5.7±0.4	6.003	k
	412	K/L_I	8.5±0.5	8.605	k
	412	$(L_I+L_{II})/L_{III}$	7.2±0.8	6.939	k
	412	L_{II}/L_I	0.30±0.03	0.2530	k
	412	L_{III}/L_I	0.18±0.02	0.1806	k
	411	K/L	3.85±0.30	6.002	e
	298	K/L	5.6±1.0	5.902	j
	140	K/L	4.35±0.30	5.559	e
	81	L_{II}/L_{III}	0.89±0.15	0.976	i
47	411	K/L	7.7±1.0	8.39	e
	140	K/L	7.2±1.0	8.25	e

[a] a means total atomic cross section.
[b] Hultberg (1959).
[c] Boyd, Brantley, and Hamilton (1965).
[d] Jansen, Hultberg, Goudsmit, and Wapstra (1962).
[e] Marty (1952).
[f] Herrlander, Stockendal, and Gupta (1960).
[g] Ryde and Sujkowski (1962).
[h] Frey, Hamilton, and Hultberg (1963).
[i] Sujkowski (1961).
[j] Grigoryev and Zolotavin (1959).
[k] Bergkvist (1964).

can be seen very clearly when comparing Scofield's (1972) theoretical results with such experimental results as given in the compilation of Veigele, Briggs, Bates, Henry, and Bracewell (1971), as we will discuss in Sec. 6.5 (cf. Tables 6.16–6.17).

The second type of data is the so called "direct" measurements. Recent and accurate data of this type is quite scarce. We present the cross section data known to us in Table 6.14 and the shell ratio data in Table 6.15 and compare this with Scofield's theoretical values. The conclusions drawn for the subtraction method remain valid. The claimed experimental errors range from 4% to 15% and the difference between theory and experiment is also within these limits (except for one case). This is also generally true for the measured ratios.

6.5 Validity of Previous and Present Tabulations

Most tabulations give total absorption cross sections together with cross sections for the various processes contributing to the total. Our comments mainly apply to the photoelectric data. Though the early tabulations we mention here (Davisson and Evans, 1952; Grodstein, 1957; and Davisson, 1965) are mainly of historical interest, we find it appropriate to comment on them for two reasons: (1) This review tries to cover, at least to some extent, the developments of the subject since the early 1950's. (2) Some semiempirical methods used in these tabulations can now be given a theoretical justification whereas some are now known to be wrong.

The tabulation of Davisson and Evans (1952) was based on the following: For the energy range 10–350-keV results of Sauter's formula (6.1.2) multiplied by Stobbe's correction factor [square brackets in Eq. (6.1.1)] or Stobbe's formula (6.1.1) were tabulated. For the range 350–2000 keV Hulme's few values served as a basis for the tables and for higher energies Hall's formula (Hall, 1934, 1936) was used. The total atomic cross section was obtained by applying the "five fourths rule" to these K-shell results. All these cross sections were plotted, the graphs "smoothed" and final results were read from these graphs.

Grodstein (1957) followed a similar pattern, but instead of using the 5/4 law she used the ratio σ_{K+L+M}/σ_K as calculated with Stobbe's and similar formulas for the M shell, thus correcting cross sections for the low-Z values for which 5/4 is an overestimate.

TABLE 6.16. Comparison between theoretical and experimental (subtraction method) photoelectric cross sections of aluminum. $a\pm n$ shall mean $a\times10^{\pm n}$.

k (keV)	Theory[a]	Experiment LLL[b]	Experiment Kaman[c]
1	5.300+4	5.263+4	5.32+4
2	1.013+5	1.032+5	1.06+5
3	3.524+4	3.608+4	3.61+4
4	1.609+4	1.649+4	1.63+4
5	8.612+3	8.814+3	8.69+3
6	5.120+3	5.224+3	5.15+3
8	2.218+3	2.246+3	2.22+3
10	1.146+3	1.151+3	1.14+3
15	3.367+2	3.330+2	3.35+2
20	1.389+2	1.359+2	1.38+2
30	3.908+1	3.784+1	3.88+1
40	1.570+1	1.517+1	1.56+1
50	7.697+0	7.453+0	7.68+0
60	4.286+0	4.171+0	4.29+0
80	1.695+0	1.673+0	1.71+0
100	8.245−1	8.266−1	8.35−1
150	2.236−1	2.327−1	2.28−1
200	8.970−2	9.609−2	9.07−2
300	2.574−2	2.839−2	2.50−2
400	1.112−2	1.224−2	1.01−2
500	6.021−3	6.477−3	5.03−3
600	3.764−3	3.895−3	2.86−3
800	1.905−3	1.787−3	1.18−3
1000	1.184−3	9.970−4	6.03−4

[a] Scofield (1972).
[b] McMaster, Del Grande, Mallett, and Hubbell (1970).
[c] Veigele, Briggs, Bates, Henry, and Bracewell (1971).

TABLE 6.17. Same as Table 6.16 except for uranium.

k (keV)	Theory[a]	Experiment LLL[b]	Experiment Kaman[c]
1	2.614+6	2.899+6	4.09+6
2	7.323+5	6.822+5	9.38+5
3	2.997+5	2.886+5	3.35+5
4	5.213+5	4.281+5	4.99+5
5	3.479+5	3.257+5	3.38+5
6	2.452+5	2.508+5	2.57+5
8	1.202+5	1.198+5	1.23+5
10	6.860+4	6.750+4	6.98+4
15	2.430+4	2.382+4	2.48+4
20	2.700+4	2.626+4	2.71+4
30	1.566+4	1.536+4	1.55+4
40	7.383+3	7.302+3	7.20+3
50	4.092+3	4.067+3	3.97+3
60	2.515+3	2.508+3	2.45+3
80	1.161+3	1.158+3	1.14+3
100	6.354+2	6.307+2	6.28+2
150	9.381+2	9.417+2	9.35+2
200	4.489+2	4.445+2	4.43+2
300	1.601+2	1.580+2	1.57+2
400	7.899+1	7.799+1	7.61+1
500	4.667+1	4.609+1	4.38+1
600	3.086+1	3.050+1	2.80+1
800	1.657+1	1.648+1	1.40+1
1000	1.049+1	1.059+1	8.29+0

[a] Scofield (1972).
[b] McMaster, Del Grande, Mallett, and Hubbell (1970).
[c] Veigele, Briggs, Bates, Henry, and Bracewell (1971).

TABLE 6.18. Scofield's HFS cross sections for aluminum (in b/atom). Here $aE\pm n$ shall mean $a\times10^{\pm n}$. Symbols $1s$, $2s$, $2p$, $2\bar{p}$, $3s$, $3p$, and $3\bar{p}$ refer to K, $L_{\rm I}$, $L_{\rm II}$, $L_{\rm III}$, $M_{\rm I}$, $M_{\rm II}$, and $M_{\rm III}$, respectively.

k (keV)	$1s$	$2s$	$2p$	$2\bar{p}$	$3s$	$3p$	$3\bar{p}$	σ_a
1.000E+00	0.0E+00	2.4855E+04	8.8278E+03	1.7374E+04	1.7826E+03	5.3490E+01	1.0531E+02	5.2999E+04
1.500E+00	0.0E+00	1.0063E+04	2.3985E+03	4.7083E+03	7.1487E+02	1.4898E+01	2.9250E+01	1.7929E+04
1.548E+00	0.0E+00	9.3479E+03	2.1602E+03	4.2396E+03	6.6382E+02	1.3434E+01	2.6370E+01	1.6451E+04
1.561E+00	1.6084E+05	9.1757E+03	2.1040E+03	4.1291E+03	6.5153E+02	1.3088E+01	2.5690E+01	1.7694E+05
2.000E+00	9.3139E+04	5.0835E+03	9.1609E+02	1.7946E+03	3.6054E+02	5.7700E+00	1.1303E+01	1.0131E+05
3.000E+00	3.2595E+04	1.8431E+03	2.2509E+02	4.3945E+02	1.3073E+02	1.4348E+00	2.7951E+00	3.5238E+04
4.000E+00	1.4921E+04	8.6818E+02	8.0659E+01	1.5705E+02	6.1665E+01	5.1800E−01	1.0061E+00	1.6090E+04
5.000E+00	7.9965E+03	4.7600E+02	3.5799E+01	6.9539E+01	3.3805E+01	2.3093E−01	4.4751E−01	8.6123E+03
6.000E+00	4.7569E+03	2.8828E+02	1.8244E+01	3.5362E+01	2.0491E+01	1.1807E−01	2.2827E−01	5.1196E+03
8.000E+00	2.0627E+03	1.2831E+02	6.1832E+00	1.1935E+01	9.1325E+00	4.0180E−02	7.7369E−02	2.2184E+03
1.000E+01	1.0657E+03	6.7476E+01	2.6318E+00	5.0605E+00	4.8077E+00	1.7149E−02	3.2897E−02	1.1458E+03
1.500E+01	3.1328E+02	2.0362E+01	5.4183E−01	1.0335E+00	1.4532E+00	3.5457E−03	6.7436E−03	3.3668E+02
2.000E+01	1.2924E+02	8.5208E+00	1.7378E−01	3.2909E−01	6.0872E−01	1.1400E−03	2.1522E−03	1.3888E+02
3.000E+01	3.6371E+01	2.4351E+00	3.4619E−02	6.4700E−02	1.7417E−01	2.2766E−04	4.2400E−04	3.9080E+01
4.000E+01	1.4613E+01	9.8670E−01	1.1018E−02	2.0282E−02	7.0628E−02	7.2366E−05	1.3321E−04	1.5702E+01
5.000E+01	7.1628E+00	4.8625E−01	4.5307E−03	8.2482E−03	3.4825E−02	2.9764E−05	5.4204E−05	7.6968E+00
6.000E+01	3.9882E+00	2.7184E−01	2.1968E−03	3.9584E−03	1.9470E−02	1.4434E−05	2.6025E−05	4.2857E+00
8.000E+01	1.5773E+00	1.0805E−01	7.0607E−04	1.2506E−03	7.7411E−03	4.6401E−06	8.2241E−06	1.6950E+00
1.000E+02	7.6715E−01	5.2721E−02	2.9589E−04	5.1580E−04	3.7777E−03	1.9426E−06	3.3947E−06	8.2447E−01
1.500E+02	2.0806E−01	1.4361E−02	6.3077E−05	1.0679E−04	1.0292E−03	4.1366E−07	7.0328E−07	2.2362E−01
2.000E+02	8.3457E−02	5.7740E−03	2.1879E−05	3.6399E−05	4.1380E−04	1.4326E−07	2.3986E−07	8.9703E−02
3.000E+02	2.3941E−02	1.6604E−03	5.3001E−06	8.7016E−06	1.1899E−04	3.4581E−08	5.7462E−08	2.5735E−02
4.000E+02	1.0340E−02	7.1801E−04	2.0679E−06	3.4264E−06	5.1452E−05	1.3446E−08	2.2704E−08	1.1115E−02
5.000E+02	5.6011E−03	3.8920E−04	1.0393E−06	1.7677E−06	2.7889E−05	6.7468E−09	1.1710E−08	6.0211E−03
6.000E+02	3.5022E−03	2.4313E−04	6.1320E−07	1.0667E−06	1.7430E−05	3.9654E−09	7.1123E−09	3.7644E−03
8.000E+02	1.7718E−03	1.2303E−04	2.8161E−07	5.2323E−07	8.8277E−06	1.8197E−09	3.5109E−09	1.9045E−03
1.000E+03	1.1015E−03	7.6480E−05	1.6341E−07	3.1698E−07	5.4961E−06	1.0487E−09	2.1700E−09	1.1839E−03
1.500E+03	5.1749E−04	3.5938E−05	6.7042E−08	1.4616E−07	2.6001E−06	4.3805E−10	1.0467E−09	5.5624E−04

TABLE 6.19. Scofield's HFS cross sections for tin (in b/atom).

k (keV)	$1s$	$2s$	$2p$	$2\bar{p}$	$3s$	$3p$	$3\bar{p}$	$3d$	$3\bar{d}$	σ_a
1.000E+00	0.0E+00	0.0E+00	0.0E+00	0.0E+00	7.6501E+04	1.0587E+05	2.3111E+05	4.0498E+05	5.9069E+05	1.6064E+06
1.500E+00	0.0E+00	0.0E+00	0.0E+00	0.0E+00	4.3891E+04	6.1593E+04	1.2556E+05	1.3629E+05	1.9671E+05	6.4827E+05
2.000E+00	0.0E+00	0.0E+00	0.0E+00	0.0E+00	2.7983E+04	3.7665E+04	7.4186E+04	5.8616E+04	8.4067E+04	3.2683E+05
3.000E+00	0.0E+00	0.0E+00	0.0E+00	0.0E+00	1.3982E+04	1.6908E+04	3.1990E+04	1.6445E+04	2.3359E+04	1.1986E+05
3.923E+00	0.0E+00	0.0E+00	0.0E+00	0.0E+00	8.5782E+03	9.3886E+03	1.7354E+04	6.7494E+03	9.5224E+03	6.0549E+04
3.954E+00	0.0E+00	0.0E+00	0.0E+00	1.2387E+05	8.4518E+03	9.2198E+03	1.7030E+04	6.5694E+03	9.2665E+03	1.8319E+05
4.000E+00	0.0E+00	0.0E+00	0.0E+00	1.2650E+05	8.2717E+03	8.9803E+03	1.6571E+04	6.3170E+03	8.9079E+03	1.8408E+05
4.157E+00	0.0E+00	0.0E+00	0.0E+00	1.1366E+05	7.6954E+03	8.2206E+03	1.5119E+04	5.5413E+03	7.8058E+03	1.6580E+05
4.190E+00	0.0E+00	0.0E+00	5.8186E+04	1.1135E+05	7.5805E+03	8.0703E+03	1.4833E+04	5.3922E+03	7.5942E+03	2.2062E+05
4.436E+00	0.0E+00	0.0E+00	5.2659E+04	9.6761E+04	6.8036E+03	7.0649E+03	1.2927E+04	4.4322E+03	6.2326E+03	1.9348E+05
4.472E+00	0.0E+00	2.8696E+04	5.1668E+04	9.4853E+04	6.7012E+03	6.9339E+03	1.2680E+04	4.3119E+03	6.0621E+03	2.1838E+05
5.000E+00	0.0E+00	2.3969E+04	3.9290E+04	7.0525E+04	5.4098E+03	5.3158E+03	9.6307E+03	2.9240E+03	4.0981E+03	1.6606E+05
6.000E+00	0.0E+00	1.7476E+04	2.3894E+04	4.2177E+04	3.7839E+03	3.3951E+03	6.0622E+03	1.5312E+03	2.1348E+03	1.0354E+05
8.000E+00	0.0E+00	1.0239E+04	1.0681E+04	1.8420E+04	2.1130E+03	1.6176E+03	2.8227E+03	5.3469E+02	7.3871E+02	4.8635E+04
1.000E+01	0.0E+00	6.5991E+03	5.5944E+03	9.4666E+03	1.3231E+03	8.8570E+02	1.5177E+03	2.3044E+02	3.1588E+02	2.6751E+04
1.500E+01	0.0E+00	2.8051E+03	1.6523E+03	2.7001E+03	5.4446E+02	2.8030E+02	4.6410E+02	4.7469E+01	6.4022E+01	8.8349E+03
2.000E+01	0.0E+00	1.4683E+03	6.7462E+02	1.0737E+03	2.8163E+02	1.1916E+02	1.9223E+02	1.4960E+01	1.9908E+01	3.9711E+03
2.916E+01	0.0E+00	6.0105E+02	2.0173E+02	3.0965E+02	1.1444E+02	3.7233E+01	5.7878E+01	3.1815E+00	4.1478E+00	1.3740E+03
2.939E+01	6.9752E+03	5.8950E+02	1.9658E+02	3.0150E+02	1.1222E+02	3.6310E+01	5.6398E+01	3.0779E+00	4.0108E+00	8.3186E+03
3.000E+01	6.7001E+03	5.6071E+02	1.8388E+02	2.8144E+02	1.0672E+02	3.4036E+01	5.2753E+01	2.8261E+00	3.6783E+00	7.9675E+03
4.000E+01	3.1603E+03	2.7393E+02	7.1601E+01	1.0625E+02	5.2071E+01	1.3602E+01	2.0431E+01	8.4965E−01	1.0858E+00	3.7186E+03
5.000E+01	1.7308E+03	1.5447E+02	3.4139E+01	4.9367E+01	2.9377E+01	6.5949E+00	9.6490E+00	3.3265E−01	4.1857E−01	2.0250E+03
6.000E+01	1.0510E+03	9.5752E+01	1.8562E+01	2.6242E+01	1.8227E+01	3.6281E+00	5.1885E+00	1.5451E−01	1.9185E−01	1.2248E+03
8.000E+01	4.7060E+02	4.4274E+01	7.0657E+00	9.6164E+00	8.4468E+00	1.4029E+00	1.9305E+00	4.6221E−02	5.6157E−02	5.4600E+02
1.000E+02	2.4972E+02	2.4050E+01	3.3397E+00	4.4046E+00	4.5980E+00	6.6976E−01	8.9289E−01	1.8258E−02	2.1814E−02	2.8906E+02
1.500E+02	7.7920E+01	7.7918E+00	8.6535E−01	1.0750E+00	1.4954E+00	1.7598E−01	2.2095E−01	3.4743E−03	4.0422E−03	8.9967E+01
2.000E+02	3.4092E+01	3.4843E+00	3.3844E−01	4.0327E−01	6.7033E−01	6.9323E−02	8.3484E−02	1.1091E−03	1.2765E−03	3.9325E+01
3.000E+02	1.0865E+01	1.1366E+00	9.4490E−02	1.0711E−01	2.1931E−01	1.9521E−02	2.2303E−02	2.3884E−04	2.7489E−04	1.2523E+01
4.000E+02	4.9876E+00	5.2763E−01	4.0043E−02	4.4367E−02	1.0189E−01	8.3069E−03	9.2682E−03	8.5609E−05	1.0086E−04	5.7458E+00
5.000E+02	2.8058E+00	2.9850E−01	2.1277E−02	2.3397E−02	5.7687E−02	4.4254E−03	4.8942E−03	4.0463E−05	4.8838E−05	3.2310E+00
6.000E+02	1.7941E+00	1.9142E−01	1.3016E−02	1.4325E−02	3.7005E−02	2.7114E−03	2.9991E−03	2.2606E−05	2.8257E−05	2.0651E+00
8.000E+02	9.2822E−01	9.9215E−02	6.2930E−03	7.0185E−03	1.9185E−02	1.3130E−03	1.4719E−03	9.4952E−06	1.3088E−05	1.0676E+00
1.000E+03	5.7979E−01	6.1966E−02	3.7424E−03	4.2333E−03	1.1980E−02	7.8278E−04	8.8958E−04	5.2896E−06	7.4034E−06	6.6643E−01
1.500E+03	2.6830E−01	2.8606E−02	1.6082E−03	1.8832E−03	5.5297E−03	3.3572E−04	3.9588E−04	1.9363E−06	3.1645E−06	3.0806E−01

TABLE 6.20. Scofield's HFS cross sections for uranium (in b/atom).

k (keV)	$1s$	$2s$	$2p$	$2\bar{p}$	$3s$	$3p$	$3\bar{p}$	$3d$	$3\bar{d}$	σ_a
1.000E+00	0.0E+00	0.0E+00	0.0E+00	0.0E+00	0.0E+00	0.0E+00	0.0E+00	0.0E+00	0.0E+00	2.6138E+06
1.029E+00	0.0E+00	0.0E+00	0.0E+00	0.0E+00	0.0E+00	0.0E+00	0.0E+00	0.0E+00	0.0E+00	2.4827E+06
1.038E+00	0.0E+00	0.0E+00	0.0E+00	0.0E+00	0.0E+00	0.0E+00	0.0E+00	0.0E+00	0.0E+00	2.6035E+06
1.264E+00	0.0E+00	0.0E+00	0.0E+00	0.0E+00	0.0E+00	0.0E+00	0.0E+00	0.0E+00	0.0E+00	1.8083E+06
1.274E+00	0.0E+00	0.0E+00	0.0E+00	0.0E+00	0.0E+00	0.0E+00	0.0E+00	0.0E+00	0.0E+00	1.8056E+06
1.421E+00	0.0E+00	0.0E+00	0.0E+00	0.0E+00	0.0E+00	0.0E+00	0.0E+00	0.0E+00	0.0E+00	1.4569E+06
1.432E+00	0.0E+00	0.0E+00	0.0E+00	0.0E+00	0.0E+00	0.0E+00	0.0E+00	0.0E+00	0.0E+00	1.4619E+06
1.500E+00	0.0E+00	0.0E+00	0.0E+00	0.0E+00	0.0E+00	0.0E+00	0.0E+00	0.0E+00	0.0E+00	1.3315E+06
2.000E+00	0.0E+00	0.0E+00	0.0E+00	0.0E+00	0.0E+00	0.0E+00	0.0E+00	0.0E+00	0.0E+00	7.3229E+05
3.000E+00	0.0E+00	0.0E+00	0.0E+00	0.0E+00	0.0E+00	0.0E+00	0.0E+00	0.0E+00	0.0E+00	2.9966E+05
3.551E+00	0.0E+00	0.0E+00	0.0E+00	0.0E+00	0.0E+00	0.0E+00	0.0E+00	0.0E+00	0.0E+00	2.0381E+05
3.579E+00	0.0E+00	0.0E+00	0.0E+00	0.0E+00	0.0E+00	0.0E+00	0.0E+00	0.0E+00	2.8529E+05	4.8538E+05
3.733E+00	0.0E+00	0.0E+00	0.0E+00	0.0E+00	0.0E+00	0.0E+00	0.0E+00	0.0E+00	2.5243E+05	4.3401E+05
3.763E+00	0.0E+00	0.0E+00	0.0E+00	0.0E+00	0.0E+00	0.0E+00	0.0E+00	1.8083E+05	2.4727E+05	6.0635E+05
4.000E+00	0.0E+00	0.0E+00	0.0E+00	0.0E+00	0.0E+00	0.0E+00	0.0E+00	1.5356E+05	2.1318E+05	5.2134E+05
4.285E+00	0.0E+00	0.0E+00	0.0E+00	0.0E+00	0.0E+00	0.0E+00	0.0E+00	1.3029E+05	1.7804E+05	4.3990E+05
4.319E+00	0.0E+00	0.0E+00	0.0E+00	0.0E+00	0.0E+00	0.0E+00	7.1224E+04	1.2768E+05	1.7419E+05	5.0222E+05
5.000E+00	0.0E+00	0.0E+00	0.0E+00	0.0E+00	0.0E+00	0.0E+00	5.6631E+04	8.5492E+04	1.1449E+05	3.4792E+05
5.178E+00	0.0E+00	0.0E+00	0.0E+00	0.0E+00	0.0E+00	0.0E+00	5.3440E+04	7.7362E+04	1.0333E+05	3.1813E+05
5.219E+00	0.0E+00	0.0E+00	0.0E+00	0.0E+00	0.0E+00	1.9350E+04	5.2699E+04	7.5609E+04	1.0093E+05	3.3100E+05
5.524E+00	0.0E+00	0.0E+00	0.0E+00	0.0E+00	0.0E+00	1.8222E+04	4.7449E+04	6.4097E+04	8.5883E+04	2.8759E+05
5.568E+00	0.0E+00	0.0E+00	0.0E+00	0.0E+00	1.2175E+04	1.8065E+04	4.6729E+04	6.2722E+04	8.3952E+04	2.9421E+05
6.000E+00	0.0E+00	0.0E+00	0.0E+00	0.0E+00	1.0873E+04	1.6812E+04	4.0400E+04	5.0950E+04	6.7276E+04	2.4523E+05
8.000E+00	0.0E+00	0.0E+00	0.0E+00	0.0E+00	7.2674E+03	1.1085E+04	2.3018E+04	2.1693E+04	2.8009E+04	1.2023E+05
1.000E+01	0.0E+00	0.0E+00	0.0E+00	0.0E+00	5.1706E+03	7.6440E+03	1.4375E+04	1.0873E+04	1.3795E+04	6.8598E+04
1.500E+01	0.0E+00	0.0E+00	0.0E+00	0.0E+00	2.5835E+03	3.5267E+03	5.6812E+03	2.9245E+03	3.5861E+03	2.4305E+04
1.716E+01	0.0E+00	0.0E+00	0.0E+00	0.0E+00	2.0187E+03	2.6616E+03	4.0939E+03	1.8615E+03	2.2560E+03	1.7143E+04
1.730E+01	0.0E+00	0.0E+00	0.0E+00	2.3311E+04	1.9891E+03	2.6170E+03	4.0145E+03	1.8121E+03	2.1943E+03	4.0104E+04
2.000E+01	0.0E+00	0.0E+00	0.0E+00	1.5490E+04	1.5153E+03	1.9090E+03	2.7932E+03	1.1054E+03	1.3204E+03	2.6999E+04
2.103E+01	0.0E+00	0.0E+00	0.0E+00	1.3534E+04	1.3763E+03	1.7087E+03	2.4602E+03	9.3067E+02	1.1060E+03	2.3635E+04
2.119E+01	0.0E+00	0.0E+00	9.7202E+03	1.3247E+04	1.3553E+03	1.6786E+03	2.4106E+03	9.0540E+02	1.0751E+03	3.2860E+04
2.178E+01	0.0E+00	0.0E+00	9.1337E+03	1.2311E+04	1.2860E+03	1.5794E+03	2.2486E+03	8.2420E+02	9.7603E+02	3.0659E+04
2.195E+01	0.0E+00	4.6686E+03	8.9940E+03	1.2048E+04	1.2663E+03	1.5513E+03	2.2029E+03	8.0170E+02	9.4867E+02	3.4734E+04
3.000E+01	0.0E+00	2.6946E+03	4.0903E+03	4.9101E+03	6.8039E+02	7.4855E+02	9.6482E+02	2.6709E+02	3.0603E+02	1.5659E+04
4.000E+01	0.0E+00	1.5379E+03	1.9042E+03	2.0958E+03	3.7384E+02	3.6896E+02	4.3584E+02	9.4727E+01	1.0515E+02	7.3834E+03
5.000E+01	0.0E+00	9.7385E+02	1.0369E+03	1.0652E+03	2.3107E+02	2.0884E+02	2.3062E+02	4.1854E+01	4.5256E+01	4.0916E+03
6.000E+01	0.0E+00	6.6030E+02	6.2533E+02	6.0771E+02	1.5442E+02	1.2969E+02	1.3553E+02	2.1340E+01	2.2566E+01	2.5154E+03
8.000E+01	0.0E+00	3.4885E+02	2.7826E+02	2.4778E+02	8.0338E+01	6.0117E+01	5.7562E+01	7.3189E+00	7.4651E+00	1.1609E+03
1.000E+02	0.0E+00	2.0884E+02	1.4750E+02	1.2275E+02	4.7765E+01	3.2751E+01	2.9287E+01	3.1888E+00	3.1626E+00	6.3537E+02
1.162E+02	0.0E+00	1.4689E+02	9.6145E+01	7.6450E+01	3.3500E+01	2.1700E+01	1.8532E+01	1.8265E+00	1.7784E+00	4.2361E+02
1.171E+02	1.3461E+03	1.4415E+02	9.3980E+01	7.4547E+01	3.2870E+01	2.1229E+01	1.8085E+01	1.7733E+00	1.7248E+00	1.7607E+03

TABLE 6.20 (*Continued*)

k (keV)	$1s$	$2s$	$2p$	$2\bar{p}$	$3s$	$3p$	$3\bar{p}$	$3d$	$3\bar{d}$	σ_a
1.500E+02	7.2575E+02	7.9777E+01	4.6335E+01	3.4103E+01	1.8148E+01	1.0716E+01	8.4617E+00	7.0993E−01	6.7104E−01	9.3813E+02
2.000E+02	3.5065E+02	3.9766E+01	2.0496E+01	1.3856E+01	9.0404E+00	4.8474E+00	3.5114E+00	2.4976E−01	2.2955E−01	4.4889E+02
3.000E+02	1.2612E+02	1.4930E+01	6.6590E+00	4.0245E+00	3.3970E+00	1.6128E+00	1.0422E+00	5.9972E−02	5.3838E−02	1.6006E+02
4.000E+02	6.2563E+01	7.5664E+00	3.0908E+00	1.7406E+00	1.7227E+00	7.5763E−01	4.5554E−01	2.2865E−02	2.0510E−02	7.8986E+01
5.000E+02	3.7111E+01	4.5370E+00	1.7451E+00	9.3635E−01	1.0331E+00	4.3076E−01	2.4647E−01	1.1211E−02	1.0156E−02	4.6670E+01
6.000E+02	2.4614E+01	3.0254E+00	1.1155E+00	5.7790E−01	6.8885E−01	2.7652E−01	1.5262E−01	6.5009E−03	5.9513E−03	3.0861E+01
8.000E+02	1.3274E+01	1.6375E+00	5.7116E−01	2.8172E−01	3.7265E−01	1.4227E−01	7.4666E−02	2.8621E−03	2.7012E−03	1.5569E+01
1.000E+02	8.4299E+00	1.0400E+00	3.5188E−01	1.6783E−01	2.3654E−01	8.7858E−02	4.4558E−02	1.5966E−03	1.5294E−03	1.0493E+01
1.500E+03	3.8927E+00	4.7868E−01	1.5857E−01	7.1593E−02	1.0874E−01	3.9733E−02	1.8962E−02	6.2316E−04	6.3271E−04	4.8296E+00

She treated screening (incorrectly as we known now) by using $Z_{\text{eff}}=Z-0.3$ and also applied semiempirical correction factors for the energy range 10–100 keV so that the tabulated values become larger and closer to the experimental values. Comparison of these Tables with the latest tabulations shows that for medium and heavy elements in the energy range of 0.1–1.0 MeV the results agree to within 5%. However, the discrepancies increase for higher energies (40% for tin and 60% for uranium at 10 MeV) or when energies drop below the K-shell threshold (35% for uranium at 10 keV). For aluminum the results given (for $k=10$–400 keV) are within 5%–10%.

Davisson's later Table (1965) used the interpolated experimental data of McGinnies (1959) for the energy range 10–50 keV, and a version of the Gavrila-Pratt formula for the energy range 400–2000 keV. Another improvement was the use of the ratios σ_a/σ_K which were taken from Kirchner's (1930) experimental values at threshold. Generally the same discrepancies exist as in Grodstein's tables with the exception that for high energies the discrepancies here are smaller (5%–10%) because of the use of the Gavrila–Pratt formula. Through not always sufficiently accurate these tabulations gave a quite fair account of the process and were extensively used in the fields of nuclear physics and radiation shielding.

In Sec. 6.3 we have discussed the accuracies involved in the theoretical tabulations of Storm and Israel (1970) and Scofield (1972) and also compared them. We will now discuss a second type of tabulations: those which combine experimental and theoretical values. One such tabulation [which evolved from the NBS Report 8681, 2nd edition by Hubbell and Berger, 1966, is that of Hubbell (1969, 1971)]. It contains photoelectric cross sections for 23 elements in the energy range 10 keV–100 MeV. For energies up to 100 keV the results are purely those of the subtraction method procedure and the scattering data are taken from Strom and Israel (1967) except for uranium where the data is taken directly from Rakavy and Ron (1967). For higher energies they used Davisson's (1965) and Hultberg, Nagel, and Olsson's (1968) theoretical values. The high-energy data are based upon the Gavrila–Pratt formula. The computed K-shell cross sections were converted to total atomic cross sections by using Kirchner's ratios and taking into account some energy dependence of this ratio for the heavier elements as deduced from the Rakavy and Ron (1967) results. Hubbell also gives analytic expressions which fit the data presented. More extensive fits of this type are given by Biggs and Lighthill (1971).

McMaster, Del Grande, Mallett, and Hubbell (1970) performed least-squares fitting to an extensive documented combination of theoretical values and experimental data in the energy range of 1–1000 keV. The experimental results were weighted according to their assessed accuracy. Extensive use was made of

the Schmickley and Pratt (1967) Tables. L- and M-shell jump ratios were calculated from the theoretical values of Rakavy and Ron (1967) and additional theoretical data was used: i.e., Davisson (1965), Hultberg, Nagel, and Olsson (1968), and Hall and Sullivan (1966). The claimed accuracy is 2%–15%. We have discussed this work in Sec. 6.4 and it is represented in Fig. 5 for elements $Z=1$–94, and $k=$ 1–1000 keV.

These last compilations were used to compose the ENDF/B (Evaluated Nuclear Data File) photon interaction cross sections library tape. Values up to 1 MeV were taken from McMaster, Del Grande, Mallett, and Hubbell (1970), and values for energies ranging between 1 MeV and 100 MeV were taken from Hubbell (1969). Simmons and Hubbell (1971) compared the ENDF/B compliation with that of Storm and Israel (1970). The differences become bigger than about 5% for elements $Z \gtrsim 26$ and photon energies in the range of about 1–5 keV and again for energies in the MeV range. The latter probably reflects the fact that different approaches to the Gavrila–Pratt formula and the ratios σ_a/σ_{1s} were taken.

The last compilation we mention is that of Veigele, Briggs, Bates, Henry, and Bracewell (1971), who gave cross sections for the elements $Z=1$–94 in the energy range of 0.1 keV to 1 MeV. These authors made an extensive survey of the experimental data existing from 1920 to 1970. Assumptions of smoothness in Z and energy allowed then to go from discrete data points to a uniform tabulation. The photoelectric cross sections presented are solely based upon the subtraction method, except for energies from 0.1 keV to between 1 keV and 10 keV for which nonrelativistic calculations, using nonrelativistic HFS potentials, were performed. The discrepancy between Scofield's results and this tabulation (Tables 6.16–6.17) is large for the higher energies were photoeffect is a small component of the total attenuation cross section (see Table 6.12) and is a consequence of the use of the subtraction method in that region. One should avoid using such cross sections at these energies. There exists also a large discrepancy for the lower energies for uranium (Table 6.16). It stems from the difference in the total attenuation coefficients which they use and we have not traced the error. The claimed uncertainties are similar to those of the other tabulation and are 2%–20%.

7. CONCLUSIONS

In this review article we have attempted to summarize our present understanding of the photoelectric process for photon energies above 10 keV. Between 10 keV and 5 MeV, theoretical predictions accurate within a few percent can be obtained with the aid of modern electronic computers; these agree with experimental results of similar accuracy. The theoretical model needed for this purpose describes the process as a first-order transition, due to the electromagnetic field of the photon, between the initial bound and final continuum state of a single electron in a central potential determined self-consistently for the atom. Both higher-order Coulomb and electron-screening effects are important, and the accurate cross sections can differ by almost an order of magnitude from simple Born approximation predictions.

Considerable insight has been obtained from the realization that throughout most of the energy range considered here the momentum transfers to the nucleus in the photoelectric process are of order unity. This means that the important regions in configuration space for the process are at electron Compton wavelength distances, well *inside* the region for which electron wave functions are large. At such distances the *shape* of electron wave functions is independent of electron screening, and the shapes of electron wave functions of the same angular momentum but different energy are similar. Consequently, screening enters only through wave function normalization. A screened cross section can be obtained from a point-Coulomb cross section simply by changing the normalization; angular distribution shapes and polarization correlations are independent of screening. For the same reason the ratios of cross sections from certain subshells (such as L_I/K) are constant; in such cases the angular distribution shapes and polarization correlations are the same.

The circumstances in which our understanding of atomic photoeffect is most deficient are at high energies (above 5 MeV), at low energies (below 10 keV), and for low Z ($Z<13$) at all energies. The problem at higher energies concerns mathematical techniques for calculating the consequences of the present model for the process, while in the second and third circumstance the problem is to extend the present model. High-energy limit results are available for the photoeffect, but in the range from 5 to 50 MeV where interpolation techniques must now be used, considerable errors may result. However, since such cross sections are small and experiments have not been possible, there is no present incentive for improving the high-energy predictions. Similarly, until considerably more accurate experimental results are in prospect, there is no great incentive to attempt to improve the numerical predictions described here for the energy range 10 keV to 5 MeV. The situation is quite different below 10 keV, where the claimed experimental accuracy remains unchanged but the expected accuracy of the theoretical predictions rapidly deteriorates, due to inadequacies of the effective central potential model. In addition, for low-Z elements bound state normalization is more sensitive to the choice of potential, so that the problem persists at higher energies. In all cases at low energies the importance of exchange and correlation effects remains to be established, and explanations are needed

for the complex structures which develop near threshold. Such subjects are not ready for review but rather are the topics for further investigation.

ACKNOWLEDGMENTS

We are grateful to Dr. J. Scofield for the extensive calculations that he performed at our request. We also thank Dr. D. Liberman for sending us his program, which calculates the HFS atomic potentials, and Drs. E. Strom, H. I. Israel, and Wm. J. Veigele for clarifying some points regarding their tables. We wish to thank Professor U. Fano for encouraging us to carry out this work and Nancy Del Grande for her continued interest and her advice on experiments and tabulations. In addition we would like to thank our many colleagues in this field for their helpful comments on the preliminary draft of this manuscript.

REFERENCES

Abramowitz, M., and I. A. Stegun, 1965, *Handbook of Mathematical Functions* (Dover, New York).
Aglintsev, K. K., V. V. Mitrofanov, A. A. Rimskii-Korsakov, V. V. Smirnov, 1961, Izv. Ak. Nauk USSR **25,** 1146
Akhiezer, A. A., and V. B. Berestetskii, 1965, *Quantum Electrodynamics* (Interscience, New York).
Alling, W. R., and W. R. Johnson, 1965, Phys. Rev. **139,** A1050.
Amusia, M. Ya., N. A. Cherepkov, and S. I. Sheftel, 1967, Phys. Letters A **24,** 541.
——, N. A. Cherepkov, L. V. Chernysheva, and S. I. Sheftel, 1969, Sov. Phys. JETP **29,** 1018.
Azaroff, L. V., and D. M. Pease, 1973, *X-Ray Absorption Spectra, X-Ray Spectra,* edited by L. V. Azaroff (McGraw-Hill, to be published).
Band, I. M., L. A. Sliv, and M. B. Trzhaskovskaya, 1970, Sov. Phys. JETP Letters **11,** 201 (1970) [Zh. Eksperim. i Teor. Fiz. Pis. Red. **11,** 306 (1970)].
Banerjee, H., 1958, Nuovo Cimento, Serie X, **10,** 863.
——, 1959, Nuovo Cimento, Serie X, **11,** 220.
Bearden, A. J., 1966, J. Appl. Phys. **37,** 1681.
Berestetskii, V. B., E. M. Lifshitz, and L. P. Pitaevskii, 1971, *Relativistic Quantum Theory* (Pergamon, New York) (translated from the Russian by J. B. Skyes and J. S. Bell).
Bergkvist, K. E., 1964, Arkiv för Fysik, **27,** p. 483–500.
——, and S. Hultberg, 1964, Arkiv för Fysik **27,** 321.
Bethe, H. A., L. Maximon, and F. Low, 1953, Phys. Rev. **91,** 417.
——, and L. C. Maximon, 1954, Phys. Rev. **93,** 768.
——, and E. E. Salpeter, 1957, *Quantum Mechanics of One and Two-Electron Atoms* (Springer-Verlag, Berlin).
Biggs, F., and R. Lighthill, 1971, *Analytical Approximations for X-ray Cross Sections II,* Sandia Corporation, Albuquerque, N. Mexico, SC-RR-71 0507.
Bjorken, J. D., and S. D. Drell, 1964, *Relativistic Quantum Mechanics* (McGraw-Hill, New York).
Bleeker, E. J., P. F. A. Goudsmit, and C. De Vries, 1962, Nucl. Phys. **29,** 452.
Boyd, H. W., W. H. Brantley, and J. H. Hamilton, 1965, Nuovo Cimento, **39,** 1.
Boyer, R. H., 1957, Ph.D. thesis, Oxford University, 1957 (unpublished).
——, 1960, Phys. Rev. **117,** 475.
Briet, G., 1929, Phys. Rev. **34,** 553.
——, 1930, Phys. Rev. **36,** 383.
——, 1931, Phys. Rev. **39,** 616.
Brenner, S., G. E. Brown, and J. B. Woodward, 1954, Proc. Roy. Soc. (London) **A227,** 59.
Brini, D., L. Peli, O. Rimondi, and P. Veronesi, 1957, Nuovo Cimento, Serie X, Vol. **6,** 98.
Brown, G. E., and D. F. Mayers, 1955, Proc. Roy. Soc. (London) **A234,** 387.
——, and D. F. Mayers, 1957, Proc. Roy. Soc. (London) **A242,** 89.
——, R. E. Peierls, and J. B. Woodward, 1954, Proc. Roy. Soc. (London) **A227,** 51.
Brysk, H., and M. E. Rose, 1958, Rev. Mod. Phys. **30,** 1169.
——, and C. D. Zerby, 1968, Phys. Rev. **171,** 292.
Burgess, A., and M. J. Seaton, 1960, M. N. Roy. Astron. Soc. **120,** 121.
Chang, E. S., and M. R. C. McDowell, 1968, Phys. Rev. **176,** 126.
Colgate, S. A., 1952, Phys. Rev. **87,** 592.
Condon, E. U., and G. H. Shortley, 1935, *The Theory of Atomic Spectra* (Cambridge U. P., London).
Conneely, M. J., K. Smith, and L. Lipsky, 1970, J. Phys. B **3,** 493.
Conner, A. L., H. F. Atwater, and E. H. Plassmann, 1970, Phys. Rev. A **1,** 539.
Cooper, J. W., 1962, Phys. Rev. **128,** 681.
——, 1964, Phys. Rev. Letters **13,** 762.
——, and S. T. Manson, 1969, Phys. Rev. **177,** 157.
Corbató, F. J., and J. L. Uretsky, 1959, J. Assoc. Comp. Mach. **6,** 366.
Coulthard, M. A., 1967, Proc. Phys. Soc. (London) **91,** 44.
Cown, R. D., A. C. Larson, D. Liberman, J. B. Mann, and J. Waber, 1966, Phys. Rev. **144,** 5.
Csavinszky, P., 1968, Phys. Rev. **166,** 53.
Dalitz, R. H., 1951, Proc. Roy. Soc. (London) **206,** 509.
Darwin, C. G., 1928, Proc. Roy. Soc. (London) **A118,** 654.
Davisson, C. M., and R. D. Evans, 1952, Rev. Mod. Phys. **24,** 79 (1952).
——, 1965, in *Alpha- Beta- and Gamma-ray Spectroscopy,* edited by K. Siegbahn (North-Holland, Amsterdam), Vol. 1, Chapt. 2.
Desiderio, A. M., and W. R. Johnson, 1971, Phys. Rev. **A4,** 1267.
Deslattes, R. D., 1958, *An Experimental Study of X-Ray Attenuation Coefficients 8-30 keV,* Florida State University, AFOSR Report TN-58-784 (1958).
Dyson, F. J., 1949, Phys. Rev. **75,** 486; **75,** 1736.
Edmonds, A. R., 1957, *Angular Momentum in Quantum Mechanics* (Princeton U. P., Princeton, N.J.).
Einstein, A., 1905, Ann. Physik **17,** 132.
Erber, T., 1958, Bull. Am. Phys. Soc. Ser. II, **3,** 53.
——, 1959, Ann. Phys. (N.Y.) **8,** 435.
Erdélyi, A., W. Magnus, F. Oberhettinger, and F. G. Tricomi, 1953, *Higher Transcendental Functions* (Bateman Manuscript Project (McGraw-Hill, New York), Vols. I/II.
Fano, U., 1969, Phys. Rev. **178,** 131.
——, and J. W. Cooper, 1968, Rev. Mod. Phys. **40,** 441.
——, K. W. McVoy, and J. R. Albers, 1959, Phys. Rev. **116,** 1147.
——, L. V. Spencer, and M. J. Berger, 1959, in *Encyclopedia of Physics,* edited by Flügge (Springer-Verlag, Berlin), Vol. XXXVIII/2.
Farnoux, F. C., 1969, J. Physique **30,** 521.
Feynman, R. P., 1949, Phys. Rev. **76,** 749; **76,** 769.
——, N. Metropolis, and E. Teller, 1949, Phys. Rev. **75,** 1561.
Fischer, J., 1931a, Ann. Physik **8,** 821.
——, 1931b, Ann. Physik **11,** 489.
Fomin, P. I., 1958, Soviet Phys. JETP **8,** 491 (1959) [Zh. Eksperim. i Teor. Fiz. **35,** 707].
——, 1960, Soviet Phys. JETP **11,** 372 [Zh. Eksperim. i Teor. Fiz. **38,** 513].
Forssner, T., 1968, Arkiv för Fysik **35,** 477.
Frey, W. F., J. H. Hamilton, and S. Hultberg, 1963 Arkiv för Fysik **24,** 503.
Furry, W. H. 1934, Phys. Rev. **46,** 391.
——, 1951, Phys. Rev. **81,** 115.
Gáspár, R., 1954, Acta Phys. Acad. Sci. Hung. **3,** 263.
Gavrila, M., 1958, Nuovo Cimento **9,** 327.
——, 1959, Phys. Rev. **113,** 514.
——, 1960, Soviet Phys. **11,** 224.
——, 1961, Phys. Rev. **124,** 1132.
Ghose, A. M., 1966, Nucl. Phys. **75,** 529.
Ghumman, B. S., S. Anand, B. S. Sood, 1967, Indian J. Pure Appl. Phys. **5,** 70.
Goldemberg, J., and R. H. Pratt, 1966, Rev. Mod. Phys. **38,** 311.
Gombás, P., 1949, *Die Statistische Theorie Des Atoms* (Springer-Verlag, Vienna).

——, 1956, *Encyclopedia of Physics*, edited by S. Flügge (Springer-Verlag, Berlin), Vol. XXXVI.
Gorshkov, V. G., 1961, Soviet Phys. JETP **13,** 1037 (1961) [Zh. Eksperim i Teor. Fiz. **40,** 1481].
——, and A. I. Mikhailov, 1963, Soviet Phys. JETP **16,** 70 [Zh. Eksperim. i Teor. Fiz. **43,** 991 (1962)].
——, and A. I. Mikhailov, 1963, Soviet Phys. JETP **17,** 1439 [Zh. Eksperim. i Teor. Fiz. **44,** 2142].
——, A. I. Mikhailov, and V. S. Polikanov, 1967, Soviet Phys. JETP **25,** 1045.
Grant, I. P., 1961, Proc. Roy. Soc. (London) **A262,** 555.
——, 1967, Advan. Phys. **82,** 747.
Grigoryev, E. P., and A. V. Zolotavin, 1959, Zh. Eksperim. i Teor. Fiz. **36,** 272.
Grodstein-White, G., 1957, *X-ray Attenuation Coefficients from 10 keV to 100 MeV*, National Bureau of Standards Circular 583.
Guttmann, A. J., and H. Wagenfeld, 1967, Acta Cryst. **22,** 334.
Guzenko, S. Y., and P. I. Fomin, 1960, Soviet Phys. JETP **11,** 372 [Zh. Eksperim i Teor. Fiz. **38,** 513 (1960)].
Hager, R. S., and E. C. Seltzer, 1968, Nuclear Data Tables **A4,** 1.
Hall, H., 1934, Phys. Rev. **45,** 620.
——, 1936, Rev. Mod. Phys. **8,** 358.
——, 1951, Phys. Rev. **84,** 167.
——, 1960, *The Atomic Photoelectric Effect at High Energies*, Preprint, University of California, LRL.
——, and J. R. Oppenheimer, 1931, Phys. Rev. **38,** 57.
——, and W. Rarita, 1934, Phys. Rev. **46,** 143.
——, and E. C. Sullivan, 1966, Phys. Rev. **152,** A4.
Harriman, J., 1956, Phys. Rev. **101,** 594.
Hartree, D. R., 1928, Proc. Camb. Phil. Soc. **24,** 89.
Hartree, D. R., 1971, *The Calculation of Atomic Structures* (Wiley, 1957).
Hedgran, A., 1952, Arkiv för Fysik **5,** 13.
——, and S. Hultberg, 1954, Phys. Rev. **94,** 498.
Heitler, W., 1954, *The Quantum Theory of Radiation* (Oxford U. P., London), 3rd ed.
Hereford, F. L., 1951, Phys. Rev. **81,** 482.
——, 1951, Phys. Rev. **81,** 627.
——, and J. P. Keuper, 1953, Phys. Rev. **90,** 1043.
Herman, F., and S. Skillman, 1963, *Atomic Structure Calculations* (Prentice-Hall, Englewood Cliffs, New Jersey).
Herrlander, C. J., R. Stockendal, and R. K. Gupta, 1960, Arkiv för Fysik **17,** 315.
Hertz, H., 1887, Ann. Physik **31,** 983.
Hubbell, J. H., 1969, *Photon Cross Sections, Attenuation Coefficients, and Energy Absorption Coefficients from 10 keV to 100 GeV*, National Bureau of Standards NSRDS-NBS29.
——, 1971, Atomic Data **3,** 241.
——, and M. J. Berger, 1968, in R. Jaeger, (Ed.) *Engineering Compendium on Radiation Shielding* (IAEA, Vienna), Vol. 1, Ch. 4, Berlin/Göttingen/Heidelberg: Springer, p. 167–202.
Hulme, H. R., J. McDougall, R. A. Buckingham, and R. H. Fowler, 1935, Proc. Roy. Soc. (London) **A149,** 131.
Hultberg, S., 1955, Arkiv för Fysik **9,** 245.
——, 1959, Arkiv för Fysik **15,** 307.
——, B. Nagel, and P. O. M. Olsson, 1962, Arkiv för Fysik **20,** 555.
——, B. Nagel, and P. Olsson, 1968, Arkiv för Fysik **38,** 1–96.
——, T. O'Conner, and J. H. Hamilton, Nucl. Phys. **22,** 306.
——, and R. Stockendal, 1958, Arkiv för Fysik **14,** 565.
——, and R. Stockendal, 1959, Arkiv för Fysik **15,** 355.
——, and Z. Sujkowski, 1959, Phys. Rev. Letters **3,** 227.
Jansen, J. F. W., S. Hultberg, P. F. A. Goudsmit, and A. H. Wapstra, 1962, Nucl. Phys. **38,** 121.
Johnson, W. R., and R. T. Deck, 1962, J. Math. Phys. **3,** 319.
Johnston, R. R., 1964, Phys. Rev. A **136,** A958.
Källen, G., 1958, in *Handbuch der Physik*, edited by S. Flügge (Springer, Berlin), Vol. V/1.
——, 1962, *Topics in Quantum Electrodynamics* (Benjamin, New York), Vol. 1.
Kelly, H. P., 1969, Phys. Rev. **182,** 84.
——, and A. Ron, 1972, Phys. Rev. **A5,** 168.
Kirchner, F., 1930, *Handbuch der Experimentalphysik*, Wien, W. and F. Harms, (eds.) (Akademische Verlagsgesellschaft, Leipzig).
Knerr, R. P., and H. Vonach, 1967, Angew. Physik **22,** 507.
Kobayashi, S., T. Matsukuma, S. Nagai, and K. Umeda, 1955, J. Phys. Soc. Japan **10,** 759.
Köhler, H. S., and Y. C. Lin, 1971, Nuc. Phys. **A167,** 305.
Kohn, W., and L. S. Sham, 1965, Phys. Rev. **140,** A1133.
Koopmans, T., 1933, Physica **1,** 104.
Krause, M. O., 1969, Phys. Rev. **177,** 151.
Landau, L. D., and E. M. Lifshitz, 1965, *Quantum Mechanics* (Pergamon Press, 1965), 2nd ed. (Translated from the Russian by J. B. Skyes and J. S. Bell.)
Latter, R., 1955, Phys. Rev. **99,** 1854.
Latyshev, G. D., 1947, Rev. Mod. Phys. **19,** 132.
Lewis, M. N., 1953, *Oscillator Strength of Ionizing Transitions*, National Bureau of Standards Report 2457, 1953.
Liberman, D., 1970, Phys. Rev. **B2,** 244.
——, D. T. Cromer, and J. T. Waber, 1971, Computer Phys. Commun. **2,** 107.
Mann, J. B., and W. R. Johnson, 1971, Phys. Rev. **A4,** 41.
Manne, R., and T. Åberg, 1970, Chem. Phys. Lett. **7,** 282.
Manson, S. T., and J. W. Cooper, 1968, Phys. Rev. **165,** 126.
——, and J. W. Cooper, 1970, Phys. Rev. A **2,** 2170.
Marty, N., 1952, Compt. Rend. **234,** 938.
Matese, J. J., and W. R. Johnson, 1965, Phys. Rev. **140,** A1.
Meldner, H. W., and J. D. Perez, 1971, Phys. Rev. **A4,** 1388.
Messiah, A., 1962, *Quantum Mechanics*, (North-Holland Publ. Co., Amsterdam). (Translated from the French by G. M. Temmer.)
Mikhailov, A. I., 1969, Sov. Phys. JETP **28,** 326.
Molière, G., 1947, Z. Naturforsch. **2a,** 133.
Moliére, G., 1948, Z. Naturforsch. **3a,** 78.
Mork, K. J., and H. Olsen, 1961, Phys. Norvegica 1: No. **1,** 23.
——, and H. Olsen, 1965, Phys. Rev. **140,** B1661.
——, and H. Olsen, 1968, Phys. Rev. **166,** 1862.
Moroi, D. S., 1961, Phys. Rev. **123,** 167.
Morse, P. M., and H. Feshbach, 1953, *Methods of Theoretical Physics* (McGraw-Hill, N.Y.).
Mott, N. F., and H. S. W. Massey, 1965, *The Theory of Atomic Collision* (Oxford U. P., Oxford), 3rd ed.
McCrary, J. H., E. H. Plassmann, J. M. Puckett, A. L. Conner, and G. W. Zimmermann, 1967, Phys. Rev. **153,** 307.
McGinnies, R. T., 1959, *X-Ray Attenuation Coefficients from 10 keV to 100 MeV*, National Bureau of Standards Supplement to Circular 583, 1959.
McGuire, E. J., 1967, Phys. Rev. **161,** 51.
——, 1968, Phys. Rev. **175,** 20.
McMaster, W. H., and F. L. Hereford, 1954, Phys. Rev. **95,** 723.
——, N. K. Del Grande, J. H. Mallett, and J. H. Hubbell, 1970, Report Lawrence Livermore Laboratory, UCRL 50174. See also Nuclear Data Tables **A8,** 443 (1970); *International Tables for X-Ray Crystallography*, edited by J. A. Ibers and W. C. Hamilton (Kynoch Press, Birmingham, England), Sec. 2.1, (in press).
McVoy, K. W., 1957, Phys. Rev. **108,** 365.
——, and U. Fano, 1959, Phys. Rev. **116,** 1168.
Nagasaka, F. G., 1955, Ph.D. Thesis, University of Notre Dame, 1955 (unpublished).
——, and E. Guth, 1958, Bull. of Amer. Phys. Soc. **4,** 13.
Nagel, B., 1960, Arkiv för Fysik **18,** 1.
——, 1963, Arkiv för Fysik **24,** 151.
——, and P. O. M. Olsson, 1960, Arkiv för Fysik **18,** 29.
Olsen, H., L. C. Maximon, and H. Wergeland, 1957, Phys. Rev. **106,** 27.
Oms, J., and P. Chedin, Journal De Physique, 1967, Tome **28,** 281.
Parthasaradhi, K., 1968, Indian J. Pure Appl. Phys. **6,** 385.
——, V. Lakshminarayana, and S. Jnanananda, 1964a, Indian J. Pure Appl. Phys. **2,** 290.
——, V. Lakshminarayana, and S. Jnanananda, 1964b, Indian J. Pure Appl. Phys. **2,** 306.
——, V. Lakshminarayana, and S. Jnanananda, 1965, Indian J. Pure Appl. Phys. **3,** 323.
——, V. Lakshminarayana, and S. Jnanananda, 1966a, Phys. Rev. **142,** 9.
——, V. Lakshminarayana, and S. Jnanananda, 1966b, Indian J. Pure Appl. Phys. **4,** 87.
Perkin, J. L., and A. C. Douglas, 1967, Proc. Phys. Soc. (London) **92,** 618.
Perlman, H. S., and B. A. Robson, 1959, Australian J. of Phys. **12,** 30.
Popov, V. S., 1970, Sov. J. Nucl. Phys. **12,** 235 (1971); [Yad. Fiz. **12,** 429].
Prange, R. A., and R. H. Pratt, 1957, Phys. Rev. **108,** 139.

Pratt, R. H., 1960a, Phys. Rev. **117,** 1017.
——, 1960b, Phys. Rev. **119,** 1619.
——, R. D. Levee, R. L. Pexton, and W. Aron, 1964, Phys. Rev. **134,** A898; **134,** A916.
——, and H. K. Tseng, 1972, Phys. Rev. A **5,** 1063.
Rakavy, G., and A. Ron, 1965, Phys. Letters **18,** 207.
——, and A. Ron, 1967, Phys. Rev. **159,** 50.
Raman, S., R. Gunnink, T. A. Walkiewicz, and B. Martin, 1972, Bull. Am. Phys. Soc. **17,** 468.
Ralston, A., and H. S. Wilf, 1962, eds. *Mathematical Methods for Digital Computers* (Wiley, N.Y.).
Rao, V. V., and K. Parthasaradhi, 1968, Indian J. Pure Appl. Phys. **6,** 642.
——, and K. Parthasaradhi, 1969, J. Appl. Phys. **40,** 5391.
——, K. Parthasaradhi, and S. Jnanananda, 1969, Indian J. Pure Appl. Phys. **7,** 271.
Reitan, A., 1961, Physica Norvegica **1,** 113.
Rimsky-Korsakov, A. A., and V. V. Smirnov, 1962, Soviet Phys. JETP **15,** 47 [Zh. Eksperim. i Teor. Fiz. **42,** 67].
Ron, A., 1966, Ph.D. Dissertation, The Hebrew University, Israel, (1966) (unpublished).
Rose, M. E., 1958, *Internal Conversion Coefficients* (North Holland Publ. Co.,).
——, 1961, *Relativistic Electron Theory* (Wiley, N.Y.).
Rose, M. E., and L. C. Biedenharn, 1954, *Theory of the Photoelectric Effect,* ORNL Report 1779.
Rosen, A., and I. Lindgren, 1968, Phys. Rev. **176,** 114.
Rotenberg, M., R. Bivins, N. Metropolis, and J. K. Wooten, Jr., 1959, *The 3-j and 6-j Symbols* (Massachusetts Institute of Technology, Cambridge, Mass.).
Roy, R. R., and R. D. Reed, 1968, *Interactions of Photons and Leptons with Matter* (Academic, N.Y.).
Rozsnyai, B. F., 1972, Phys. Rev. **A5,** 1137.
Ryde, H., and Z. Sujkowski, 1962, Arkiv för Fysik **20,** 289.
Sauter, F., 1931a, Ann. Physik **9,** 217.
——, 1931b, Ann. Physik **11,** 454.
——, and H. O. Wuster, 1955, Z. Physik **141,** 83.
Scheck, F., and M. Stingl, 1968, Z. Physik **209,** 93.
Schmickley, R. D., 1966, Ph.D. Dissertation, Stanford University, 1966 (unpublished).
——, and R. H. Pratt, 1967, Phys. Rev. **164,** 104.
Schweber, S. S., 1961, *An Introduction to Relativistic Quantum Field Theory* (Row, Peterson and Co., New York), pp. 243 and 566.
Scofield, J., 1972, private communication.
Seemann, K. W., 1956, Bull. Am. Phys. Soc. **1,** 198.
Shalitin, D., 1965, Phys. Rev. **140,** A1857.
Simmons, G. L., and J. H. Hubbell, 1971, *Comparison of Photon Interaction Cross Section Data Sets. I. Storm-Israel and ENDF/B,* National Bureau of Standards Report 10668, 1971. Also reports 10818, 10842, 10847.
Singh, M. I., and B. S. Sood, 1972, Nuovo Cimento **8B,** 261.
Slater, J. C., 1951, Phys. Rev. **81,** 385.
——, 1960, *Quantum Theory of Atomic Structure* (McGraw-Hill N.Y.), Vol. I and II.
——, 168, Phys. Rev. **165,** 658.
Sliv, L., and J. Band, 1956, *Tables of Internal Conversion Coefficients of Gamma-rays* (Academy of Sciences USSR).
Sommerfeld, A., 1939, *Atombau and Spektrellinien* (F. Vieweg and Son, Braunschweig, 1939), Vol. 2, p. 457.
——, and A. W. Maue, 1935, Ann. Physik **22,** 629.
——, and G. Schur, 1930, Ann. Physik **4,** 409.
Starace, A. F., 1970, Phys. Rev. **A2,** 118.
Stobbe, M., 1930, Ann. Physik **7,** 661.
Storm, E., and H. I. Israel, 1967, LA-3753 (1967).
——, 1970, Nuclear Data Tables **A7,** 565.
Sujkowski, Z., 1961, Arkiv för Fysik **20,** 269.
Swirles, B., 1935, Proc. Roy. Soc. (London) **152,** 625.
Taylor, B. N., W. H. Parker, and D. N. Langenberg, 1969, Rev. Mod. Phys. **41,** 375.
Titus, F., 1958, Bull. Am. Phys. Soc. **4,** 269.
——, 1959, Phys. Rev. **115,** 351.
——, 1965, Nucl. Phys. **69,** 179.
Tolhoek, H. A., 1956, Rev. Mod. Phys. **28,** 277.
Tseng, H. K., 1970, Ph.D. Dissertation, University of Pittsburgh, 1970 (unpublished).
——, and R. H. Pratt, 1971, Phys. Rev. A **4,** 1835.
——, and R. H. Pratt, 1972, Phys. Rev. A **6,** 2049.
Tucker, T. C., L. D. Roberts, C. W. Nestor, T. A. Carlson, and F. B. Malik, 1968, Phys. Rev. **174,** 118.
Veigele, Wm. J., E. Briggs, L. Bates, E. M. Henry, and B. Bracewell, 1971, *X-Ray Cross Section Compilation from 0.1 keV to 1 MeV,* Kaman Science Corporation, DNA2433F, Vols. I and II, Rev. 1 KN-71-431(R), 1971, (also to be published in Atomic Data).
Weber, T. A., and C. J. Mullin, 1962, Phys. Rev. **126,** 615.
Weinberg, S., 1965, Phys. Rev. **140,** B516.
Wiedenbeck, M., 1962, Phys. Rev. **126,** 1009.